



UNITED NATIONS
UNIVERSITY

UNU-GTP

 **ORKUSTOFNUN**



Silica rich waters in Köldulaugagil, Hengill area, SW-Iceland

Selamawit Worku Sisay

SUB-SURFACE GEOLOGY, HYDROTHERMAL ALTERATION AND 3D MODELLING OF WELLS LA-9D AND LA-10D IN THE ALUTO LANGANO GEOTHERMAL FIELD, ETHIOPIA

Report 6
December 2016



UNITED NATIONS
UNIVERSITY

UNU-GTP

Geothermal Training Programme

Orkustofnun, Grensasvegur 9,
IS-108 Reykjavik, Iceland

Reports 2016
Number 6

SUB-SURFACE GEOLOGY, HYDROTHERMAL ALTERATION AND 3D MODELLING OF WELLS LA-9D AND LA-10D IN THE ALUTO LANGANO GEOTHERMAL FIELD, ETHIOPIA

MSc thesis

School of Engineering and Natural Sciences
Faculty of Earth Sciences
University of Iceland

by

Selamawit Worku Sisay
Geological Survey of Ethiopia
P.O. Box 2302,
Addis Ababa,
ETHIOPIA
soliethio@yahoo.com

United Nations University
Geothermal Training Programme
Reykjavík, Iceland
Published in December 2016

ISBN 978-9979-68-410-7
ISSN 1670-7427

This MSc thesis has also been published in August 2016 by the
School of Engineering and Natural Sciences, Faculty of Earth Sciences
University of Iceland

INTRODUCTION

The Geothermal Training Programme of the United Nations University (UNU) has operated in Iceland since 1979 with six month annual courses for professionals from developing countries. The aim is to assist developing countries with significant geothermal potential to build up groups of specialists that cover most aspects of geothermal exploration and development. During 1979-2016, 647 scientists and engineers from 60 developing countries have completed the six month courses, or similar. They have come from Africa (38%), Asia (36%), Latin America (14%), Europe (12%), and Oceania (1%). There is a steady flow of requests from all over the world for the six-month training and we can only meet a portion of the requests. Most of the trainees are awarded UNU Fellowships financed by the Government of Iceland.

Candidates for the six-month specialized training must have at least a BSc degree and a minimum of one-year practical experience in geothermal work in their home countries prior to the training. Many of our trainees have already completed their MSc or PhD degrees when they come to Iceland, but many excellent students with only BSc degrees have made requests to come again to Iceland for a higher academic degree. From 1999 UNU Fellows have also been given the chance to continue their studies and study for MSc degrees in geothermal science or engineering in co-operation with the University of Iceland. An agreement to this effect was signed with the University of Iceland. A similar agreement was also signed with Reykjavik University in 2013. The six-month studies at the UNU Geothermal Training Programme form a part of the graduate programme.

It is a pleasure to introduce the 51st UNU Fellow to complete the MSc studies under a UNU-GTP Fellowship. Selamawit Worku Sisay, BSc in Geology from the Geological Survey of Ethiopia, Ethiopia, completed the six-month specialized training in Borehole Geology in 2012. Her research report was entitled: *Borehole geology and hydrothermal mineral alteration of well HN-3, Hellisheidi geothermal field, SW-Iceland*. After two years of geothermal work in Kenya, she came to Iceland for MSc studies at the University of Iceland, School of Engineering and Natural Sciences, starting in August 2014. In July 2016, she defended her MSc thesis presented here, entitled: *Sub-surface geology, hydrothermal alteration and 3D modelling of wells LA-9D and LA-10D in the Aluto Langano geothermal field, Ethiopia*. Her studies in Iceland were financed by the Government of Iceland through a UNU-GTP Fellowship from the UNU Geothermal Training Programme. We congratulate her on her achievements and wish her all the best for the future. We thank the School of Engineering and Natural Sciences, Faculty of Earth Sciences at University of Iceland for the co-operation, and her supervisors for the dedication.

Finally, I would like to mention that Selamawit's MSc thesis with the figures in colour is available for downloading on our website www.unugtp.is, under publications.

With warmest greetings from Iceland,

Lúdvík S. Georgsson, Director
United Nations University
Geothermal Training Programme

ACKNOWLEDGEMENTS

My heartfelt gratitude to the Icelandic Government and the United Nation University Geothermal Training Programme (UNU-GTP) director, Mr. Lúdvík S. Georgsson for granting me to study in Iceland, and the staff members Mr. Ingimar G. Haraldsson, Ms. Thórhildur Ísberg, Mr. Markús A.G. Wilde and Mrs. Málfrídur Ómarsdóttir for providing all facilities and support. My special thanks to Ato Solomon Kebede, geothermal resource exploration and evaluation core process owner and Ato Hundie Melka, chief geologist of Geological Survey of Ethiopia for allowing me to attend the MSc study in Iceland.

I am highly indebted and thankful to my supervisors Anette K. Mortensen, Björn S. Hardarson and Gudmundur Gudfinnsson for the excellent guidance, constant support and invaluable help during my project work. My warm thanks goes to to Sigurdur. S. Jónsson for his help with XRD analysis, Júlíana Signý Gunnarsdóttir for her assistance during my laboratory analysis at ISOR, Saemundur Ari Halldórsson for the guidance and assistance during ICP-OES sample analysis at University of Iceland and the external examiner Dr. Vigdis Hardardottir.

My very sincere gratitude goes to my beloved friends and UNU MSc and PhD fellows, I am so thankful for the good time we spent together and for your encouragement and motivation. May God bless you all.

My deepest gratitude goes to my family for their unflagging love and unconditional support throughout my life and my studies. Your support and encouragement was worth more than I can express on paper.

Above all, Glory to the Almighty God who made all things possible. Without his protection and guidance none of this work would have been possible.

DEDICATION

This work is dedicated to my beloved parents.

ABSTRACT

Aluto Langano geothermal field is located in the Aluto volcanic complex (AVC), within the Central Main Ethiopian Rift System (CMERS). AVC is a silicic peralkaline complex, which is affected by Wonji fault belt (WFB), trending NNE-SSW. Ten exploratory wells (LA-1 to LA-10D) have been drilled in Aluto Langano geothermal field, with a maximum depth of 2500 m and maximum measured temperature of 335°C.

This study focused on sub-surface geology and hydrothermal alteration of wells LA-9D and LA-10D. The wells were drilled directionally on the top of AVC. Data from neighbouring wells (wells LA-3 to LA-8) are used for comparison purposes. Lithologies that are found in the study wells, identified with the aid of binocular microscopy and petrographic microscopy, are pyroclastics, silicic tuff and breccia, sediments, rhyolite, trachyte, basalt and ignimbrite, while ICP-OES analyses also led to the identification of very scarce and thin layers of trachyandesite, basaltic trachyandesite, trachydacite, basaltic andesite and andesite units. Hydrothermal alteration minerals are found as replacement of primary minerals and as fillings of veins and vesicles. Four alteration zones are recognized in both study wells, and include an unaltered zone, smectite zone, illite/chlorite zone and illite/chlorite/epidote zone.

Eight feed zones (with one major and seven minor) were identified in well LA-9D and seven (one major with six minor) feed zones in LA-10D are observed. Most of the feed zones are located in fractured basaltic units. The highest temperature recorded was more than 300°C in well LA-9D below 1560 m depth, and below 1600 m in LA-10D, the recorded temperature indicated is more than 300°C. Both wells appear to be in the upflow zone of the system.

TABLE OF CONTENTS

	Page
1. BACKGROUND.....	1
1.1 Objectives of the study	3
2. TECTONIC AND GEOLOGICAL SETTING	4
2.1 Structural setting of Main Ethiopian Rift (MER)	4
2.2 Regional geology.....	5
2.3 Geology of Aluto Langano geothermal field.....	7
2.3.1 Surface geology.....	7
2.3.2 Structure of the Aluto-Langano Area.....	9
2.3.3 Geothermal surface manifestation.....	10
2.3.4 Subsurface geology of Aluto Langano area	11
2.3.5 Hydrogeological setting	13
2.3.6 Geophysical exploration of Aluto Langano area.....	14
3. METHODOLOGY.....	16
3.1 Sampling.....	16
3.2 Analytical methods.....	16
3.2.1 Binocular microscope analysis.....	16
3.2.2 Petrography microscope analysis	16
3.2.3 X-ray diffractometer analysis.....	17
3.2.4 Inductively Coupled Plasma-Optical Emission Spectroscopy (ICP-OES)	17
4. RESULTS	18
4.1 Drilling activity	18
4.2 Lithology	19
4.2.1 Main rock units identified by binocular, petrography and ICP-OES method.	19
4.2.2 Rock units identified by ICP-OES analysis	22
4.3 Hydrothermal alteration mineralogy	23
4.3.1 Alteration of primary mineral assemblage	23
4.3.2 Distribution of hydrothermal alteration minerals.....	24
4.4 Vein and vesicle fillings	28
4.5 Mineral depositional sequence	29
4.6 Hydrothermal mineral zonation.....	30
4.7 Feed zones	32
4.8 Distribution of temperature at Aluto Langano geothermal field	32
4.9 Whole rock chemistry.....	37
4.9.1 Classification of rock type.....	37
4.9.2 Effects of hydrothermal alteration on the rock chemistry	39
4.10 3D geological and geothermal model.....	41
5. DISCUSSION	45
5.1 Lithology	45
5.2 Hydrothermal alteration.....	48
5.3 2D interpretation of hydrothermal alteration mineral zonation vs resistivity.....	49
5.4 2D interpretation of formation temperature vs hydrothermal alteration mineral zonation.....	52
6. CONCLUSION AND RECOMMENDATIONS.....	55
6.1 Conclusions	55
6.2 Recommendations	55
REFERENCES.....	56

APPENDIX I	Page 60
APPENDIX II	63
APPENDIX III	66
APPENDIX IV	67

LIST OF FIGURES

1. Location map of the Main Ethiopian Rift (MER) and Aluto geothermal field.....	1
2. Wells LA-1 to LA-8 located in Aluto Langanu geothermal field.....	2
3. Tectonic setting of the Main Ethiopian Rift (MER)	5
4. Geological map of Ethiopia	6
5. Geology of Aluto Langanu volcanic complex	8
6. Structural map of Aluto Langanu volcanic complex (AVC)	10
7. Distribution of surface manifestations in Aluto Langanu geothermal field.....	11
8. Aluto Langanu and the surrounding area - ASTER RGB 321 imagery.....	12
9. Deep well cross-section	12
10. Regional hydrological map of the Aluto Langanu area	13
11. Regional Bouguer anomaly map.....	14
12. Station map of MT survey	15
13. Apparent Resistivity Map with a frequency of 1 Hz at (-1000 m a.s.l.)	15
14. Lithology, alteration minerals and alteration zones of well LA-9D.....	20
15. Lithology, alteration minerals and alteration zones of well LA-10D.....	21
16. Smectite peaks in LA-10D.....	28
17. Chlorite and illite peaks in LA-9D.....	28
18. A) Quartz veinfilling found in LA-10D at 1530 m; and B) calcite veinfilling at LA-10D at 1890 m depth.....	29
19. Mineral depositional sequence.....	30
20. Cross-section of alteration zones in Aluto Langanu geothermal wells.....	31
21. Feed zones in well LA-9D inferred from loss of circulation, temperature logs, alteration intensity and abundance of alteration minerals.....	33
22. Feed zones in well LA-10D inferred from loss of circulation, temperature logs, alteration intensity and abundance of alteration minerals.....	34
23. Distribution of temperature in Aluto Langanu geothermal field at 800 m.a.s.l.	35
24. Distribution of temperature with lithology and alteration in Aluto Langanu geothermal wells ..	36
25. TAS diagram showing the Aluto Langanu sub-surface rock samples (LA-9D and LA-10D) with surface data fields from the northern MER.....	38
26. Al ₂ O ₃ vs FeO diagram of the Aluto Langanu samples from wells LA-9D and LA-10D	39
27. Major elements vs SiO ₂ for subsurface samples of Aluto Langanu wells LA-9D and 10D	40
28. Trace elements vs Zr for subsurface samples of Aluto Langanu wells LA-9D and 10D.....	41
29. 3D view of topography map with wells (vertical exaggeration by factor 2x).....	42
30. 3D view of alteration horizon with geothermal wells at Aluto Langanu geothermal field.....	43
31. 3D property model of temperature at Aluto Langanu geothermal field.....	43
32. 3D property model of resistivity at Aluto Langanu geothermal field	44
33. The rock units observed in wells LA-9D and LA-10D, Aluto Langanu geothermal field.....	45
34. Main lithologies identified in Aluto Langanu geothermal fields	46
35. NW-SE cross-section through well field showing simplified stratigraphy and structural controls in Aluto Langanu geothermal fields.....	47
36. Cross-sections of resistivity vs. hydrothermal alteration zone.....	50
37. Resistivity data at 800 m a.s.l., Aluto Langanu geothermal field	51

	Page
38. Cross-sections of formation temperature vs. hydrothermal alteration zone.....	53
39. Conceptual model of Aluto Langanu field in relation to alteration mineral zones and formation temperatures	54

LIST OF TABLES

1. Summary of Aluto Langanu wells (LA-1 to LA-8)	11
2. Wells LA-9D and LA-10D of Aluto Langanu geothermal field.....	16
3. Well configuration of LA-9D.....	18
4. Well configuration of LA-10D.....	18
5. Alteration minerals and their temperature based on data from Icelandic geothermal systems	23
6. Primary minerals and alteration products of wells LA-9D and LA-10D.....	24
7. Results of XRD analysis of clay minerals from well LA-9D (d in Å).....	26
8. Results of XRD analysis of clay minerals from well LA-10D (d in Å).....	27
9. Mineral depositional sequence in well LA-9D and LA-10D	29
10. Whole rock chemical analysis data for major elements (wt.%) and trace elements (ppm) of drill cuttings from well LA-9D.....	37
11. Whole rock chemical analysis data for major elements (wt.%) and trace elements (ppm) of drill cuttings from well LA-10D	38

ACRONYMS AND ABBREVIATIONS

AVC	Aluto volcanic complex
CMERS	Central Main Ethiopian Rift
EARS	East African Rift System
GEARS	Great East Africa Rift System
HCl	Hydrochloric acid
ICP-OES	Inductively Coupled Plasma – Optical Emission Spectroscopy
ISOR	Icelandic GeoSurvey
Ka	Thousand years
KOP	kick-off point
Ma	Million years
m a.s.l.	metre above sea level
MER	Main Ethiopia Rift
MERS	Main Ethiopian Rift System
MLC	Mixed layer clays
MT	Magneto telluric
MWe	Megawatt electricity
PPL	Plane Polarised Light
ppm	parts per million
TAS	Total Alkali versus Silica
WFB	Wonji fault belt
XPL	Cross polarised light
XRD	X-ray diffractometer

1. BACKGROUND

Ethiopia is one of the East African countries with the most significant geothermal resources. Geothermal resources are present in the Main Ethiopian Rift System (MERS) and in the Afar depression, which are a part of the Great East Africa Rift System (GEARS). More than sixteen geothermal prospects are located along this rift that are believed to have the potential for electricity production. Aluto Langano, Tendaho, Corbetti, Abaya, Tulumoye-Gedemsa, Dofan and Fantale are a few of the prospect areas in which detailed exploration study and drilling have started due to their expected potential and their strategic location relative to the national grid. Aluto Langano geothermal field is one of geothermally active areas and the first geothermal field to be developed in Ethiopia but the field is located about 200km south of the capital Addis Ababa (coordinates: N 7.60°-7.96°, E 38.68°-38.92°). The Aluto Langano geothermal field is located within the Aluto volcanic complex (AVC) on the eastern margin of the Main Ethiopian Rift valley in the Lake District between Lake Ziway, to the north, and Lake Langano, to the south (Figures 1 and 2).

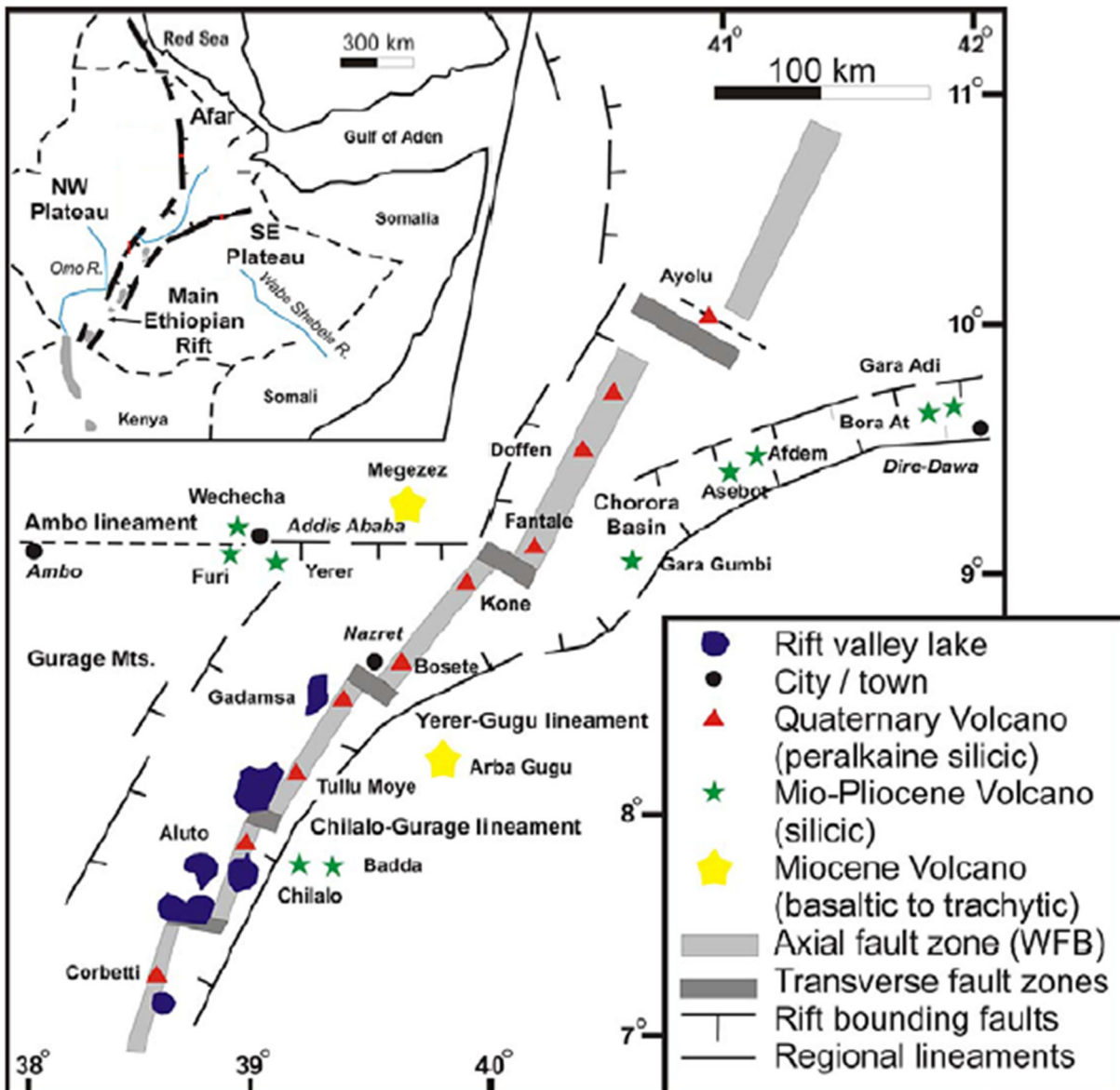


FIGURE 1: Location map of the Main Ethiopian Rift (MER) and Aluto geothermal field

AVC is situated in the eastern side of the Central Main Ethiopian Rift (CMER) floor, which covers an area of about 100 km², reaching an elevation of 2328 m a.s.l. and rising about 700 m above the rift floor (Teklemariam, 1996). AVC is dominated by a ~14 km-wide, 700 m-high edifice composed of a thick pile of rhyolitic lava flows and domes, pumice cones, and ignimbrite deposits (Hutchison et al., 2015).

Aluto caldera is extended in the WNW direction with a size of 6 km by 9 km (Kebede et al., 1984) and covered by alluvial sediments. According to Lloyd (1977), pyroclastics and rhyolites were erupted through vents or centres, which are controlled by the Wonji fault belt (WFB) trending in NNE direction. The initial Aluto volcanic activity is estimated to have taken place between 150 and 130 ka (Electroconsult, 2016). In the northwest of the complex, there is a significant number of smaller volcanic vents and domes located. The Aluto volcanic complex appears to be limited to the west by one of the numerous WFB faults and to the east by a series of step faults, which progressively rise above the rift floor to form the Eastern Escarpment (Hutchison et al., 2015).

Geothermal resource exploration and study in Ethiopia started in 1969 with a collaboration work of the Ethiopian Geological Survey and the United Nations. Geological, geochemical and hydrological surveys have been performed.

Aluto Langanu is the first geothermal field in Ethiopia to be exploited. In this area, eight deep exploration wells (LA- 1 to LA-8) were drilled in 1981 to 1986 with a maximum depth of 2500 m, reaching temperature of up to 335°C (Teklemariam and Beyene, 2000). Wells LA-1 and LA-2 were drilled at the southern and western flanks of Aluto volcanic complex (AVC), respectively (Figure 2), and were characterized by low temperature and permeability. Wells LA-3 to LA-8 were sited on top of Aluto Langanu in the south-eastern part of the area (Figure 2). LA-3 and LA-6 were drilled in the most active fault system, Wonji Fault Belt (WFB), trending in NNE direction, and where maximum temperature recorded was 315 and 335°C, respectively (UNDP, 1986). LA-4 and LA-5 were drilled in the eastern part of Wonji fault Belt and LA-7 and LA-8 in the western part (Figure 2).

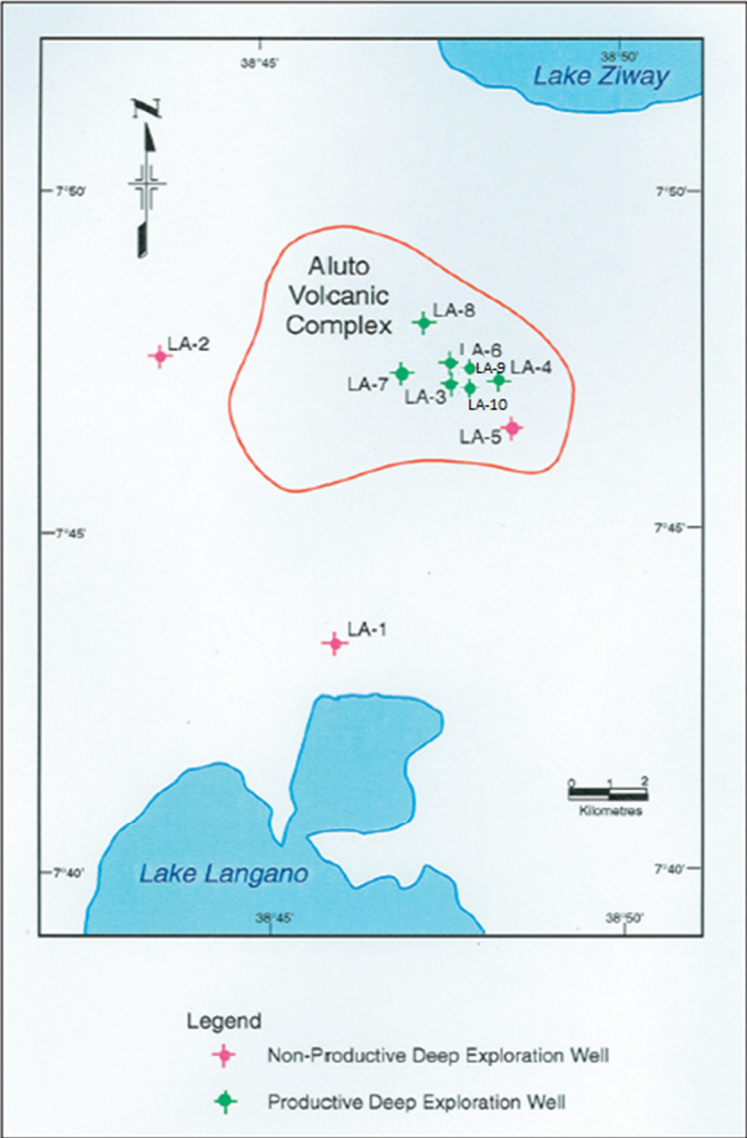


FIGURE 2: Wells LA-1 to LA-10 located in Aluto Langanu geothermal field

The first 7.2 MW pilot power plant was installed by the Ethiopian Electric Power Corporation, and connected to the national power grid in May 1998. It was started by four production wells (LA-3, LA-4, LA-6 and LA-8, and with one reinjection well, LA-7) (Teklemariam and Beyene, 2000). The expected capacity of this geothermal field was 30 MW over for 30 years. The pilot power plant has not been in full operation due to problems related to the production wells (e.g. decline of well pressures, scaling and wellhead valve problems) and problems related to the power plant involving cooling tower fan breakdowns, Pentane leakage from the heat exchangers and so on. According to Kebede (2012), the plant has been partially renewed and started to produce 4 MWe in 2007. In 2013, expansion work in Aluto Langanu geothermal field was started.

The project is a collaboration of and financed by the Ethiopian government, the World Bank and the government of Japan (Tassew, 2015). The expansion is expected to produce 70 MWe in two phases. Two exploration wells have been drilled, LA-9D and LA-10D, with the use of a rig owned by the Geological Survey of Ethiopia.

LA-9D and LA-10D are the first directional wells in Ethiopia with a depth of 1920 and 1940 m, respectively, and were drilled within the Aluto volcanic complex. LA-9D was drilled directionally from 700 m to N70°W and 51° inclinations; and LA-10D from 450 m with a direction of N43°W and 25.75° inclination.

1.1 Objectives of the study

The main objective of this study is to understand the sub-surface geology of the Aluto Langanu geothermal field by using cuttings samples and various data from wells LA-9D and LA-10D. The detailed objectives include:

- ✓ Identify the subsurface geology and lithological units of the study wells by using different analytical method.
- ✓ Identify the hydrothermal alteration minerals and the history of alteration, and to understand the thermal evolution of the wells.
- ✓ Identify and categorize the feed zones in the study wells in relation to structures, alteration minerals and alteration intensity, lithological contacts and temperature logs. To understand the permeability of the well.
- ✓ Determine the distribution of temperature in the study wells together with the neighbouring wells.
- ✓ Understand the relation between the alteration and temperature in the wells and the resistivity in the field.
- ✓ Outline the geological characteristics controlling the distribution of temperature, alteration and permeability within the geothermal reservoir at Aluto-Langanu geothermal field.

2. TECTONIC AND GEOLOGICAL SETTING

2.1 Structural setting of Main Ethiopian Rift (MER)

The East African Rift System (EARS) originated during the Oligocene with the progressive uplifting of East Africa and part of the Arabian Peninsula to form the Afro-Arabian Dome in the Early Tertiary (Upper Eocene), along with tensional tectonic movements. This process caused a continental break-up with intense normal faulting and associated widespread flood basalt eruptions of the Trap Series (Corti, 2009). The East African Rift System (EARS) extends for about 6,500 km from the Dead Sea Rift in the north to Mozambique in the south. This rift system is divided into an eastern branch and western branch, and is composed of several interacting segments. The Ethiopian rift system is located in the eastern branch of EARS, and started to develop during Miocene time. The MER is an oblique rift, exhibiting an overall NE–SW trend, formed by E–W extension between the Nubia and Somalia plates via both magmatic intrusion and tectonic faulting (Ebinger, 2005; Corti, 2009; Corti et al., 2013a). According to Bendick et al. (2006), Keir et al. (2006) and Stamps et al. (2008), the geodetic and seismic data show that the current E–W extension rates are 4–6 mm per year. The rift gives a complete picture of how rift morphology develops through time, from fault-dominated in the southern MER to magma-dominated in the northern MER (Corti, 2009). Active faulting and volcanic activity is mostly localized along N-S trending fault system (Wonji Fault Belt), developed within the rift floor (Kazmin, 1980). Wonji Fault Belt (WFB) is characterized by active extension fractures and normal faults, which are related to fissural or central volcanic activity.

The Ethiopian Rift is divided into two main physiographic segments, called the southern Afar and the Main Ethiopian Rift; the rift morphology is typically developed in the latter segment, where a ~80-km wide rift valley (Mohr, 1983) separates the uplifted western (Ethiopian) and eastern (Somalian) plateaus. Mohr (1962) states that the boundary between the Main Ethiopian Rift (MER) and southern Afar does not correspond to any physiographic feature, as the rift valley gradually funnels outwards into the wide Afar depression. MER is traditionally subdivided into three main sectors (Northern MER, Central MER and Southern MER) (Figure 3) that reflect differences in terms of the spatial pattern of the faulting (Agostini et al., 2011), the timing of major faulting episodes and lithospheric characteristics (Molin and Corti, 2015).

The Northern MER is considered to extend from the true Afar depression up to the Lake Koka region, following the middle course of the Awash River valley. The main boundary faults in this region formed about 10-11 Ma ago (Kazmin et al., 1980; Mohr, 1983). The Northern MER is characterized by two distinct fault sets. These are NE–SW trending border faults on the boundaries of the rift, and a set of closely spaced NNE–SSW-trending faults (Hutchison et al., 2015).

The Central MER contains most of the Lakes Region, up to the Lake Awasa area. In the Central MER, the faults were formed at 6–8 Ma (WoldeGabriel et al., 1990; Bonini et al., 2005); while the Wonji faults initiated 2 Ma (Corti, 2009). The main boundary faults are well developed at the age of late Miocene–Pliocene post-6–7 Ma (Bonini et al., 2005). In the CMER, the border faults are still seismically active (Hutchison et al., 2015) and much of the active tectonic deformation occurs in the magmatic segments through NNE–SSW Wonji faults (Keir et al., 2006). These could be related to the hydrothermal system.

The Southern MER extends south of Lake Awasa into the ~300-km-wide system of basins and ranges (Figure 3). The first extensional structures in Southern MER developed as N-S trending Kenya Rift related structures at about 20–21 Ma and lasted up to 11 Ma. According to Molin and Corti (2015), in the southern MER, a few major boundary faults accommodate the largest part of recent and active deformation.

Most recent silicic products in the northern Ethiopian rift have erupted from central volcanoes with large summit calderas, such as Gedemsa, Kone and Fantale and forming very thick pyroclastic deposits, thought to have been partially produced from fissures. These volcanic products are about 5 Ma and are known as the Nazret group (Electroconsult, 2015). Quaternary volcanism in the northern Ethiopian rift consists of dominant peralkaline rhyolites, minor trachytes, and transitional basalts. Intermediate

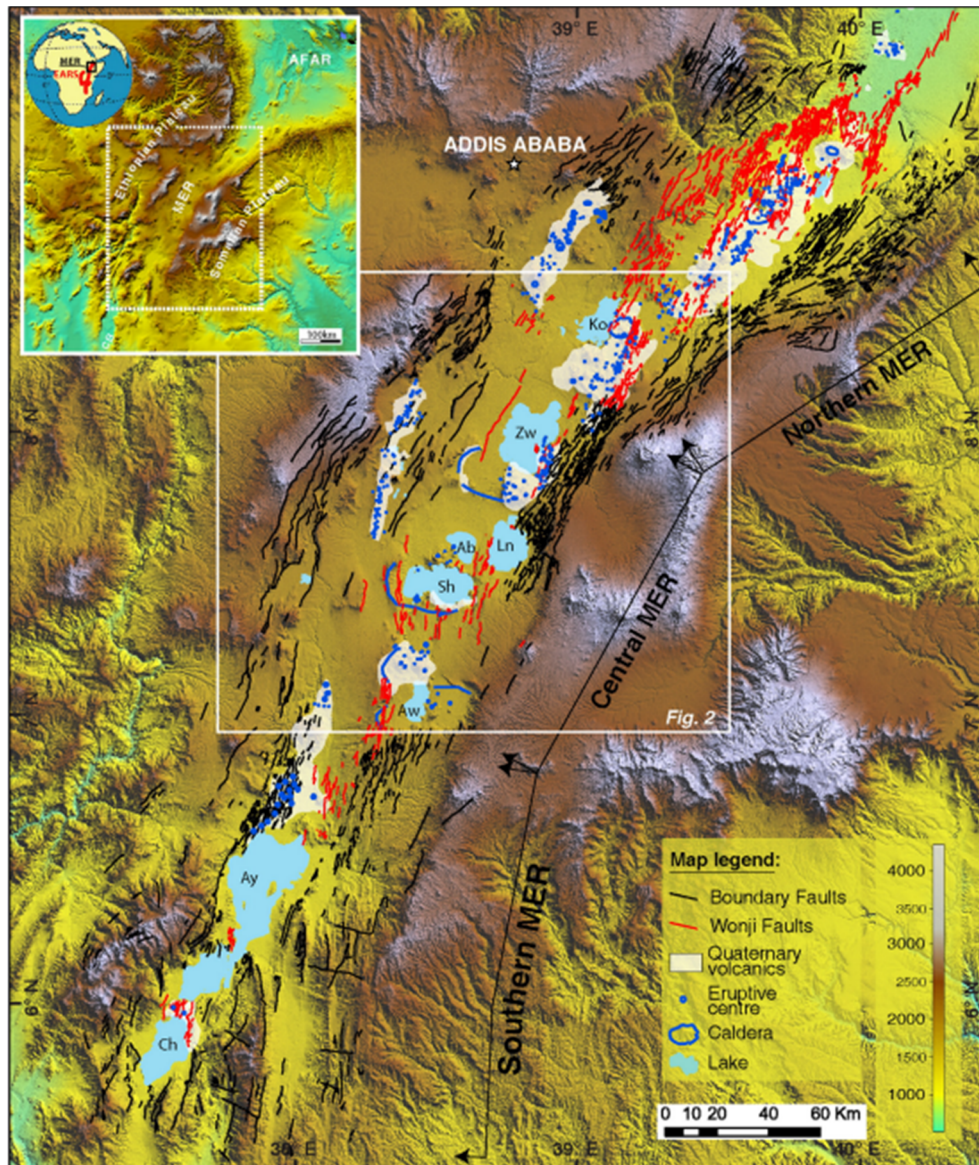


FIGURE 3: Tectonic setting of the Main Ethiopian Rift (MER) (Molin and Corti, 2015)

composition rocks are very rare or absent. Some trachytic volcanoes occur on the margins of the rift (Acoccella et al., 2002).

2.2 Regional geology

The oldest basement rocks in Ethiopia, especially in the south and in the western part of the country, are Precambrian with an age of more than 600 million years (Figure 4). The Precambrian formations contain a wide variety of sedimentary, volcanic and intrusive rocks which have been subjected to varying degrees of metamorphism and deformation. These rocks are impermeable, except where they are fractured. The fractured zones are an important source of groundwater and for economically exploitable mineral deposits (Alemu, 2012).

Uplift occurred during Palaeozoic time, which was followed by a long period of erosion. The sediments, which were deposited during this time interval that took place around 375 million years ago, were mostly removed by erosion, except for shales that were deposited in the northern and central part of Ethiopia.

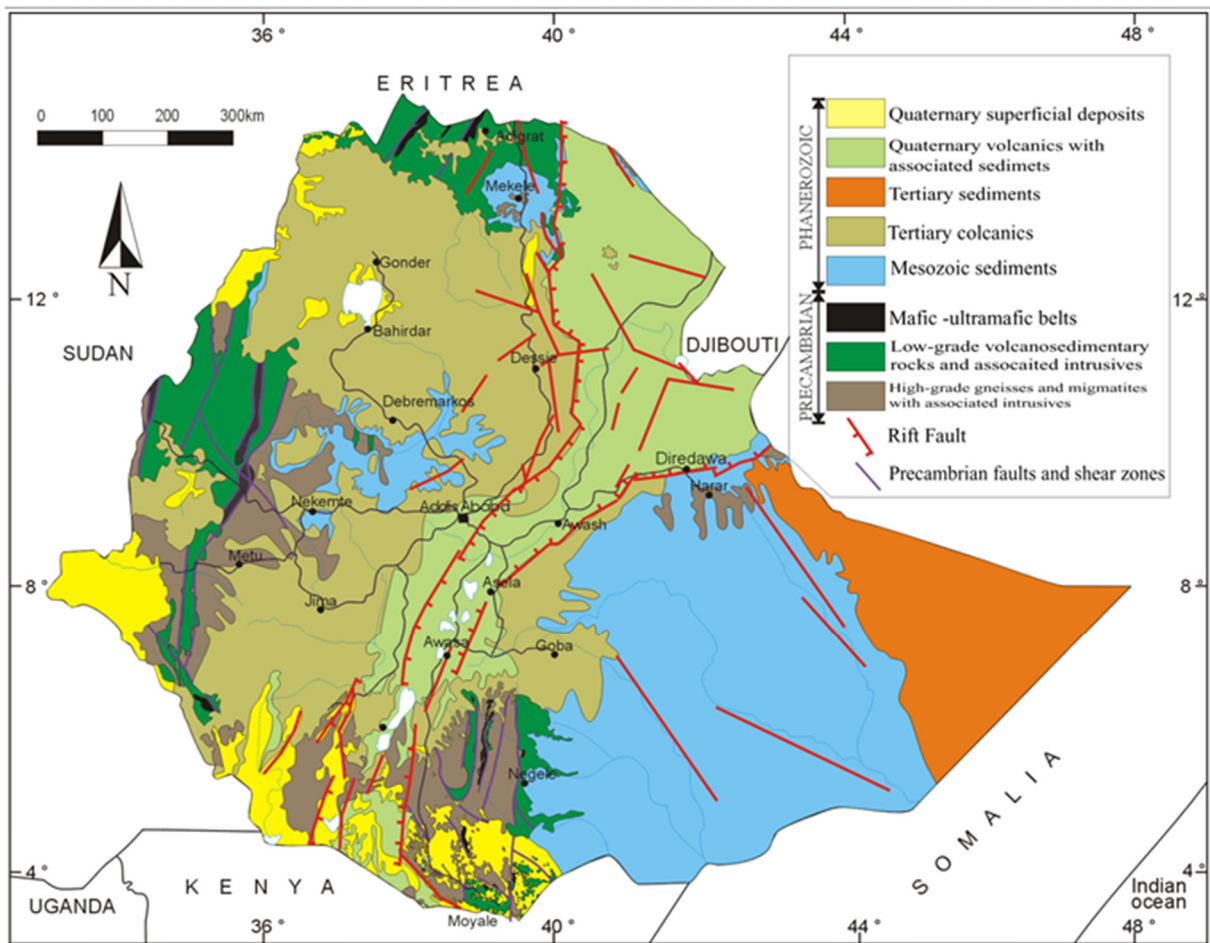


FIGURE 4: Geological map of Ethiopia from (Alemu, 2012)

Subsidence began around 225 million years ago in the Mesozoic period. A shallow sea spread, starting from Ogaden and extending to the northern and western parts of the area. Mudstone and limestone were deposited when the depth of the water increased. At the end of this period, the sea started withdrawing due to the uplift of the landmass, and deposition of clay, silt and sand and occurred on land (Teklemariam, 1996). Mesozoic rocks have the potential for oil and gas formations.

In the Cenozoic period, uplift started with normal faults and related widespread volcanic activity. The earliest and most extensive group of volcanic rocks (Trap Series) erupted from fissures during 54–13 Ma (Tadesse et al., 2003). The Trap Series consists of piles of flood basalts and minor ignimbrites; the basalt has a transitional composition between alkaline and tholeiitic. Many large shield volcanoes developed on the surface of the volcanic plateau after the peak of flood basalt emplacement from 30 to 10 Ma (Ring, 2014). A second episode of flood basalt volcanism has been described in southern Ethiopia at 18 to 11 Ma and in MER to Afar at about 10 to 11 Ma (Bonini et al., 2005).

During the Eocene to late Oligocene, volcanism started by the eruption of flood basalts that have generally been attributed to either one or two mantle plumes affecting the base of the lithosphere under Afar or the Afar to Northern Kenya rifts (Alemu, 2012). Extensive late Miocene-Pliocene rhyolitic ignimbrites (~7-3 Ma) with intercalated minor mafic lavas were emplaced throughout the northern and central MER (Kazmin et al., 1980). Early eruptions of flood basalts in the central MER were followed by alkaline intermediate and acidic rocks at ~17-12 Ma (Kazmin et al., 1980) and by the eruption of basalts and subordinate silicic flows in the late Miocene ~11-8 Ma (Abebe et al., 1998; Kazmin et al., 1980).

Bimodal volcanic rocks with widespread flood basalts and subordinate felsic products such as lavas and pyroclastic strata were closely related with the Wonji Fault Belt that formed in the rift floor during the

Quaternary about <1.6-1.8 Ma ago (WoldeGabriel et al., 1990). The presence of a complete magmatic differentiation series extending from a mildly alkaline basaltic parental magma to comenditic and pantelleritic end members is seen in some segments of the Wonji Fault Belt. This indicates the existence of magma beneath the Wonji Fault Belt (Paola, 1986). According to Zanettin et al. (1978) and Ebinger et al. (1993), in the southern MER, volcanic activity continued in the early Pleistocene with the eruption of ignimbrites and basalts. The Main Ethiopian Rift (MER) is mostly covered by volcanic rocks, except for the lacustrine deposits in the Lakes District, the alluvial, colluvial and erosion products of the volcanic rocks. Quaternary deposits, represented by sand, clay, conglomerate and reef limestone, are commonly found in the Afar depression. Geothermal activity and groundwater resources are associated with the Cenozoic deposits (Ernst & Young and ShinNihon, LLC, 2010).

Tensional tectonic movement and progressive uplift played a significant role in the process of continental breakup. EARs is one of the major tectonic structures globally. It extends from the Red Sea to Malawi. The rift valleys are a system of normal faults bordering a 40-60 km wide trough, funnelling out toward north in the Afar region. Recent volcanism is associated with the development of this rift valley.

2.3 Geology of Aluto Langano geothermal field

2.3.1 Surface geology

Aluto Langano is an active volcanic system with a caldera in the Main Ethiopian Rift System (MER). According to Electroconsult (1986), the caldera collapse occurred between 50 to 80 ka, for the reason that the post/syn caldera rocks are dated at about 55 ka, whereas the oldest rocks are dated at about 150 ka. The outcropping rocks in and around the Aluto-Langano geothermal field are mainly volcanic along with some lacustrine sediments (Figure 5). The volcanic activity started around 150 ka ago with an explosive eruption of ignimbrite (Electroconsult, 2015) and with the build-up of a rhyolite flow dome, which was interrupted by explosive pyroclastic pumice eruptions and a major caldera forming pyroclastic eruption (Ernst & Young and ShinNihon, LLC, 2010). Post-caldera collapse rhyolite flows, domes with minor pyroclastic products, formed along the NE-SE segment of the Aluto caldera rim on a basement of pumiceous ignimbrites and older rhyolite.

The rhyolite flow dome was followed by strong uplift, controlled by E-W faults. After the uplifting phase, volcanic activity continued with the emplacement of several rhyolite domes. Mostly rhyolite post-caldera lavas and pyroclastics erupted from several craters, with all vents showing a clear control by either the caldera ring fracture or the NNE trending faults of the Wonji Fault Belt (WFB). Minor basaltic lavas erupted from the NNE trending faults east of Aluto massif. The Aluto caldera is covered by alluvial sediments. According to Ernst & Young and ShinNihon, LLC (2010), the most recent volcanic products in Aluto Langano is a series of obsidian lava flows, the youngest of which likely erupted around 2000 yrs ago, and commonly concentrated in the eastern and western part of the caldera.

Based on geological maps the rock units from the oldest to the youngest are described below.

Bofa basalt

This basalt sequence is mostly found in the eastern part of the Aluto volcanic complex in deep gorges and the marginal lowlands. It is elongated in the NE-SW direction, following the Ethiopian rift trend. The exposed thickness varies from a few meters to 30m along fault escarpments. The sequence has numerous flows of porphyritic lava and breccia with intercalation of rhyolite and pyroclastics. The basaltic flows are dominantly plagioclase phyric with minor olivine and pyroxene phenocrysts. The rocks frequently show prominent veins and amygdales filled by secondary minerals. The age of the Bofa basalts ranges between 3.5 and 1.5 Ma (Teklemariam, 1985).

Hulo Seyno ignimbrite

Hulo Seyno ignimbrite is found in the southeast and northwest corners of the area, and is assumed to be one of the oldest volcano products of the silicic complex of Aluto (Electroconsult, 1986). It forms a

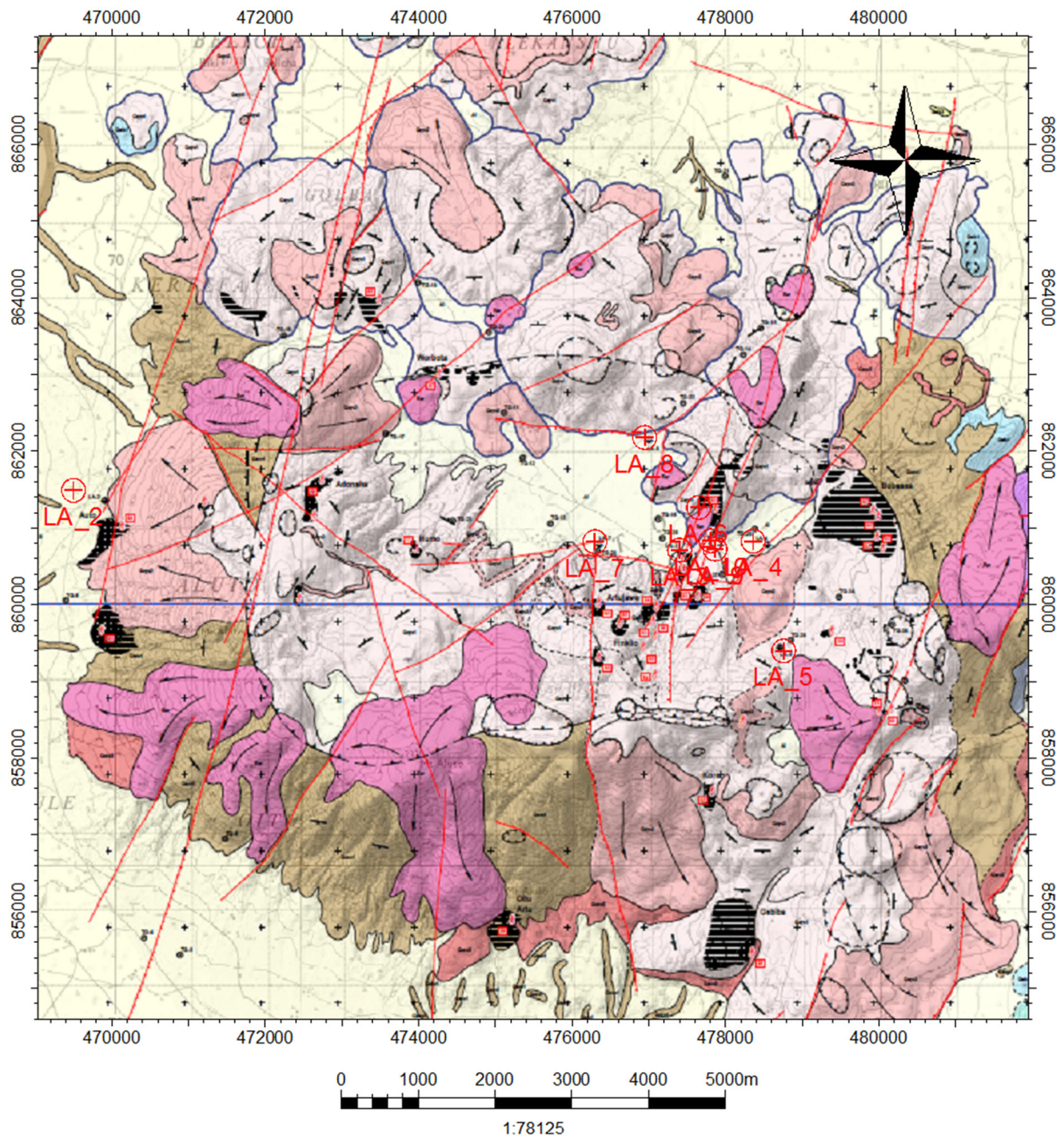


FIGURE 5: Geology of Aluto Langano volcanic complex (modified from Electroconsult, 2015)

sequence of poorly to moderately compacted (welded) lithic, crystal tuff and ash with minor intercalations of lacustrine sediments (Kebede et al., 1984). These pyroclastic flow deposits have filled the old grabens and step faults that cut the Bofa basalt. The Hula Senyo Ignimbrite is dated between 2.54 and 1.7 Ma (Electroconsult, 2015).

Wenshe Danta basalt

This volcanic unit is mainly exposed in the southeast of Ziway Lake (Figures 1 and 2) and at northern bay of Langano, within the NNE-SSW trending structure of the Wonji Fault Belt (WFB) (Kebede et al., 1984). Wenshe Danta basalts formed in fissure eruptions, are mostly vesicular and have aphyric to porphyritic texture. Wenshe Danta basalt is only found in well LA-1 at a depth of 186-217 m.

Aluto older volcanic products

Aluto older volcanic products are found in the north-eastern and southern part of the area and follow a NNE trending fault system. They are silicic in composition and cover the external part of the Aluto volcanic complex (AVC). The products of this unit could be as old as 150 ka (Electroconsult, 2016). Pumiceous pyroclastic deposits and rhyolite lava flows are subunits of the Aluto older volcanic unit. The pumiceous pyroclastics consist of flow deposits with different grain size from very coarse grained pumice with blocks of lava to fine grained ash deposits. Flows are most abundant but many layers of fall deposits can be found. Aluto older rhyolite lava flows consist of glassy rhyolite flows and obsidian lava flows. They are located in the eastern and south-western part of Aluto volcanic centre (AVC). These lava flows are fine-grained flow-banded crystalline rhyolite. Mostly they are found as intercalations with pumiceous pyroclastics deposits (Electroconsult, 2015).

Aluto younger volcanic products

These rock units are found in the south-eastern and north-western parts of the area. Aluto younger volcanic products contain pumiceous pyroclastics, rhyolite and obsidian lava flows. The Pumiceous pyroclastic deposits contain fine to coarse grained pumice, lithic fragments and crystals. Aluto Younger rhyolite lava flows cover the northern part of the area. They are silicic in composition and erupted as viscous lavas through fissures and vents. These rhyolite lava flows are exposed in the faulted hillsides and form domes. Aluto youngest obsidian flow is exposed in the southern, western and eastern rim of the caldera and within the caldera (Kebede et al., 1984). It contains coarsely porphyritic obsidian with phenocrysts of feldspars and quartz. The rocks are black in colour but some greenish black colour is also seen in the obsidian in the south-eastern part of AVC. The youngest flow is dated at 2 ka (Electroconsult, 1986).

Lacustrine deposit

The Lacustrine sediment formation covers a very wide portion of the Aluto-Langano area. This unit covers a large area of the AVC, particularly along gorges and streams. The existence of lacustrine deposits at an elevation of 1850 m shows that the lake level was higher in the past (Lloyd, 1977). The lacustrine deposits vary from sandy gravel to fine silt and are rich in diatomite with intercalations of pumice and ash deposits.

2.3.2 Structure of the Aluto-Langano area

The Aluto volcanic complex is affected by Wonji Fault Belt (WFB), which is trending NNE-SSW. In Aluto-Langano geothermal field, there are several faults, number of a complex sets of intersecting structural lineation, discontinuities and open fissures located and trending in NNE-SSW, NW-SE, N-S, NE-SW and E-W direction (Figure 6). The eastern part of Aluto Langano is intersected by NE trending structural alignments, and the western part has NNE trending fracture lines.

Most of the recent volcanoes and craters are aligned along the NNE-SSW trend of the Wonji fault belt, and to some extent, in E-W direction (Teclu, 2004). The fault that strikes in NNE-SSW direction, dipping towards the west, is located west of wells LA-3 and LA-6, and has similar orientation as the Wonji fault belt. Similarly, a fault that is located between wells LA-4 and LA-5 has NNE-SSW strike, dips towards west, and caused a total loss of circulation during drilling. The discontinuity is also associated with circulation loss zones trending NNE-SSW direction, dipping towards the west at wells LA-3, LA-6 and LA-8; and in the southern part of LA-7 discontinuity structure located with a direction of NW-SE direction dipping towards NE (Ernst & Young and ShinNihon, LLC, 2010) (Figure 6).

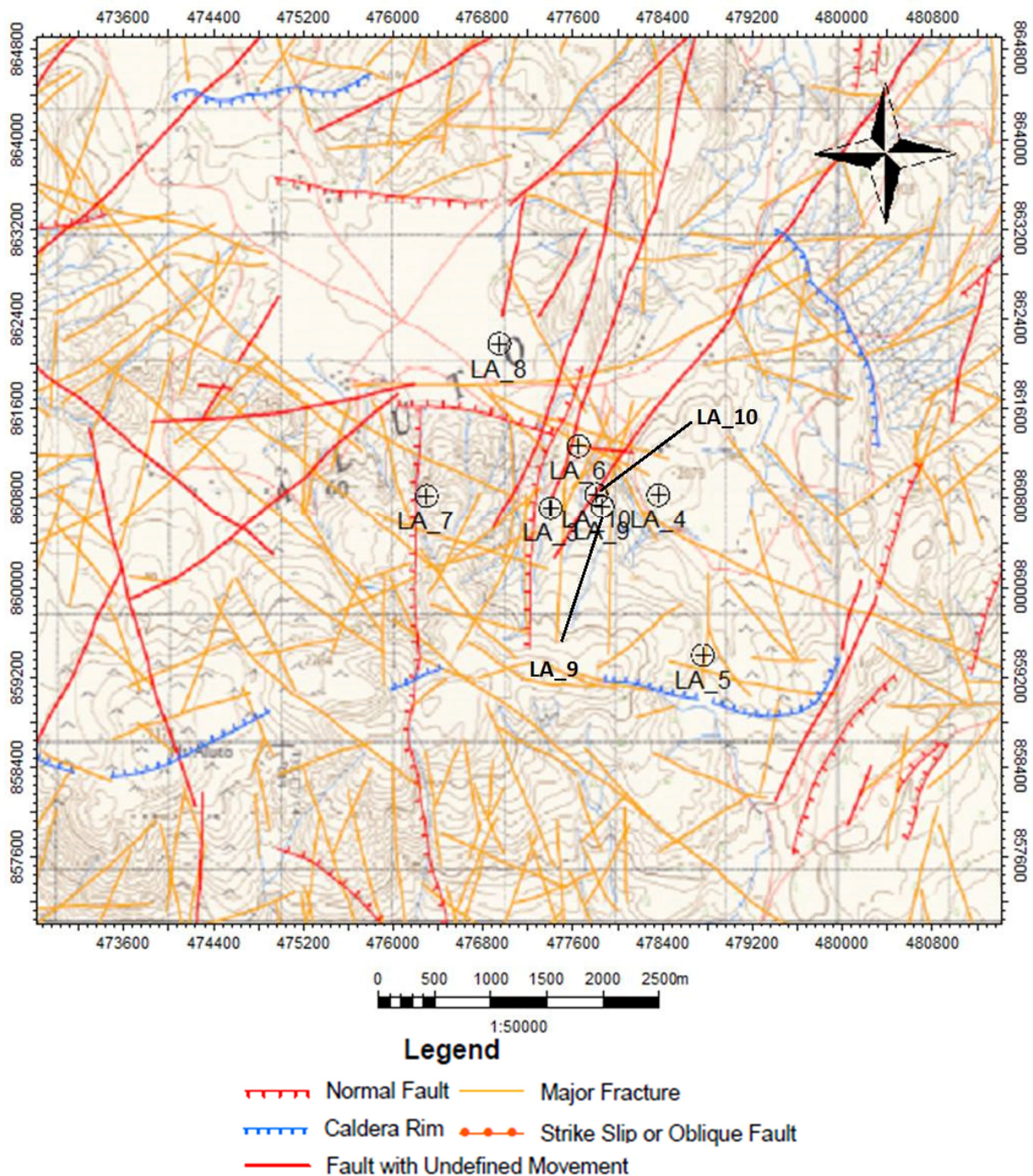


FIGURE 6: Structural map of Aluto Langano Volcanic Complex (AVC) (modified from Electroconsult, 2015)

2.3.3 Geothermal surface manifestation

Hydrothermal manifestations on the AVC include hot springs, fumaroles, and hot and warm ground. According to Electroconsult (2015), all the fumaroles are located over 1700 m a.s.l. and the hot springs are sited below 1700 m a.s.l. Some of the boiling thermal springs are located south of the volcanic complex near the shore of Lake Langano and on an island in Oitu bay in Lake Langano, trending NW-SE (Figure 7). There are also abundant small low-pressure fumaroles clustered mostly in the eastern and southern parts of the volcanic complex and a few of them scattered in the western part of the complex (Kebede et al., 1984) following the trend of E-W and N-S alignments. Some areas are covered by hot/warm grounds together with fumaroles.

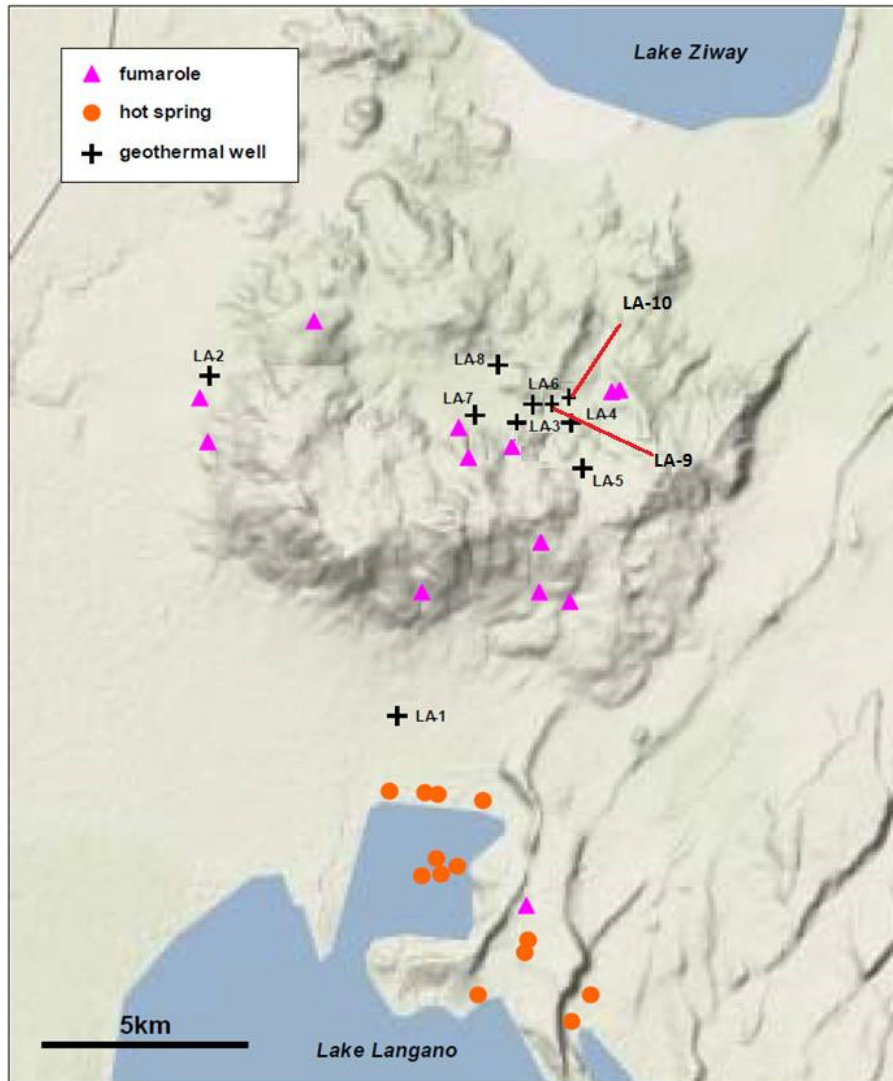


FIGURE 7: Distribution of surface manifestations in Aluto Långano geothermal field

2.3.4 Subsurface geology of Aluto Långano area

Eight deep exploratory wells (LA-1 to LA-8) (Figures 6 and 8) have been drilled in the Aluto-Långano geothermal field with a maximum depth of 2500 m and with a maximum measured temperature of 335°C (Table 1).

TABLE 1: Summary of previous wells of Aluto Långano from (LA-1 to LA-8)

Wells	Total depth (m)	Temperature (°C)	Permeable zone (m)	Aquifer (m)	Enthalpy (kJ/kg)	Year of drilling
LA-1	1317	88	-	-	-	7/11/81-11/6/82
LA-2	1602	110	-	-	-	6/7/82-15/10/82
LA-3	2144	320	2000	2117	1610	21/1/83-13/6/83
LA-4	2062	235	1445	1445	1000	6/7/83-23/10/83
LA-5	1867	208	-	-	-	15/11/83-11/3/84
LA-6	2203	335	2000	2000-2200	1650	24/3/84-2/7/84
LA-7	2449	226	2100	2100	850	12/7/84-21/10/84
LA-8	2500	270	2300	1900-2100	1150	26/10/84-13/5/84

The stratigraphic sequence based on information from geothermal wells that have been drilled in Aluto Långano from older to younger formations is outlined below.

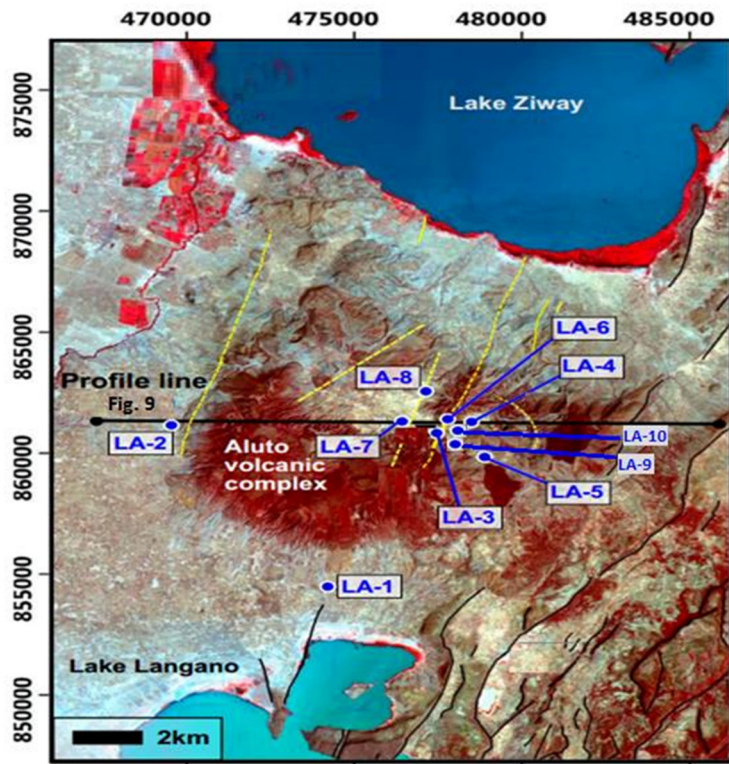


FIGURE 8: Aluto Langanu and the surrounding area. ASTER RGB 321 imagery. Geothermal wells are labelled in blue and faults are indicated with broken yellow lines (revised figure from Hutchison et al., 2015)

According to Kebede et al. (2002), the oldest rock unit in Aluto Langanu is Tertiary ignimbrite formation that is exposed in the eastern rift escarpment. It has a thickness of up to 700 m in all wells, except well LA-2, and an age of about 2.3 Ma. It consists of hard, crystalline ignimbrite with minor intercalations of rhyolite lava, ash and basalt lava layers. The ignimbrites are mostly brecciated and fractured (Teklemariam, 1985). The Tertiary ignimbrites are overlapped by alkali to transitional basalts (Bofa basalts).

The deep geothermal wells show that Bofa basalt overlies a crystal-rich ignimbrite. Bofa basalt formed in fissure eruptions during late Palaeocene to late Pleistocene and was later affected by the rift faulting. It is found in all deep wells and is used as a marker bed from 340 to 1000 m. The texture varies from aphyric to porphyritic and the thickness also varies from well to well. It was encountered in wells LA-3 and LA-6 at a depth of about

1,700 m below ground level and elevation of 300 m a.s.l. (Electroconsult, 1986).

Lacustrine sediment is observed in well LA-2, LA-7, LA-8, LA-3 and LA-6 (Figure 9). It covers a very wide portion of the Aluto Langanu area. It is thinner towards east, being absent in wells LA-4 and LA-5, and thicker in the western part with a maximum thickness of 400 m in well LA-2 (Teklemariam et al., 1996). The age of the lacustrine sediments is estimated at about 0.1 Ma. At this time, a large lake occupied all of the central part of the Main Ethiopian Rift (Laury and Albritton, 1975).

Aluto volcanic products are encountered in all wells. They are silicic in composition, and consist of a complex sequence of alternating pyroclastics, such as pumice falls, surge, pumice flows, tuff breccia

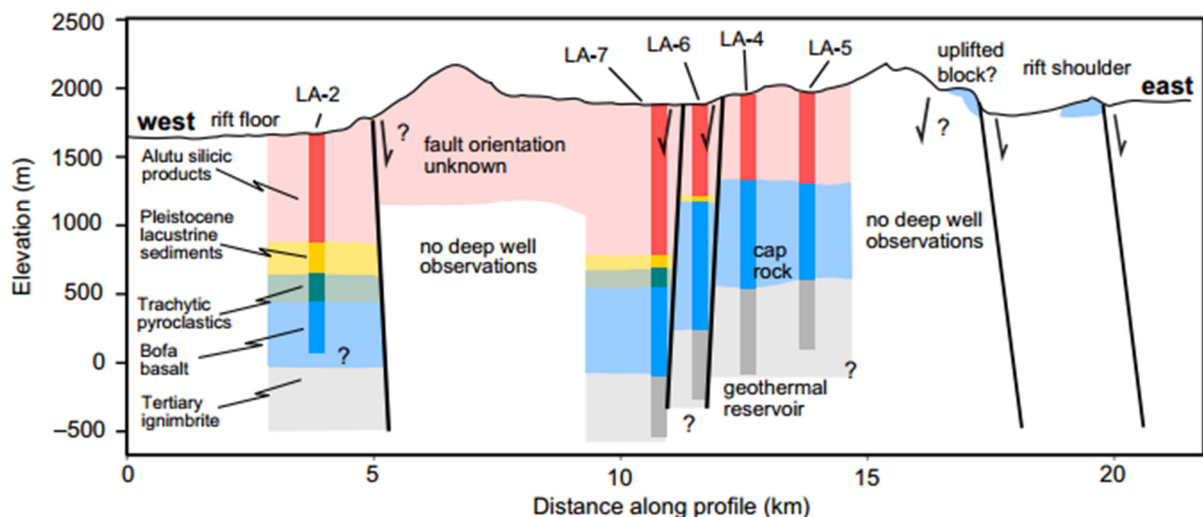


FIGURE 9: Deep well cross-section west to east from (Hutchison et al., 2015)

with very viscous lava flows and domes (Electroconsult, 1986). The formation is found in the upper part of all deep wells.

A W-E stratigraphic cross-section of the Aluto Langanu area shows subsurface lithology and structures found in the drill holes (Figures 8 and 9). The lithological sequences encountered in all the wells are very similar, but there are thickness variations of individual units between the wells. Tertiary ignimbrites have been located in all the wells, except in LA-2, but the ignimbrites occur at shallower depth towards the east (Figure 9). Bofa basalt is found in all wells with different thicknesses (for example LA-3 1000 m, LA-6 903 m and LA-4 700 m). The Lacustrine Sediments formation shows a thinning pattern from west (LA-2) to east (shown by its nonappearance in wells LA-4 and LA-5). Therefore, the deposition is controlled by faults that precede volcanic activity at Aluto (Hutchison et al., 2015). Aluto Volcanic Products have been located in all wells. As a result of the rift faults, the formation has become thicker towards the west.

As a result of the higher relief of the western rim of the caldera, younger lava flows and hydrothermal manifestations may be in less abundance as compared to the eastern rim. However, the western sector of AVC is expected to have a greater geothermal potential due to large hydraulic recharge and thicker lacustrine sediments that may act as a cap rock for the geothermal system (Electroconsult, 2015).

In all the geothermal wells of the Aluto Langanu field, most of the hydrothermal minerals are observed at a depth of 1320 m to 2500 m. As a result of water-rock interaction, secondary minerals indicate different hydrothermal mineral groups and alteration zones. According to Teklemariam et al. (1996), two types of alteration groups are identified in Aluto Langanu geothermal field. The first group is identified as prophylic and consists of hydrothermal minerals that are found in the deepest and highest temperature zone. Some of the minerals are garnet, epidote, chlorite and quartz. The second group is called argillic, formed at low-temperature conditions, some may occur at atmospheric conditions and mostly contain calcite and clay minerals.

2.3.5 Hydrogeological setting

The Aluto Langanu geothermal field is related to a hydrothermal system controlled by the recent Wonji Fault Belt that acts as an upflow area for the geothermal reservoir (Endeshaw, 1988). The area is characterized by two rainy seasons in summer (July–September) and spring (March–April). The climate in the rift is semi-arid with a mean annual temperature of 18°C, with an average maximum and minimum of 25 and 12°C, respectively, and a total mean annual rainfall of 725 mm (Reimann et al., 2003).

The geological structures and volcanic series associated with the extensional tectonics are important for groundwater occurrence in the region due to their high permeability. Groundwater infiltrating either through primary porosity or, more commonly, through secondary permeability (mainly related to faults, fractures and caldera collapse) will flow like the surface water to the west. Rainfall from the eastern highlands of Chilalo and Kubsa feeds the river Kefar and its catchment area (Figure 10), which helps to recharge groundwater and geothermal fluids. The Kefar River basin and the Munesa highlands are

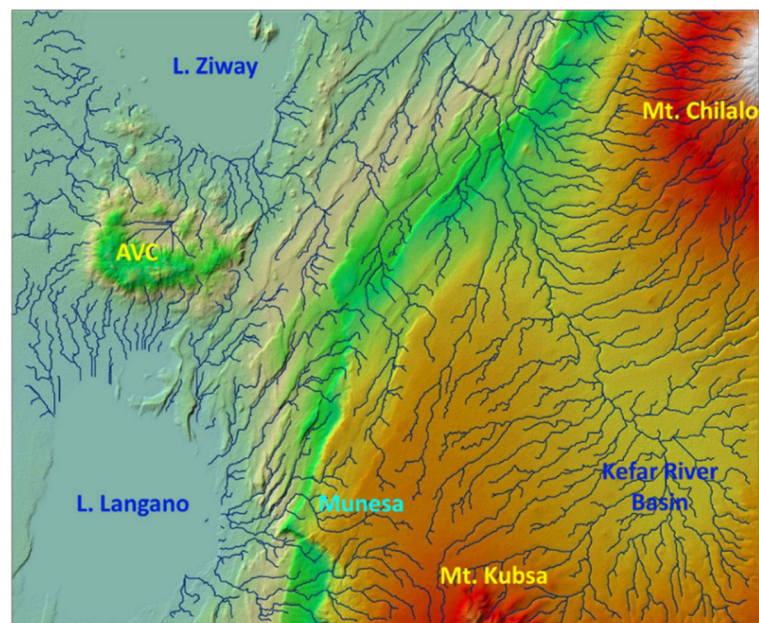


FIGURE 10: Regional hydrological map of the Aluto Langanu area from (Electroconsult, 2015)

the major recharge zones for the geothermal reservoir (Electroconsult, 2015). The scoriaceous basalts, trachytes and the uncompacted, crystalline and vesicular ignimbrite could hold water as a reservoir for the geothermal system. Ignimbrites and fractured, interlayered basalts are the major aquifers in this zone (Kebede et al., 2008). In the wells of Aluto Langano, the deepest aquifers are found in ignimbrites and basalt units.

2.3.6 Geophysical exploration of Aluto Langano area

The first geophysical surveys were performed in the Aluto-Langano area in the middle of the 1970's. Different techniques were employed during the year of exploration, including Schlumberger Electrical Sounding, gravity and magnetotelluric (MT) surveys. These surveys were conducted to outline the regional and subsurface structure in and around the Aluto Langano geothermal field.

The regional Bouguer anomaly map covers a large area of the Main Ethiopian Rift System (MERS) and outlines deep structures. Two relatively high-anomaly zones are seen in the regional Bouguer anomaly map. These are located in the northeastern and central parts of the area. There is also a low-anomaly zone located between high-Bouguer anomaly zones. There are gravity lineaments (Figure 11) located between the two high- and low-Bouguer anomaly zones trending in NE-SW direction (G1 and G2) and at the southeast corner of a high-anomaly zone (G3) (Figure 11). These zones may be interpreted as lineaments or faults that could control the underground movement of geothermal fluids (Ernst & Young and ShinNihon, LLC, 2010).

Recent MT surveys done by Ernst & Young and ShinNihon, LLC (2010) cover the caldera and the surrounding area, with a total of 40 stations in each survey (Figure 12). To detect fault systems, measuring stations were placed in a grid configuration from 600 to 800 m. To get resistivity information on an expected drilling target at 1000-2500 m depth, more than 50 frequencies, ranging from 320 to 0.001 Hz, were used for MT data acquisition. Apparent resistivity at low frequencies reflects resistivity structure in a deep zone, whereas high frequencies reflect the resistivity structure in a shallow zone. Low apparent resistivity zone is mostly seen in the northern part of the area (Figure 13). This low apparent resistivity zone is related to a hydrothermal alteration zone found at relatively shallow depth and characterized by smectite (Ernst & Young and ShinNihon, LLC, 2010).

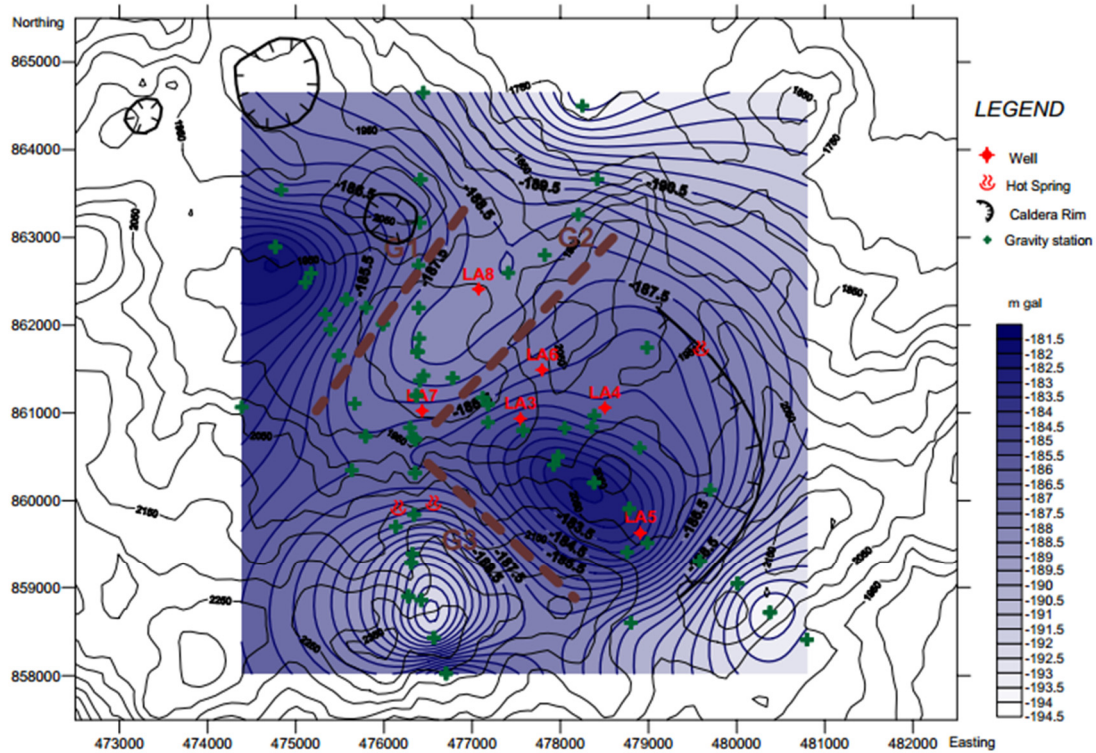


FIGURE 11: Regional Bouguer anomaly map red broken line shows G1, G2 and G3 fault lines (Ernst & Young and ShinNihon, LLC, 2010)

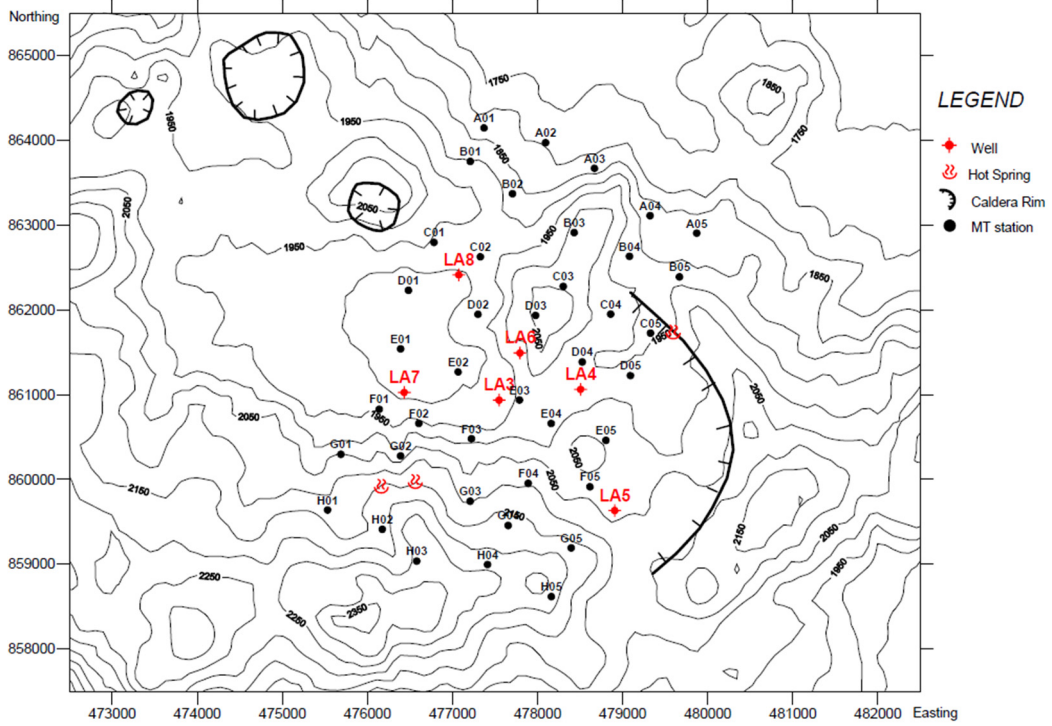


FIGURE 12: Station map of MT survey

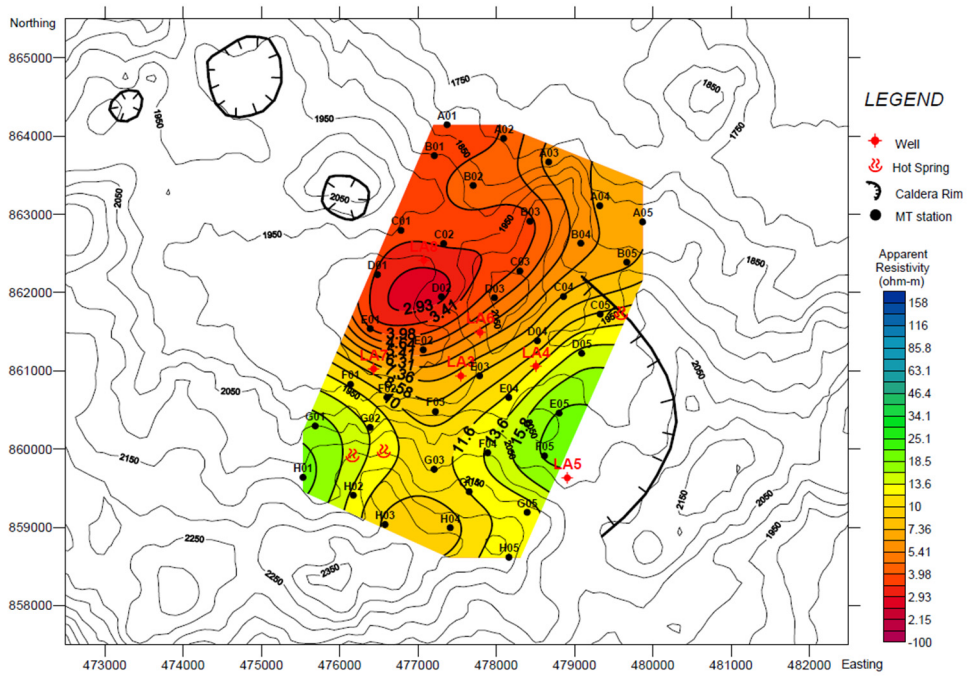


FIGURE 13: Apparent resistivity map with a frequency of 1 Hz at (-1000 m a.s.l.) (Ernst & Young and ShinNihon, LLC, 2010)

3. METHODOLOGY

3.1 Sampling

In this study, drill cuttings were analysed from well LA-9D and well LA-10D from Aluto Langanu geothermal field (Table 2). The wells were drilled in the years of 2013 to 2015. The samples were collected every 5-meter interval during drilling at the rig site. However, in this study, samples have been used to analyse every 10-meter interval. In addition, at some depth intervals, samples were not retrieved due to circulation losses in the wells. Before analysing the samples, they were washed to remove dust and drilling material.

TABLE 2: Well LA-9D and LA-10D of Aluto Langanu geothermal field

Wells	Total depth (m)	Easting (E)	Northing (N)	Elevation (m)
LA-9D	1920	477863	860736	1956
LA-10D	1940	477807	860846	1956

3.2 Analytical methods

For borehole and hydrothermal alteration mineral studies, different analytical methods were used. The methods included binocular microscope analysis, petrography microscope analysis, X-ray diffractometer analysis, fluid inclusion analysis and Inductively Coupled Plasma-Optical Emission Spectroscopy (ICP-OES).

3.2.1 Binocular microscope analysis

The binocular microscope is one of the primary rock cuttings analysing techniques used to identify rock lithology, hydrothermal alteration minerals, primary minerals, rock texture and grain size, intensity of rock alteration and oxidation, rock porosity, fractures and vein fillings. Dilute hydrochloric acid (HCl) was used to identify the presence of calcite; caution was taken in areas where foreign material from cement plugging or cementing of casing was suspected. Rock samples (cuttings) from 10-meter interval were inspected with a Wild Heerbrugg binocular microscope at the Icelandic GeoSurvey (ÍSOR) laboratory. Cuttings samples are very important, as they provide information about subsurface formations, lithological boundaries and permeable zones. However, sometimes it becomes challenging to recognize the rock type when the grain size of the lithology is larger than the cuttings chips. Also, it is difficult to distinguish the rock texture and structure of the rock if the veins and vesicles are damaged.

Detailed description of this analysis is presented in Appendices I and II and the summary plotted in Petrel software and LogPlot software (Rock Ware Inc.).

3.2.2 Petrography microscope analysis

Petrography microscope analysis was very helpful to identify/confirm rock types, texture, porosity, vein fillings, evolutionary sequences of secondary minerals, alteration of primary and secondary minerals and to identify additional minerals not seen in the binocular microscope.

In this study, 24 thin sections from the study wells were inspected at the ÍSOR petrography laboratory with the use of a Leitz Wetzlar petrographic microscope and the thin sections were made at the Institute of Earth Sciences, University of Iceland. In petrography microscope analysis, minerals are identified according to their properties in plane-polarized and cross-polarized light. It includes birefringence, cleavage, colour, pleochroism, twinning and the interference properties. The description of this analysis is described in Appendices I and II. The summary is presented with the help of Petrel and LogPlot software (Rock Ware Inc.).

3.2.3 X-ray diffractometer analysis

XRD analysis is used to examine crystallized materials based upon the scattering of X-rays, which depends on the crystal structure of the material (Koestono, 2010). The X-ray diffractometer analyses (Appendix IV) were carried out to identify different clay minerals, such as smectite, mixed layer clay, illite and chlorite, with depth and infer the temperature regime in the system. XRD analysis also helps to determine alteration zones together with other index minerals found in binocular and petrographic analysis. In this study, 36 samples were chosen according to the rock type with depth and degree of alteration.

A tea spoon of dried samples was placed in crucibles with enough amount of water, then the crucibles were put in a shaker machine for about four hours to separate the clays from the rock matrix. After this process, the clays were placed in a glass slide to dry for about 12 hours, which were then put in the XRD instrument for 15 minutes. Subsequently, the slides with clay on were stored in a container with glycol solution for 24 hours, and then run with the XRD instrument. The final step was to heat the samples at 550°C for an hour, and then run in the XRD instrument. The analyses were done at the ÍSOR XRD laboratory.

3.2.4 Inductively Coupled Plasma-Optical Emission Spectroscopy (ICP-OES)

ICP-OES is one of the most used analytical tools for the determination of trace elements. The technique is based upon the spontaneous emission of photons from atoms and ions. ICP is a high-temperature excitation source that can efficiently excite and ionize atoms. The ICP source consists of a quartz torch inside a radio frequency (RF) coil. Argon is passed through the torch and RF energy is applied to the coil. When a spark is added to the highly energized argon atoms, electrons are stripped from the argon, and plasma is formed. The argon ions and free electrons are further disturbed by the RF field, causing the temperatures within the plasma to reach approximately 8000-10,000 K (Hou and Jones, 2000).

During analysis, the sample solution is converted to an aerosol and directed into the central channel of the plasma. At its core, the inductively coupled plasma (ICP) sustains a temperature of approximately 10 000 K, so the aerosol is quickly vaporized (Hou and Jones, 2000). In this study, 19 samples were selected based on rock type and depth by using the binocular microscope. The purpose of using this analytical method was to distinguish the rock units of wells LA-9D and LA-10D. The analyses were done at the university of Iceland laboratory. The detailed procedure for sample preparation and analysis is presented in Appendix III.

4. RESULTS

4.1 Drilling activity

Drilling of wells LA-9D and LA-10D started on November 12, 2013 and June 25, 2015, respectively, and was completed on April 30, 2015 and October 2, 2015, respectively. The directional drilling kick-off point (KOP) in LA-9D is at 700 m to a direction of N 70° W with 51° maximum inclinations, whereas the KOP in LA-10D is at 450 m to a direction of N43W with a maximum inclination of 27.75°.

In LA-9D (Table 3), the first section of the well was drilled with a 26" bit to a depth of 60m and 20" casing was put down to 56.7 m. Seven times cement plugging was conducted to stop circulation losses. The second section was drilled with a 17 1/2" bit and borehole assembly down to 210 m. 13 3/8" casing was put at 207.9 m. The third section was drilled with 12 1/4" bit to 608 m, and the 9 5/8" casing reaches 605 m. During this part of the drilling, cement plugging was conducted 34 times because of circulation losses. The production section of the well was drilled vertically with an 8 1/2" bit to the KOP at 700 m. Then directional drilling started with the use of a mud-motor and an 8 1/2" bit down to 1,588 m. A 7" slotted liner was run in the hole to a total depth of 1,915 m. The 7" x 9 5/8" liner hanger was set at 571.3 m.

TABLE 3: Well configuration of LA-9D

Drilling		Casing	
Hole diameter (")	Interval (m)	Casing diameter (")	Interval (m)
26	0 – 60	20 Surface	0 – 56.7
17 ½	60 – 210	13 ¾ Anker	0 – 207.9
12 ¼	210 – 608	9 ⅝ Production	0 – 605.0
8 ½	608 – 1,920	7 Blind liner	571.3 – 599.2
		7 Slotted liner	599.2 – 1,915.0

LA-10D (Table 4) is the second directional well in Aluto Langanu geothermal field. The first section of the well was drilled with a 26" bit to 60 m depth using drilling mud fluid. Circulation loss was encountered below 14.5 m, where the shoe of the 30" conductor casing was located. The 20" surface casing was set at 57.11 m depth. The cementing operation was not successful with no return at the annulus. The second section of the well was drilled with a 17½" bit. At 108 m depth, total circulation loss was encountered. The loss zone was sealed off with a cement plug, and drilling continued with 17½" drillbit down to 186 m with full mud return. From 186 m depth and down to 347 m depth drilling of the second section was completed water. A 13¾"stab-in casing was set at 343 m depth. Cementing of the casing was not successful with no return of cement slurry from the annulus.

The third section was drilled with a 12¼" drillbit. The section was directionally drilled and at 667 m depth the wellbore had reached an angle of 9° in the direction N44°W. Directional drilling continued to 809 m depth. The 9⅝" production casing was placed at 807 m. The top cement job was successful with no return of cement slurry from the annulus.

The final section was drilled with an 8½" drillbit from 809 m depth. At 937 m depth the string was pulled out of hole in order to remove the slick bottom hole assembly and run in hole with a correction assembly consisting of mud motor, bent sub and a nonmagnetic drill collar thereafter proceeded to correct the inclination from 822 m to 937 m. After correction drilling commenced conventional drilling to 1951 m and subsequently the 7" slotted liner was landed at this depth.

TABLE 4: Well configuration of LA-10D

Depth (m)	Bit size (")	Casing type (")	Casing depth (m)
60	26	20	57.11
347	17 ½	13 ¾	345
809	12 ¼	9 ⅝	807
1951	8 ½	7	1951

4.2 Lithology

Different lithologies are identified according to the analysis from binocular, petrography and ICP-OES methods. Rock units that were identified by binocular and petrographic analysis are pyroclastic, rhyolite, trachyte, basalt and ignimbrite, whereas thin layers of andesite, trachyandesite, basaltic andesite, basaltic trachyandesite, dacite and trachydacite rock units are identified by their chemical composition from ICP-OES whole rock analysis (Figures 14 and 15). All rock types are found in the LA-10D well. On the other hand, in well LA-9D andesite, basaltic andesite and ignimbrite rock units are not identified. A description of the rock units follows.

4.2.1 Main rock units identified by binocular, petrography and ICP-OES method

Pyroclastic

Pyroclastic deposits are mostly found in the uppermost part of both well LA-9D and LA-10D and are typically observed as intercalations within rhyolite lavas. They are light to dark grey in colour with fine to medium grained rock units. Slightly altered rock samples and hint of oxidation are noted. They contain crystalline rhyolite, showing flow bands with spherulitic texture, slightly vesicular pumice breccia and dark grey to black obsidian. Sanidine, magnetite, quartz and pyroxene (aegirine) are observed as small crystals in the groundmass together with partially altered amphibole and sanidine phenocrysts. Glass fragments are common, some are fresh and others have been replaced by calcite and clays. The pyroclastic deposits are vesicular and fractured, but vesicles and veins are filled with quartz, calcite and clay minerals. Fragments of obsidian, vitric tuff, rhyolite and basalt are noted. Pyroclastic deposits are found in LA-9D at a depth of 10-130, 320-340, 400-410 and 840-880 m and in LA-10D pyroclastic deposits are noted at a depth of 10-70, 100-120, 810-820 m as well as at 1140-1210 m depth.

Sediments

Dark grey to brownish, fine grained rock units. No crystals were seen. Black fine grained silt fragments dominate. Also fragments of fractured basalt, altered pumice, rhyolite and tuff noted. They are vesicular and fractured, the vesicles and veins being filled with quartz, calcite and clays. High alteration is noted in these rock units. Sediments are found at a depth of 590-650 m in LA-9D and 580-620 m in LA-10D.

Silicic tuff and breccia

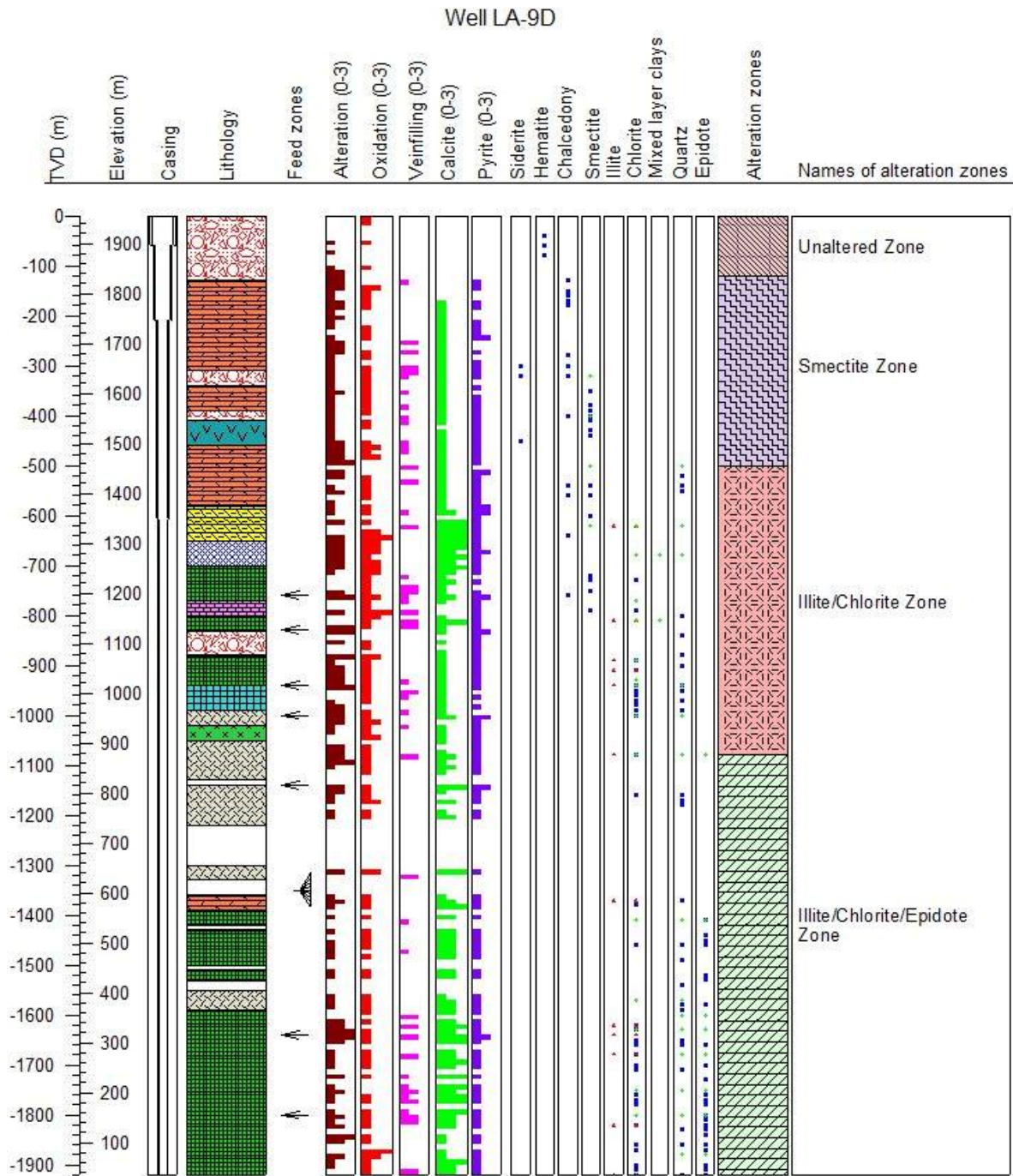
Light grey, fine grained, vesicular rock type. Some veins and vesicles are filled with siliceous material. Fragments of rhyolite with plagioclase phenocrysts and fragment of fractured and silicified obsidian units are noted. Medium to high alteration and slight oxidation was observed. Alteration minerals: few pyrite, smectite, chalcedony, quartz and clays. It is found at a depth of 590-650 m at LA-9D and 450-490 m in LA-10D wells.

Rhyolite

A sequence of rhyolitic lavas is distributed at different depth intervals in well LA-9D and LA-10D. In LA-9D, they are observed at a depth of 140-310, 350-390, 470-580, and 1150-1210 m depth, and in LA-10D at 80-90, 130-150, 340-440, 520-570, 850-900, 1070-1100 and 1400-1540 m depth. The rhyolites are light grey to brownish and light pinkish, the colour varies due to alteration intensity. Alteration of the rocks is slight at their top parts and showing a bit increase towards the bottom parts. They are fine to medium grained, banded and exhibit some trachytic texture with aligned sanidine and magnetite phenocrysts. Phenocrysts of plagioclase, quartz and sanidine are noted within a groundmass composed of glass and crystallites of aegirine, alkali feldspar, magnetite and riebeckite. Some veins and vesicles are observed and most of them are filled with quartz, calcite and clay minerals. Fragments of obsidian (both fresh and silicified), tuff and basalt are found within these rock units.

Trachyte

A sequence of trachytic lavas is found in LA-9D at depth of 1000-1020, 1060-1120, 1310-1325 and 1560-1590 m, representing different thicknesses. Circulation losses were encountered in these units. In well LA-10D, trachyte lavas occurred at a depth of 630-640, 740-770, 1000-1010, 1040-1060 and 1220-1390 m. They are light grey to brownish, have trachytic texture, fine to medium grained with sanidine phenocrysts. The groundmass is dominated by alkali feldspar, sanidine and magnetite. However, the



Legend

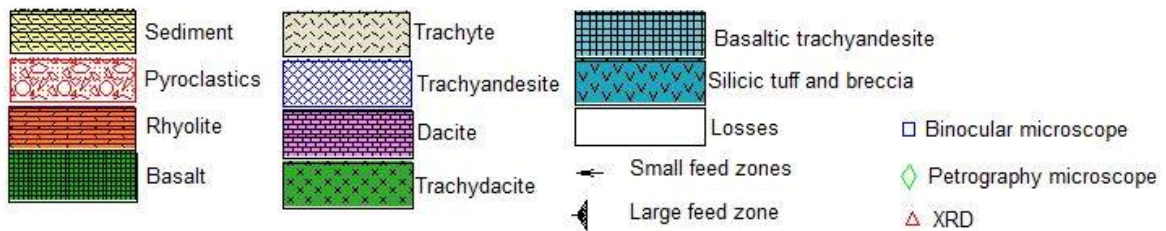


FIGURE 14: Lithology, alteration minerals and alteration zones of well LA-9D

feldspar and glass are getting altered and changing into albite and chlorite, respectively. Vesicles, fractures and veins are noted at 1000-1020 m depth in both wells and filled with quartz, chlorite and calcite hydrothermal minerals. Welded tuff, obsidian, banded rhyolite and basalt are some of the fragments that are found associated with trachyte.

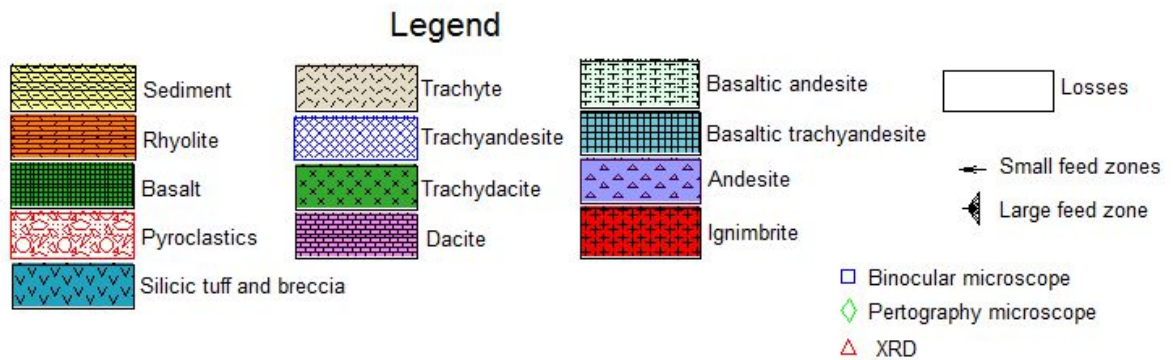
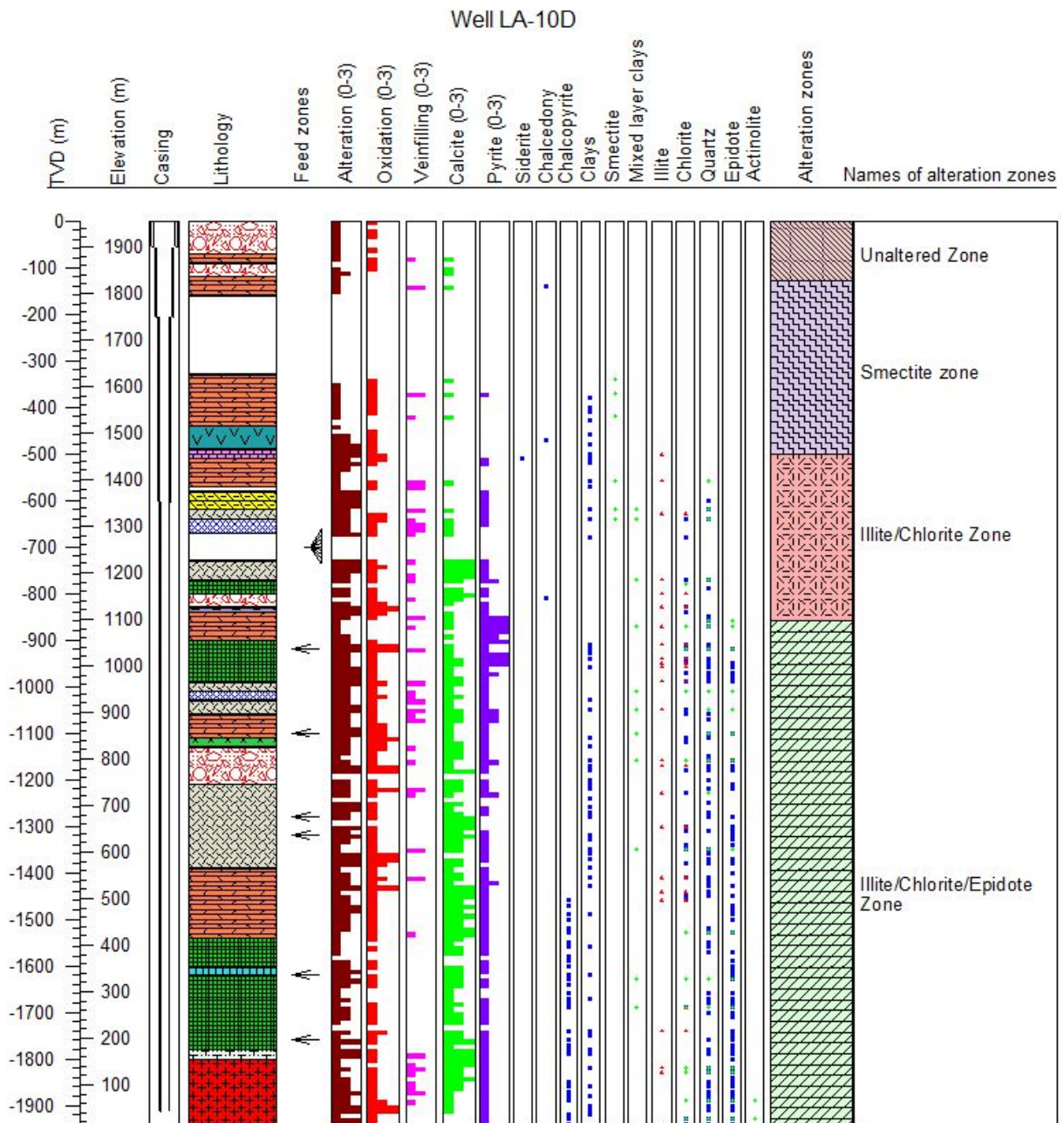


FIGURE 15: Lithology, alteration minerals and alteration zones of well LA-10D

Basalt

Basalt is found in both the LA-9D and LA-10D wells. The colour ranges between dark grey, shiny black and light grey to greenish. Fine to coarse grained. Plagioclase and sanidine are found as phenocrysts, pyroxene as microphenocrysts and alkali feldspar and magnetite as groundmass minerals. Highly altered plagioclase and pyroxene are replaced by epidote and chlorite, respectively. Also, the amount of epidote increased at 1630 m in LA-10D well. A few veins and vesicles are filled with calcite and quartz. Abundant vesicles are seen in LA-10D at 910-990 m. This rock type is found in different thicknesses and at several depths. Mixed in are fragments of welded tuff, trachyte and rhyolite. In well LA-9D, basalt is observed at 710-770, 810-830, 890-940, 1400-1410, 1440-1490, 1520-1530 and 1600-1920 m and in LA-10D, at 780-800, 940-950, 960-990, 1550-1600 and 1630-1780 m depth.

Ignimbrite

A single ignimbrite rock unit occurred in the bottom part of well LA-10D at a depth of 1810-1940 m. It is light green to greyish in colour, fine to medium grained, with fiamme/brecciated texture. It has phenocrysts of plagioclase and quartz. Alkali feldspar, pyroxene and magnetite dominate in the groundmass. Ignimbrite is found with rhyolite, trachyte, tuff and glassy and altered basalt fragments. Actinolite appears at 1890 m for the first time as a replacement of pyroxene. It is identified by under petrographic microscope by its high interference colours and relief. The amount of quartz increases at the bottom of the well.

4.2.2 Rock units identified by ICP-OES analysis

Trachyandesite

This rock type was identified by its chemical composition with the use of the ICP-OES method (Figure 10 and Tables 5 and 6). It is light grey to brownish, fine to medium grained rock. Trachyandesite has trachytic texture, and is vesicular and fractured. Very few veins and vesicles occur and are filled with calcite, quartz and chlorite. Plagioclase and pyroxene (aegirine) are observed as phenocrysts and microphenocrysts, respectively, and the groundmass is dominated by alkali feldspars. Fragments of fractured tuff and basalts are noted. This rock unit has a thickness of approximate 10-40 m in both wells at different depths. In well LA-9D, a trachyandesite rock unit is found at a depth of 660-700 m, and also in LA-10D located at 650-670 m and 1020-1030 m.

Basaltic trachyandesite

This rock type is light grey to greenish, fine to medium grained. Plagioclase is found as phenocrysts together with alkali feldspar and sanidine in the groundmass. Vesicles are noted and filled with calcite and quartz. Alteration of plagioclase occurs as replacement by epidote. Moderate to high alteration and slight oxidation are noted. This rock type is identified by its chemical composition and found as thin layers and is mixed with fragments of basalt and tuff. It is found in both wells, in LA-9D at a depth of 550-990 m and in LA-10D at 1610-1620 m.

Trachydacite

The trachydacite unit was identified by its chemical composition. The colour ranges from dark grey to brownish and whitish to light greenish. It is fine grained with phenocrysts of plagioclase. It is found as a thin layer with a thickness of 20 m. Trachydacite contains a few fragments of tuff, rhyolite and basalt. Slight oxidation and moderate alteration are noted. In LA-9D, it is located at a depth of 1030-1050 m, while it occurs slightly deeper in LA-10D at 1110-1130 m.

Dacite

Dacite is light grey to brownish, porphyritic rock type, identified by its chemical composition. Quartz is found as phenocrysts. The rock unit observed together with highly altered flow banded silicified rhyolite, altered basalt and minor amount of tuff. It is seen in both wells, at a depth of 780-800 m in LA-9D and 470-510 m in LA-10D. The rocks show high alteration and moderate oxidation.

Andesite

Andesite is found only in well LA-10D at a depth of 830-840 m. It is brownish, coarse grained rock unit with plagioclase phenocrysts. As previous rock types, it is identified by its chemical composition.

Andesite is found together with fragments of black shiny aphyric basalt and white tuff. It is moderately to highly altered. Augite, hornblende and alkali feldspar occur in the groundmass.

Basaltic andesite

This rock unit is also found in LA-10D at a depth of 1790-1800m. It is pale greenish, fine grained, found as a thin layer between basalt and ignimbrite units. The basaltic andesite is vesicular and fractured with slight oxidation and alteration.

4.3 Hydrothermal alteration mineralogy

Hydrothermal alteration refers to rock formations interacting with hot hydrothermal fluids. Hydrothermal alteration is seen as change in mineralogy, texture and chemistry of rocks due to thermal and environmental changes facilitated by geothermal fluids and gases. The intensity of the changes also depends on texture and time. The factors that control alteration in geothermal systems are temperature, rock type, permeability, fluid composition and the duration of fluid-rock interactions (Reyes, 2000). Primary minerals are replaced by secondary minerals as a result of changes in the prevailing conditions. The fluids carry metals in solution, either from a nearby igneous source, or from leaching out of nearby rocks. Hydrothermal fluids cause hydrothermal alteration of rocks by passing hot fluids through the rocks and changing their composition by adding or removing or redistributing components. They may contain various types of gases, salts (brines), water, and metals. The metals are carried as different complexes, thought to involve mainly sulphur and chlorine (Lagat, 2009). Commonly, hydrothermal minerals are useful geothermometers (Table 5) and are used to reveal the history of the system; to determine the depth of the production casing during drilling; to determine the alteration temperatures of wells and by comparing alteration and formation temperatures, one can predict whether the system is heating or cooling; estimating fluid pH and other chemical parameters; as well as predicting scaling and corrosion tendencies of fluids and estimating permeability (Reyes, 1990).

TABLE 5: Alteration minerals and their temperature range based on data from Icelandic geothermal systems (Kristmannsdóttir, 1979; Franzson, 1998)

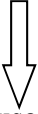
Minerals	Min. temp. (°C)	Max. temp. (°C)
Smectite	30	<200
Calcite	50-100	280-300
Quartz	180	>300
MLC	200	230
Illite	220	>300
Chlorite	220	>300
Epidote	240	>300
Actinolite	280	>300

4.3.1 Alteration of primary mineral assemblage

Primary minerals are rock forming minerals. These minerals tend to be unstable in geothermal environment, where lower temperatures and pressures governed. Primary minerals undergo chemical reaction with the hydrothermal fluid and change to secondary minerals, which are more stable at geothermal conditions (Reyes, 1990). Hence, secondary minerals are formed by the replacement of primary minerals. Plagioclase, sanidine, pyroxene, glass and oxide minerals are the main primary minerals in wells LA-9D and LA-10D (Table 6). The ferromagnesian minerals are mostly associated with basaltic rocks, while feldspar (sanidine) and oxide minerals also found in silicic rocks.

Volcanic glass: It is highly susceptible to be altered and replaced by calcite and clay alteration minerals. In thin-section, it is transparent and has vitreous lustre.

TABLE 6: Primary minerals and alteration products of well LA-9D and LA-10D

Most susceptible	Primary minerals	Alteration products
 Least susceptible	Volcanic glass	Clay, quartz, calcite
	Pyroxene	Chlorite, illite, actinolite
	Plagioclase	Calcite, albite, epidote, illite
	Fe-Ti oxides	Haematite, pyrite

Feldspars: They are abundantly found in both LA-9D and LA-10D wells as groundmass and phenocrysts. They are divided into plagioclase (mostly seen in basalt) and sanidine in silicic rock units. In thin-section, plagioclase shows low relief and twinning, while sanidine shows low relief with weak birefringence.

Pyroxene: It is varying from aegirine to augite and occurs as a groundmass constituent in rocks from the wells. It is also observed as being replaced by a high-temperature alteration mineral (actinolite) in LA-10D below 1850 m depth.

Fe-Ti oxides: They are highly resistant to alteration, and occur in both study wells. Mostly found as groundmass in the rock matrix with slight alteration intensity but when it altered, form haematite and pyrite.

4.3.2 Distribution of hydrothermal alteration minerals

The main hydrothermal alteration minerals in wells LA-9D and LA-10D are calcite, pyrite, chalcopryrite, siderite, haematite, chalcedony, smectite, illite, mixed layer clays (MLC), quartz, chlorite, epidote and actinolite. The distribution of alteration minerals with depth in wells LA-9D and LA-10D is described below and shown in Figures 14 and 15.

Calcite

Calcite is found in both the LA-9D and LA-10D wells. It is observed throughout the wells. It was identified by binocular and petrography analysis. In binocular microscope it is white in colour and is deposited in veins and vesicles of the rock cuttings. In thin section, calcite is mostly observed as platy calcite, occurring as vein and vesicle fillings, as well as being deposited in the groundmass. It was seen as a replacement mineral of plagioclase and pyroxene. In the alteration log (Figure 14 and 15) the abundance of calcite is presented with a range from 0 to 3, where 0 indicates lack of calcite and 3 indicates high abundance. High abundance of calcite observed in LA-9D and LA-10D at a depth of approximately 600-800 m and below 1100 m.

Pyrite

Pyrite is abundant in both wells. It is occurring as yellow, cubic crystals, which are disseminated in the rock matrix. In thin section, it was identified by its black euhedral shape in both cross and plane polarized setting. It is used as an indicator of permeability in geothermal systems (Reyes, 2000). It is mostly found together with calcite. Pyrite first appeared at a depth of 140 m and 460 m in wells LA-9D and LA-10D, respectively, and continues to the bottom of the wells. In the alteration log (Figures 14 and 15), the abundance of pyrite is presented with a range from 0 to 3, where 0 indicates lack of pyrite and 3 indicates high abundance. It is more abundant in well LA-10D, particularly at a depth of 850-900 m, than in LA-9D.

Siderite

Siderite is identified by using a binocular microscope. It has a radiating textural pattern and a yellowish colour. Siderite is found in minor amounts in the shallower parts of both wells (10, 100, 300 and 320 m in LA-9D and 510 m depth in LA-10D). It is a low-temperature hydrothermal alteration mineral typically associated with groundwater.

Haematite

Haematite is reddish brown in colour and mostly found in the groundmass together with magnetite. It is observed in the shallower part of well LA-9D at 40, 60 and 80 m depth. In thin section, the crystals are opaque and have hexagonal needle shape structure. It is a low-temperature mineral and formed due to percolation of rain through the surface layers.

Chalcedony

Chalcedony appears in both wells LA-9D and LA-10D at depths from 130 to 760 m and 140 to 810 m, respectively. It is greenish to greyish blue in colour, semi-transparent to translucent and found as a vesicle filling. The depositional temperature of chalcedony ranges from 120 to 180°C.

Quartz

Quartz is a whitish to colourless, transparent mineral mostly found filling vesicles and veins. It is observed at a depth of 500 m to 1920 m and 600 to 1940 m in LA-9D and LA-10D respectively. Quartz is stable at temperatures greater than 180°C. In thin section, it is identified by its undulating extinction and lack of cleavage. Quartz is more abundant in LA-10D than LA-9D and the amount increases below 800m in both wells.

Epidote

Epidote is a prismatic mineral with a yellowish green colour. In thin section, it shows high interference colour with parallel extinction and displays pleochroism. Epidote was observed at 1080 m to 1920 m and 860 to 1940 m in wells LA-9D and LA-10D, respectively. It occurs as vein and vesicle fillings, as well as it is observed replacing minerals, such as feldspars and pyroxene. Epidote is a high-temperature mineral formed at temperatures of $\geq 240^\circ\text{C}$. Therefore, the first appearance of epidote indicates that the wells have entered into the geothermal reservoir.

Actinolite

Actinolite is a high-temperature mineral that is formed at temperatures above 290°C. It was first observed in well LA-10D at a depth of 1890 m and down to the bottom of the well. In thin section, actinolite is characterised by a fibrous texture, while it has a pale green to whitish colour, high relief and displays pleochroism. It is formed by the replacement of ferromagnesian minerals, such as pyroxene, and occurs in association with epidote and chlorite.

Clays

Clays are the most common hydrothermal minerals in the geothermal wells. Various clay types form in different temperature intervals. The primary rock forming minerals alter to different types of clays depending on temperature, pH, fluid composition and the permeability of the formation. Clays occur as vein and vesicle fillings together with epidote, quartz and calcite, as well as replacement minerals. Most of the primary minerals such as pyroxene and volcanic glass are the major rock forming minerals that are replaced by clay. Four types of clays are identified in wells LA-9D and LA-10D. These are smectite, mixed layer clays (MLC), illite and chlorite. The identification of clays is based on binocular microscope, petrographic microscope and XRD analysis (Tables 7-8).

Smectite

Smectite is fine grained, brownish, low-temperature hydrothermal mineral. It is formed at a temperature range between 50-200°C. It is deposited in vesicles and is also found as a replacement mineral of volcanic glass and feldspars. Smectite is identified by binocular and petrographic microscope analysis and found at a depth between 350 and 790 m in LA-9D as well as 340 and 640 m depth in LA-10D well. In thin section, smectite shows radiating extinction and first order interference colour. XRD analysis of samples from well LA-10D shows smectite at 1560 m, which indicates the swelling nature of smectite clays, as the layer spacing of the untreated sample was 12.56 Å, while the layer spacing swelled to 13.52 Å in glycolated samples and collapsed to 10.16 Å in heated samples (Figure 16).

Mixed layer clays (MLC)

Mixed layer clays are an intermediate product of pure end members of clay. MLC was identified by petrographic analysis. In thin section, it is greenish and shows high interference colour compared to

TABLE 7: Results of XRD analysis of clay minerals from well LA-9D (d in Å)

Sample no.	Depth (m)	D(001) Unaltered sample	d (001) Glycolated sample	d (001) Heated sample	d(002)	Alteration minerals	Other
1	240	14.752 13.362 6.562	14.752 13.362 6.562	14.752 13.362 6.562	-	Chlorite	- Feldspar
2	370	10.275 8.621 6.558 6.479	10.275 8.621 6.558 6.479	10.275 8.621 6.558 6.479	-	Illite	- Amphibole Feldspar Feldspar
3	620	14.714 10.275 6.479	14.714 10.275 6.479	14.714 10.275 6.479	7.193	Chlorite Illite	- - Feldspar
4	730	-	-		-	no clay	-
5	890	14.595 10.263	14.595 10.263	14.595 10.263	7.729 7.164	Chlorite Illite	- -
6	910	14.595 10.263	14.595 10.263	14.595 10.263	7.221	Chlorite Illite	- -
7	940	14.595 10.263	14.595 10.263	14.595 10.263	7.221	Chlorite Illite	- -
8	1080	14.595 10.113	14.595 10.113	14.595 10.113	7.708 7.164	Chlorite Illite	- -
9	1370	14.735 10.308	14.735 10.308	14.735 10.308	7.232	Chlorite Illite	- -
10	1620	14.664 10.308	14.664 10.308	14.664 10.308	7.231	Chlorite Illite	- -
11	1640	14.664 10.147	14.664 10.147	14.664 10.147	7.708 7.169	Chlorite Illite	- -
12	1680	14.592 10.147	14.592 10.147	14.592 10.147	7.169	Chlorite Illite	- -
13	1800	-	-		-	no clay	-
14	1820	14.592 10.147	14.592 10.147	14.592 10.147	7.169	Chlorite Illite	- -
15	1920	14.757 10.318	14.757 10.318	14.757 10.318	7.236	Chlorite Illite	- -

chlorite. It occurs at a depth interval between 680 and 810 m in LA-9D well and 620 and 1690 m in LA-10D well.

Illite

Illite was identified through petrographic microscope analysis and XRD analysis. In thin section, it shows yellow brownish colour, low relief and high interference colour compared to chlorite. XRD analysis indicates a peak corresponding to layer spacing ranging from 10.11 Å and 10.54 Å. It was observed from 620 and 1920 m depth in well LA-9D and from 500 to 1940 m in LA-10D well. Illite is stable at a temperature range between 180 to > 220°C (Teklemariam, 1986). It is mostly found together with chlorite and occurs as a replacement of feldspars.

Chlorite

Chlorite is a high-temperature mineral, identified by binocular analysis, petrographic analysis and XRD analysis. It forms at temperatures of >280°C (Teklemariam, 1986). This mineral was observed from 620 to 1920 m in LA-9D and 640 to 1940 m in LA-10D. In thin section chlorite is light greenish to brownish in colour, fine to coarse grained, with low interference colour and moderate relief. It is observed together with illite as well as with epidote, quartz and actinolite. Chlorite is found as depositional in LA-9D at 890, 1410, 1460 and 1800 m and also found as a replacing alteration mineral of pyroxene at 810 m depth (Figure 17).

TABLE 8: Results of XRD analysis of clay minerals from well LA-10D (d in Å)

Sample no.	Depth (m)	d(001) Unaltered sample	d(001) Glycolated sample	d(001) Heated sample	d(002)	Alteration minerals	Other
1	360	8.64 6.58 6.49	8.64 6.58 6.49	8.64 6.58 6.49	-	- - -	Amphibole Feldspar Feldspar
2	470					-	No clay
3	500	10.24 6.58	10.24 6.58	10.24 6.58	- 7.21	- -	- Feldspar
4	580	10.54	10.54	10.54		Illite	-
5	640	14.58 10.41	14.58 10.41	14.58 10.41	7.20 7.20	Chlorite Illite	- -
6	810	14.53 10.41	14.53 10.41	14.53 10.41	7.20	Chlorite Illite	- -
7	830	14.67 10.49	14.67 10.49	14.67 10.49	7.21	Chlorite Illite	- -
8	920	14.81 10.28	14.81 10.28	14.81 10.28	7.25	Chlorite Illite	- -
9	940	14.86 10.36	14.86 10.36	14.86 10.36	7.82	Chlorite Illite	- -
10	950	14.67 10.34	14.67 10.34	14.67 10.34	7.79	Chlorite Illite	- -
11	960	14.62 10.25	14.62 10.25	14.62 10.25	7.24 7.76	Chlorite Illite	- -
12	990	14.62 10.25	14.62 10.25	14.62 10.25	7.20 7.76	Chlorite Illite	- -
13	1180	14.71 10.25 8.47	14.71 10.25 8.47	14.71 10.25 8.47	7.20 7.78 7.25	Chlorite Illite	- - Amphibole
14	1310	14.71 10.24	14.71 10.24	14.71 10.24	7.75	Chlorite Illite	- -
15	1410	14.39 10.16	14.39 10.16	14.39 10.16	7.20 7.13	Chlorite Illite	- -
16	1440	14.56 10.16	14.56 10.16	14.56 10.16	7.23	Chlorite Illite	- -
17	1460	14.56 10.16	14.56 10.16	14.56 10.16	7.23	Chlorite Illite	- -
18	1560	13.52	12.56	10.56		Smectite	-
19	1690	14.74 9.2	14.74 9.2	14.74	7.25 7.24	Chlorite	- -
20	1740	14.67 10.13	14.67 10.13	14.67 10.13	7.21	Chlorite Illite	- -
21	1910	14.79 10.29	14.79 10.29	14.79 10.29	7.22	Chlorite Illite	-

58321/LA-10 1560 m OMH

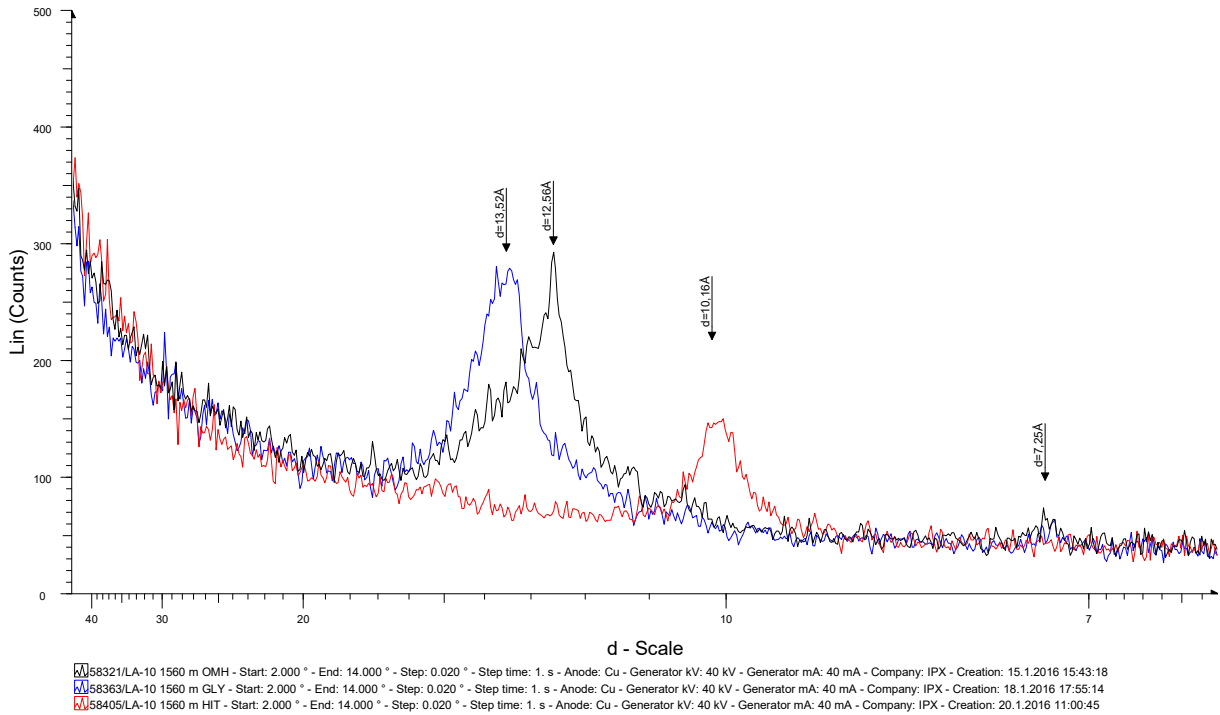


FIGURE 16: Smectite peaks in LA-10D

58296/LA-9 1080 m OMH

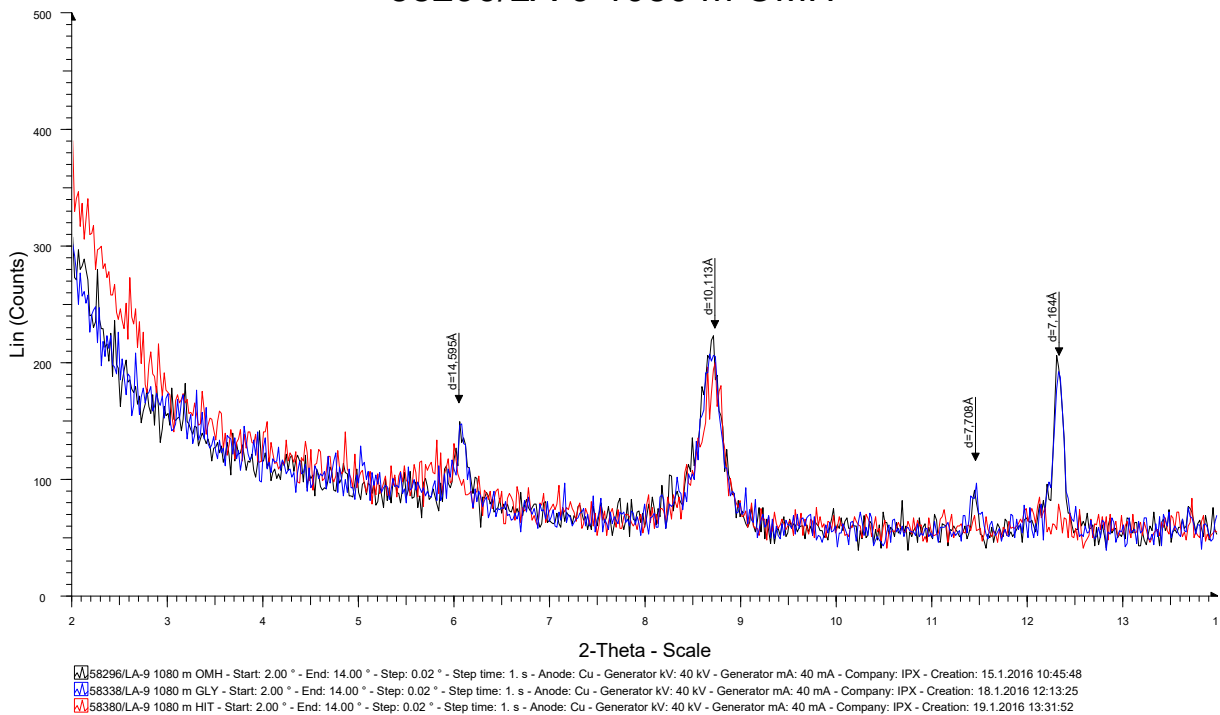


FIGURE 17: Chlorite and illite peaks in LA-9D

4.4 Vein and vesicle fillings

Vein and vesicles are indicating porosity and permeability of the formations that the well intersects, as well as they can be hosts for alteration minerals. Vein and vesicle fillings were observed in well LA-9D at 260-320, 750-830, 940-1000, 1630-1650 and 1730-1800 m depth and also in LA-10D found at 630-730, 990-1030, 1790-1810 and 1850-1870 m. Most of veins and vesicles are found in basaltic rocks and

a few of them in trachyte and rhyolite units in both wells. Commonly they are filled with chalcedony, calcite, quartz, smectite, MLC, chlorite, illite and epidote alteration minerals (Figure 18), but the sequences of alteration mineral deposition observed in veins and vesicles are outlined in the following subchapter. They were identified by binocular and petrographic analysis. Temperature and fluid composition are the main factors controlling sequence of alteration minerals deposited in veins and vesicles.

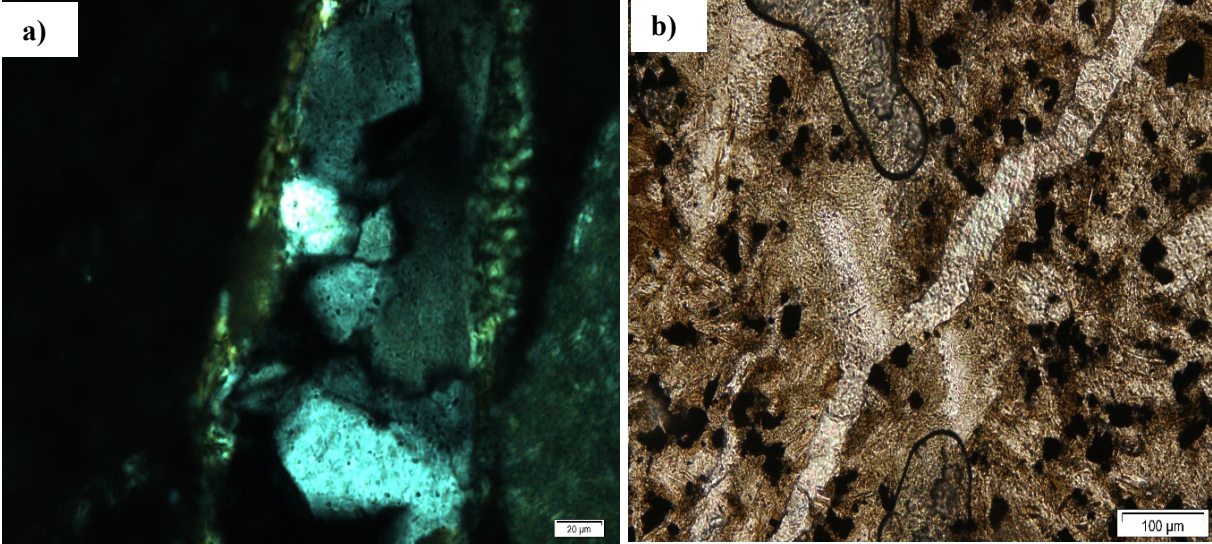


FIGURE 18: (A) Indicates quartz veinfilling found in LA-10D at 1530 m; and (B) shows calcite veinfilling at LA-10D in 1890 m depth

4.5 Mineral depositional sequence

A sequence of depositional minerals shows the relative time scale of hydrothermal alteration minerals in the geothermal system and hence thermal history (Table 9 and Figure 19). Hydrothermal alteration mineral assemblages are evaluated according to temperature, rock type and fluid-rock interaction. The youngest minerals precipitate at the centre of the sequence. The alteration mineral sequences observed in well LA-9D and LA-10D show that the temperature in the system has evolved progressively from

TABLE 9: Mineral depositional sequence in wells LA-9D and LA-10D

Depth	Alteration sequence		Lithology
	Older	→ Younger	
LA-9D			
	< : followed by		
LA-9D 320 m	Chalcedony < coarse grained clay < fine grained clay		Pyroclastic
LA-9D 680 m	Mixed layer clays (MLC) < quartz < calcite		Trachyandesite
LA-9D 810 m	Chlorite < MLC < smectite		Basalt
LA-9D 1410 m	Chlorite < calcite		Basalt
LA-9D 1460 m	Quartz < chlorite		Basalt
LA-10D			
LA-10D 790 m	Chlorite < quartz		Rhyolite
LA-10D 970 m	Epidote < calcite		Basalt
LA-10D 1010 m	Chlorite < quartz		Trachyte
	Quartz < MLC		
LA-10D 1350 m	Quartz < chlorite		Trachyte
	Calcite < epidote		
LA-10D 1530 m	Quartz < chlorite		Rhyolite
	Clay < quartz		
LA-10D 1630 m	Calcite < chlorite < quartz		Basalt
LA-10D 1690 m	Chlorite < quartz		Basalt

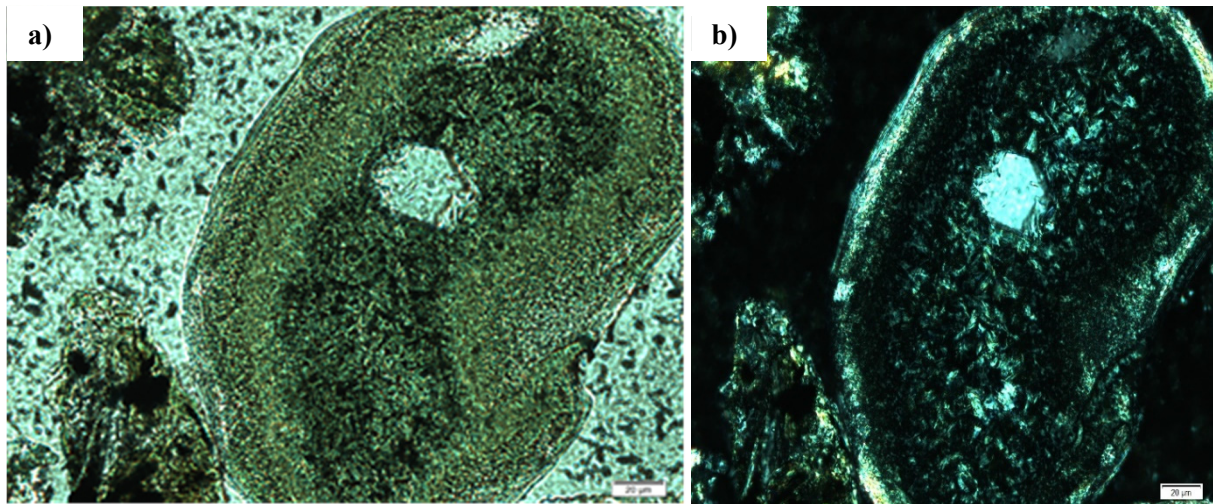


FIGURE 19: Mineral depositional sequence, Calcite < chlorite < quartz at LA-10D at 1630m; (A) PPL; and (B) XPL

low temperature to higher temperature. Generally, the alteration depositional sequence in wells LA-9D and LA-10D indicates the temperature increases down to the bottom of the wells with no cooling intervals.

4.6 Hydrothermal mineral zonation

In wells LA-9D and LA-10D, three alteration zones have been identified below the unaltered zone based on the distribution of alteration minerals with depth. The distribution of alteration minerals gives information about formation temperature at the time of deposition. The boundary from one zone to another was defined by the first appearance of selected alteration minerals. The alteration zones that have been identified in two wells are: unaltered zone, smectite zone, illite/chlorite zone and illite/chlorite/epidote zone (Figure 20).

Unaltered zone: This zone is characterized by pyroclastics at a depth of 0-120 m in LA-9D as well as pyroclastics and rhyolite at a depth of 0-129 m in well LA-10D. Oxidation, calcite and haematite are observed in this zone. Alteration temperature is below 50°C.

Smectite zone: This zone is located below the unaltered zone at a depth of 121-500 m in LA-9D and 130-500 m in LA-10D wells. It is found in a rhyolite unit with intercalations of pyroclastics and silicic tuff and breccia in LA-9D and intercalations of dacite in LA-10. A few alteration minerals were observed in this interval, such as chalcedony, smectite and siderite. The temperature in this zone reaches 75-130°C in LA-9D and 75-150°C in LA-10D wells.

Illite/chlorite zone: This zone is dominated by illite and chlorite alteration minerals together with scarce quartz, pyrite, calcite, mixed layer clays, chalcopryrite and smectite. In LA-9D, it is found from 501-1020 m depth within basalt, rhyolite, sediments, pyroclastics, trachyandesite, basaltic trachyandesite, dacite and trachyte units. In LA-10D the zone is located at a depth of 501-859 m within trachyandesite, pyroclastics, basalt, trachyte and rhyolite units. The temperature in this zone is more than 200°C.

Illite/chlorite/epidote zone: This alteration zone starts from the depth where the first appearance of epidote is observed and extends down to the bottom of the wells. It is located at depth of 1021-1920 m in LA-9D within a lithology of trachyte and basalt. In well LA-10D, it is found at 860-1940 m depth within units of rhyolite, pyroclastics, trachyte, basalt and ignimbrite. Alteration minerals like calcite, pyrite, chalcopryrite, quartz, mixed layer clays and actinolite are found together with illite, chlorite and epidote in this zone. The temperature in this zone reaches above 240°C. Deposition of epidote is more abundant in well LA-10D compared to well LA-9D.

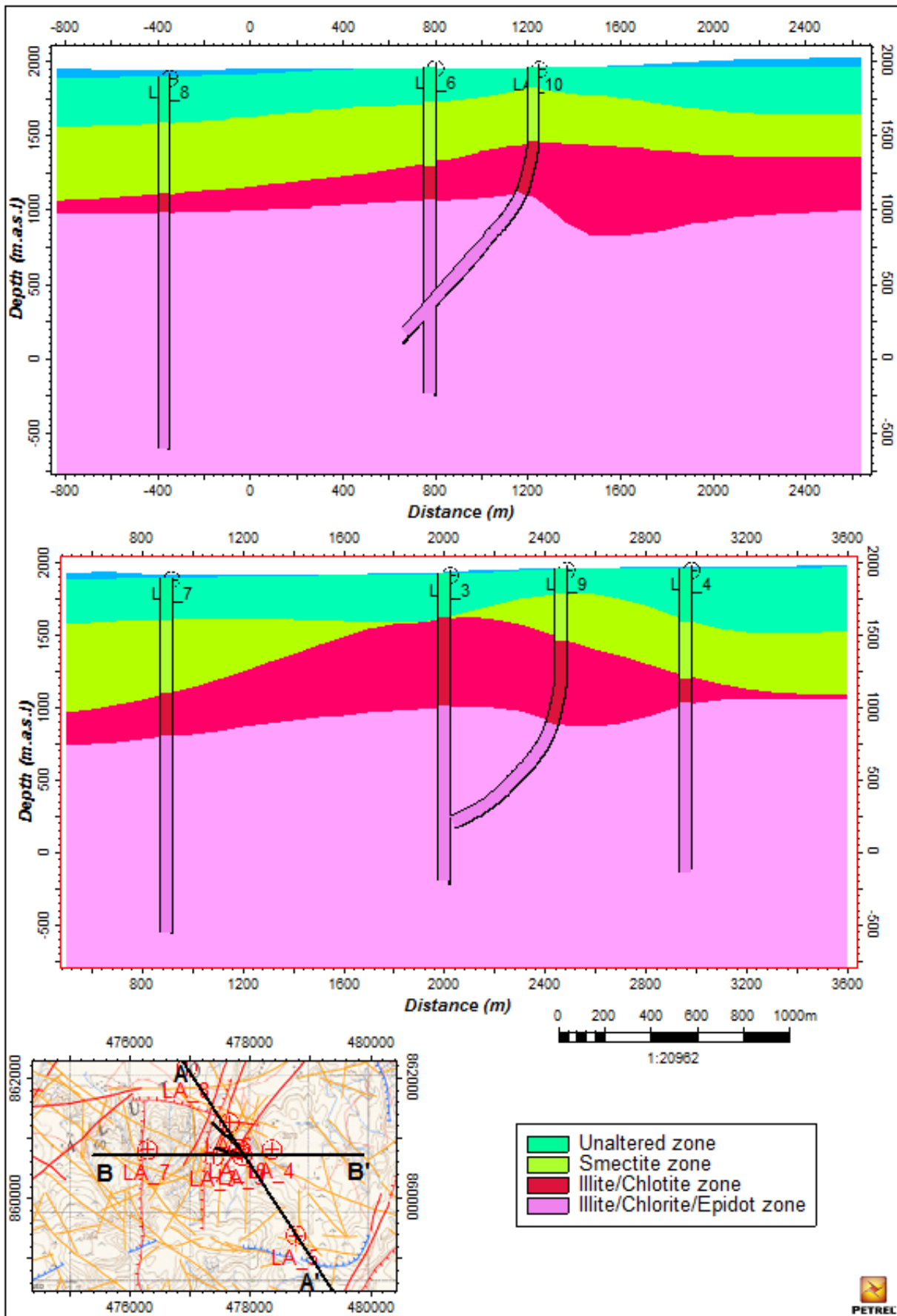


FIGURE 20: Cross-section of alteration zones in Aluto Langano geothermal wells

4.7 Feed zones

Feed zones are located in the water-saturated regions in the subsurface. The movement of the subsurface water is controlled by permeability, porosity, temperature, types of rock formations and the nature of recharge. According to Reyes (2000), feed zones are associated with structural formations such as faults, fractures, joints, lithological contacts and paleosoils in geothermal systems. Abundance of calcite and pyrite can be indicators of feed zones. Additionally, increased intensity of alteration can be an indicator of a feed zone as local increase in alteration may imply more water-rock interaction. Alteration intensity and permeability are directly proportional. When alteration intensity increases, permeability also increases. The feed zones in these wells are identified on the basis of temperature recovery profiles and the intensity of alteration, abundance of calcite and pyrite, lithological contacts and circulation losses.

In well LA-9D seven small feed zones were located at a depth of 760, 830, 940, 1000, 1140, 1640 and 1800 m, while large feed zone is encountered at depth of 1350 m. The feed zones were identified through temperature recovery measurements which were taken in May 5, 6, 8, 9, 10 and June 1, 2015 (Figure 21). The first three small feed zones (760, 830 and 940 m) and the last two small feed zones (1640 and 1800 m) were located in units of basalt. The alteration intensity was high, while a medium to low abundance of calcite and pyrite were observed. The feed zone at 1000 m was located at boundary contact between basalt and basaltic trachyandesite where the alteration intensity was moderate and the abundance of calcite and pyrite was low. At 1140 and 1350 m feed zones were encountered with circulation losses.

In well LA-10D, six small feed zones were located at 920, 1160, 1280, 1320, 1620, 1760 and one large feed zone at 700 m (circulation loss zone) (Figure 22). The small feed zones at 920, 1100, 1280 and 1320 m were located in trachyte units, while the feed zone at 1620 m depth is the contact between a unit of basaltic trachyandesite and basalt. The feed zone at 1760 m depth is located in a basaltic unit. All feed zones are associated with high alteration intensity and medium to high abundance of calcite and medium to low abundance of pyrite. The feed zones were identified through temperature recovery measurements that were taken on October 5, 6, 24 and November 18, 19, 28, 2015 (Figure 22).

4.8 Distribution of temperature at Aluto Langano geothermal field

In Aluto Langano geothermal field, a high-temperature anomaly is located in the central part of the field, where wells LA-3, LA-6, LA-9D and LA-10D are located. The highest recorded temperature is about 335°C at the bottom of LA-3 and LA-6 at an elevation of 500 m b.s.l. (Ernst & Young and ShinNihon, LLC, 2010). The zone with the highest temperature in the wells is located within the basalt formation.

The wells that are located outside the up-flow zone, such as LA-4, LA-5, LA-7 and LA-8, (Figure 23) show temperature inversion at a depth of 1600-2014, 1000-1848, 1600-1900 and 2150-2400 m, respectively. In well LA-7, temperature decreases to 140°C in the inversion zone at 1900m depth, which indicates cold inflow (Electroconsult, 1986). No temperature inversion is recorded in wells LA-3, LA-6, LA-9D and LA-10D, which are located at the main up-flow zone of the geothermal field.

The temperature decrease towards the east, the south and the western part of the Aluto Langano area gives a mushroom-like shape to the thermal dome. From the up-flow zone the high-temperature geothermal fluid travels along the (the fault that cuts well LA-3 and LA-6) and the faults (Figure 23) that strike NNE-SSW, but these faults are located to the west of the LA-3 and LA-6 wells. The NNE-SSW strike of the faults is corresponding to the alignment of Wonji Fault Belt.

In the upper part of LA-9D and LA-10D wells from surface to 550-450 m, respectively, the temperature is below 150°C. The temperature increases with depth in well LA-9D and at 1120-1560 m depth temperature increases from 250 to 300°C, while temperature is higher than 300°C below 1560 m depth. The highest temperature recorded in well LA-9D is 307°C at 1909 m. In well LA-10D, temperature increases from 250 to 300°C between 740 and 1600 m. Below 1600 m depth, temperature is higher than 300°C, but the highest temperature measured in the well is 305°C at 1801 m depth (Figure 24).

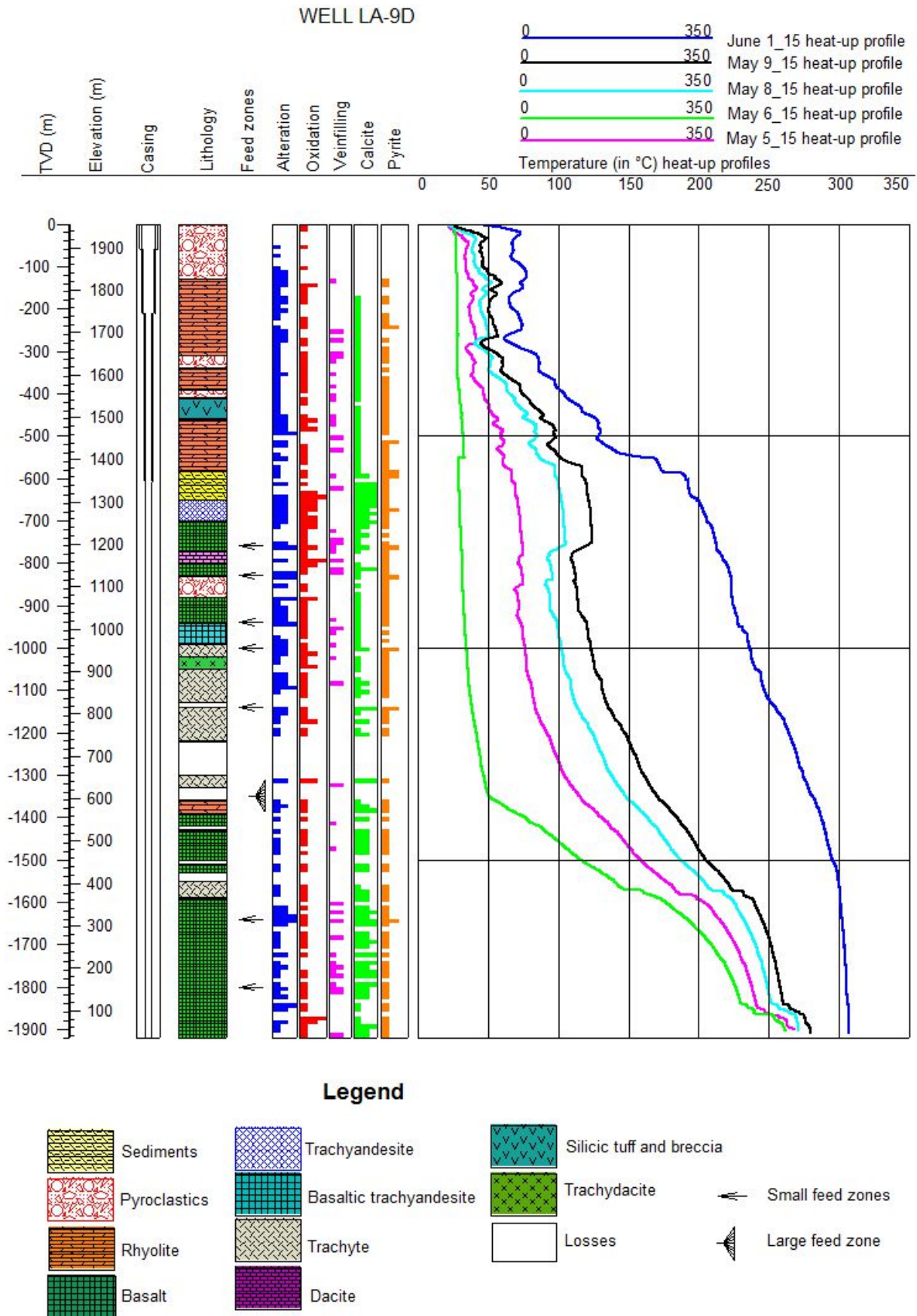


FIGURE 21: Feed zones in well LA-9D inferred from loss of circulation, temperature logs, alteration intensity and abundance of alteration minerals

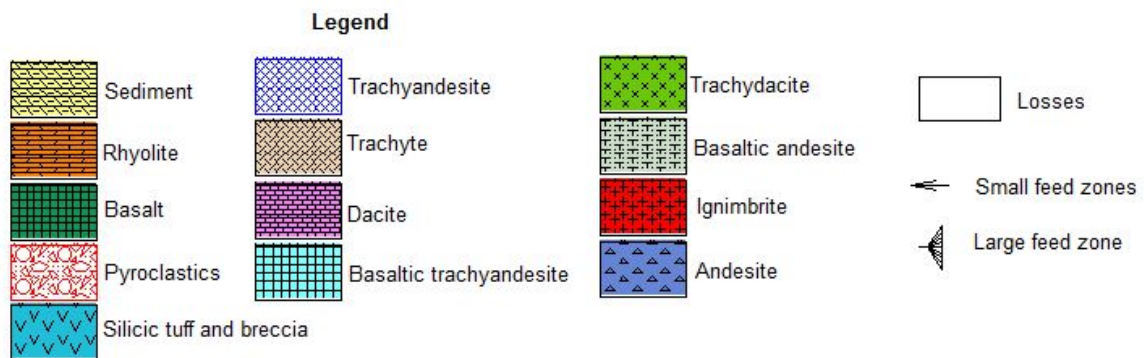
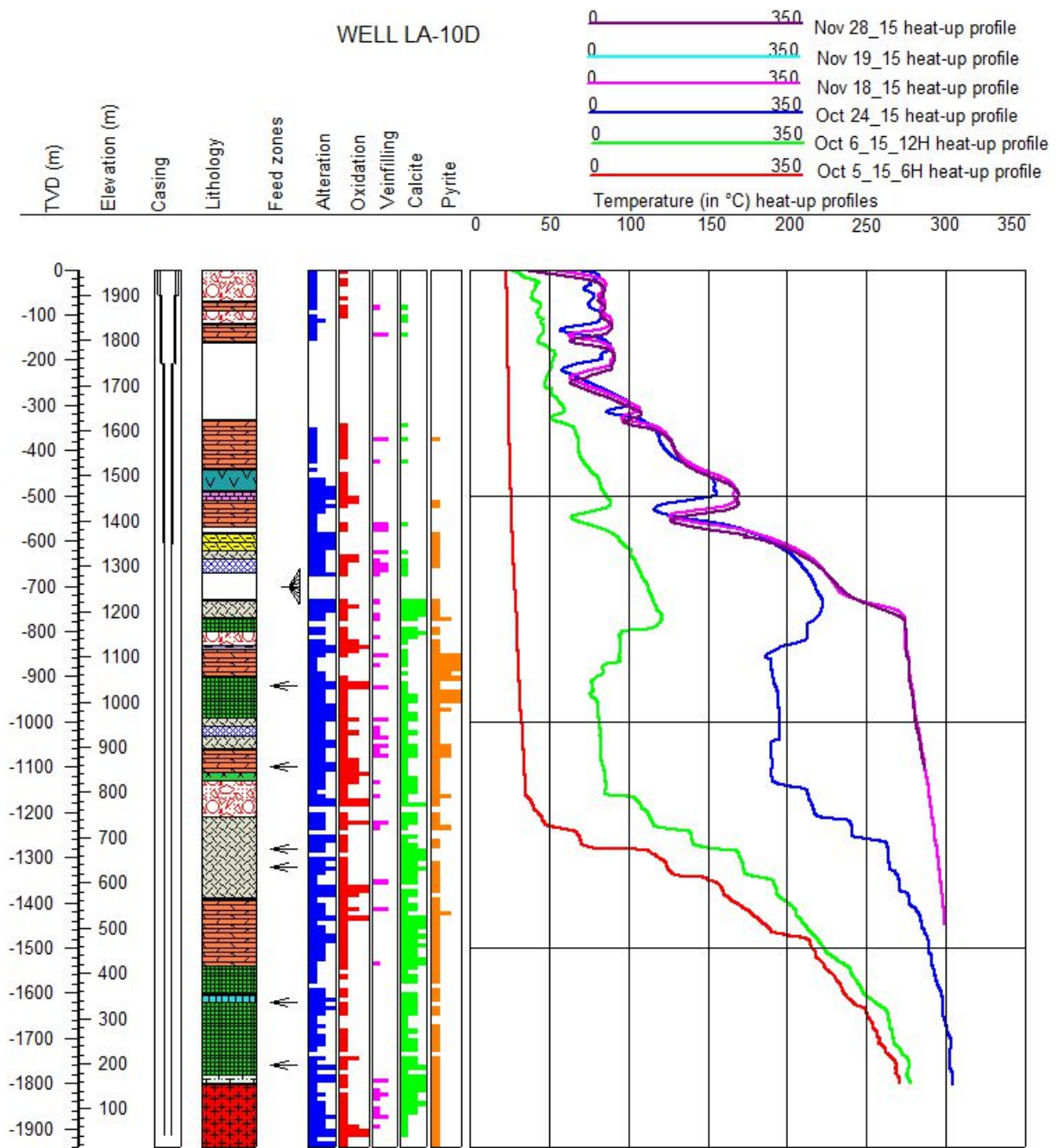


FIGURE 22: Feed zones in well LA-10D inferred from loss of circulation, temperature logs, alteration intensity and abundance of alteration minerals

In general, the highest temperature is recorded in the central part of the Aluto Langanu field, while a decrease of underground temperature is observed towards eastern and western parts of the field. It seems to indicate that there may be lateral outflow along NNE trending faults of the Wonji Fault Belt and also that the faults that are aligned in NNE-SSW and NW-SE direction surrounding the main up-flow of the field acts as a hydrological barrier.

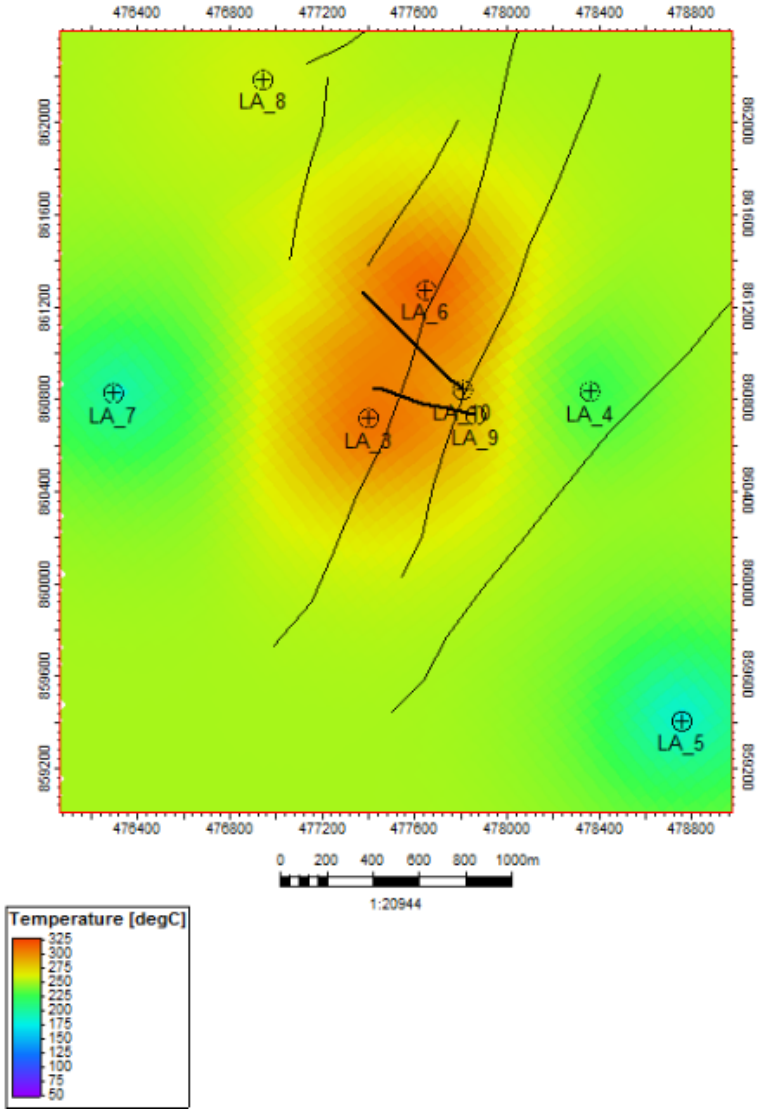


FIGURE 23: Distribution of temperature in Aluto Langanu geothermal field at 800m a.s.l.

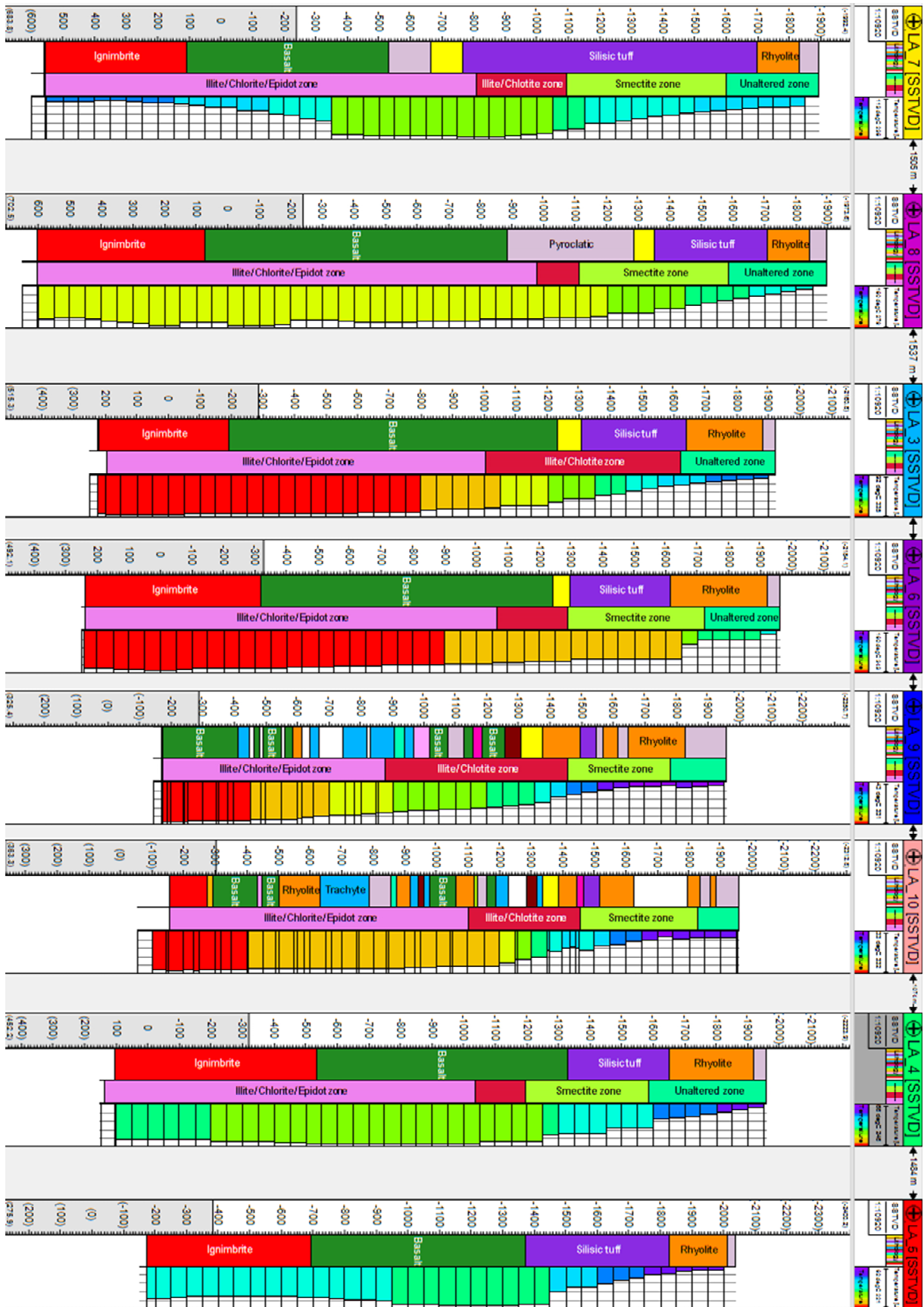


FIGURE 24: Distribution of temperature with lithology and alteration in the Aluto Langano geothermal wells

4.9 Whole rock chemistry

4.9.1 Classification of rock type

Igneous rocks can be classified using their chemical properties by analysing the major and trace element of the rocks. Several methods are used to identify the chemical composition of the rocks, but in this study, Inductively Coupled Plasma-Optical Emission Spectroscopy (ICP-OES) was used. ICP-OES analyses for major and trace elements were carried out on rock cuttings at different depths from wells LA-9D and LA-10D (Tables 10 and 11). After analysing the major and trace elements, the data were presented in Total Alkalis vs. Silica diagrams. The TAS plot shows the total alkali ($\text{Na}_2\text{O} + \text{K}_2\text{O}$) versus silica concentration, and can be used to separate alkalic and subalkalic rocks (Figure 25).

TABLE 10: Whole rock chemical analysis data for major elements (wt.%) and trace elements (ppm) of drill cuttings from well LA-9D

WELL LA-9D										
Depth (m)	350	390	490	550	660	780	950	1030	1060	1560
Element (wt.%)										
SiO ₂	76.43	70.91	75.16	76.22	61.42	65.60	54.63	63.89	65.24	50.67
Al ₂ O ₃	7.43	14.80	10.36	9.44	14.55	15.03	16.54	14.97	14.29	15.00
FeO	6.49	3.95	5.55	5.91	8.10	6.88	10.81	6.21	5.94	10.20
MnO	0.17	0.18	0.20	0.21	0.19	0.13	0.17	0.19	0.15	0.17
MgO	0.04	0.05	0.25	0.10	1.38	0.69	1.53	1.29	0.96	5.20
CaO	0.21	0.23	0.62	0.57	3.41	2.82	6.06	3.09	2.10	8.81
Na ₂ O	4.33	4.79	2.57	2.73	4.47	4.30	4.11	5.18	5.38	4.97
Na ₂ O+K ₂ O	8.70	9.30	7.27	7.00	7.88	7.06	5.49	8.74	9.81	6.16
K ₂ O	4.37	4.51	4.70	4.27	3.41	2.76	1.38	3.56	4.42	1.19
TiO ₂	0.32	0.38	0.34	0.33	1.96	1.16	3.64	1.02	0.97	3.15
P ₂ O ₅	0.02	0.02	0.05	0.02	0.89	0.43	0.95	0.32	0.29	0.48

WELL LA-9D										
Depth (m)	350	390	490	550	660	780	950	1030	1060	1560
Elements (ppm)										
Ba	336.7	451.0	255.0	419.0	713.9	633.1	400.6	1372.3	109.8	358.9
Co	0.53	1.39	1.81	1.68	18.49	13.98	47.09	8.67	9.42	53.94
Cr	3.29	0.09	4.02	8.75	4.82	2.13	6.67	0.63	7.95	16.24
Cu	11.89	7.18	11.54	8.61	12.02	14.43	24.41	9.22	9.15	16.59
La	97.04	117.1	128.6	117.5	51.20	59.13	26.84	53.87	48.82	15.07
Rb	353.6	223.1	197.3	252.1	180.6	80.5	25.5	170.7	194.0	0.0
Sc	1.70	4.09	2.03	1.88	18.28	12.30	27.78	14.57	13.45	29.23
Sr	10.55	10.61	29.76	18.5	419.4	316.4	624.1	375.6	321.9	490.4
V	6.09	7.27	13.16	7.7	41.8	26.2	253.5	12.1	22.3	275.1
Y	107.4	80.2	114.1	100.7	61.7	53.5	41.3	64.2	59.0	27.3
Zn	174.3	135.2	210.5	187.9	144.3	127.8	118.8	151.6	123.2	117.3
Zr	833.3	699.6	901.5	801.0	404.8	403.2	228.5	497.2	484.6	199.0

In Figure 25 the composition of rocks from the two wells in the Aluto-Langano field are plotted on a TAS diagram. The recognized method of classifying most volcanic rocks is the total alkali–silica (TAS) diagram (Le Bas *et al.*, 1986). The total alkali ($\text{Na}_2\text{O} + \text{K}_2\text{O}$) axis mainly distinguishes alkalic from sub-alkalic rock types, whereas the silica axis mainly distinguishes primitive from evolved rock types. It has long been recognized that the TAS diagram is not robust in classifying altered volcanic rocks, and proxies using more immobile elements have been developed for that purpose. However, several previous studies on cuttings from geothermally altered rocks from Kenya (Mbia, 2014; Musonye, 2015) have shown that the TAS diagram is indeed very useful in identifying the various rock types encountered. The effects of hydrothermal alteration on the rock chemistry are discussed below. It should be emphasised, though that when analysing rock cuttings, even if samples are carefully selected and preferably from thick lithological units, there is always the danger of mixing, which could distort the chemical range, i.e. intermediate compositions could be the result of mixing end-members, in particular at deeper levels in the wells. The subsurface samples taken from wells LA-9D and LA-10D show a chemical variation ranging from basalt through to trachyte and rhyolite in composition. The samples

TABLE 11: Whole rock chemical analysis data for major elements (wt.%) and trace elements (ppm) of drill cuttings from well LA-10D

WELL LA-10D									
Depth (m)	90	490	530	650	840	1020	1110	1610	1800
Element (wt. %)									
SiO ₂	73.47	68.64	72.93	58.64	57.59	60.25	65.27	53.02	56.09
Al ₂ O ₃	9.92	10.55	10.96	16.43	18.03	16.35	14.56	15.43	14.75
FeO	5.61	9.61	6.66	9.54	9.47	7.18	6.48	10.62	9.38
MnO	0.18	1.47	0.28	0.28	0.22	0.18	0.15	0.16	0.19
MgO	0.03	0.46	0.10	1.49	2.06	0.80	0.94	3.95	3.26
CaO	0.60	0.88	0.83	3.70	3.40	3.78	1.72	5.68	8.91
Na ₂ O	4.96	0.20	3.62	4.02	4.03	4.86	5.33	5.56	2.48
K ₂ O	4.72	7.56	4.06	2.83	1.88	4.29	3.86	1.52	1.97
Na ₂ O + K ₂ O	9.68	7.76	7.68	6.85	5.91	9.16	9.19	7.08	4.45
TiO ₂	0.32	0.37	0.35	1.98	2.59	1.46	1.12	3.34	2.29
P ₂ O ₅	0.01	0.03	0.01	0.90	0.59	0.59	0.31	0.57	0.51

WELL LA-10D									
Depth (m)	90	490	530	650	840	1020	1110	1610	1800
Element (ppm)									
Ba	170.64	328.17	121.61	671.33	386.91	1020.09	1055.74	434.98	488.40
Co	0.79	1.04	1.60	20.50	36.59	14.70	10.80	58.24	41.98
Cr	9.76	2.54	22.32	0.00	8.93	1.90	3.44	19.99	115.19
Cu	11.84	8.56	9.47	11.88	19.55	10.30	10.12	19.94	37.07
La	127.09	175.92	147.03	72.33	55.46	65.12	52.65	20.54	42.02
Rb	253.45	183.20	179.18	38.73	38.64	107.39	364.82	0.00	18.42
Sc	0.74	1.20	1.38	19.81	21.69	16.83	13.69	29.68	26.03
Sr	12.10	29.98	20.49	409.20	353.59	515.01	296.96	376.07	333.00
V	7.86	5.86	8.62	45.66	149.26	37.83	21.43	295.96	215.32
Y	115.93	142.78	136.50	66.07	53.48	58.45	61.28	33.06	40.25
Zn	222.31	319.20	244.70	152.06	132.38	133.69	128.11	115.51	118.81
Zr	892.04	1123.63	1008.45	426.05	396.57	421.87	505.75	230.69	303.65

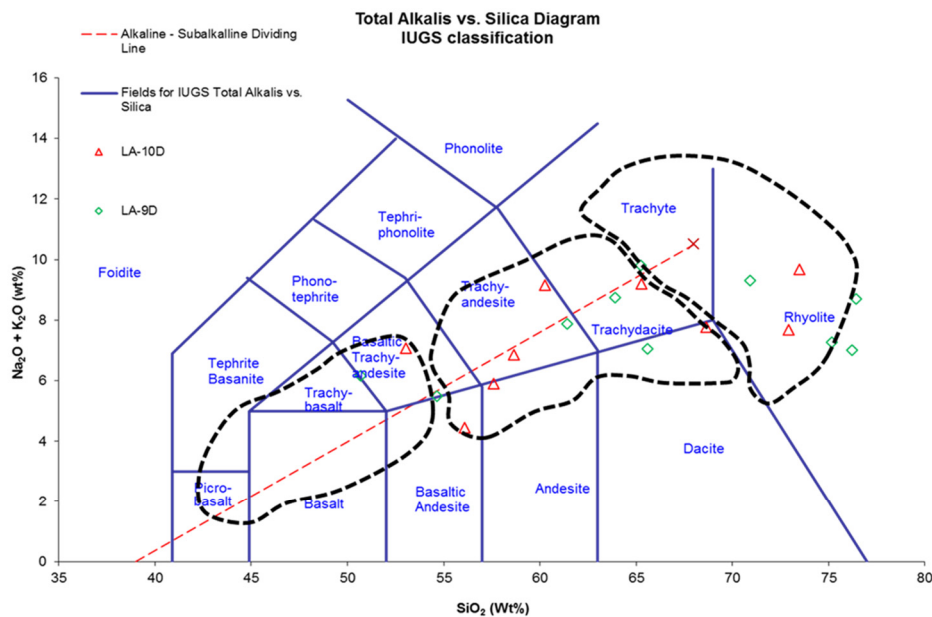


FIGURE 25: TAS diagram showing the Aluto Langanu sub-surface rock samples (LA-9D and LA-10D) with surface data fields from the northern MER, outlined by black broken lines (from Peccerillo et al., 2007) and rocks from Aluto Langanu outlined by a blue broken line (Teklemariam, 1996)

from LA-9D plot in basaltic trachyandesite, trachyandesite, dacite and rhyolite fields (Figure 25). Similarly, LA-10D contains all these rock types as well as basaltic andesite and andesite rock units. Some of the rocks, like dacite, show high intensity of alteration through binocular analysis.

The trend of subsurface rock samples from the Aluto Langano wells (LA-9D and LA-10D) seems to have a similar compositional range as surface rock samples from the northern part of Main Ethiopian Rift (MER) (Peccerillo et al., 2007). The surface samples form fields outlined by black broken lines in Figure 25. Most of the surface samples plot within the basalt, rhyolite and trachyte zones. However, the plot also shows rocks of intermediate composition, but they are rare in the Ethiopian rift. Surface samples from Aluto Langano (Teklemariam, 1996) are entirely bimodal, with no intermediate compositions (Figure 25). According to Peccerillo et al., (2007), the silicic rocks are derived from basalts by fractional crystallization with minor interaction of the crust, and the transitional rock units are generated during fractional crystallization, with rare intermediate melts.

On the Al_2O_3 versus FeO classification diagram (Figure 26), four fields are recognised, comendite, comenditic trachyte, pantelleritic trachyte and pantellerite (MacDonald, 1974). Figure 26 shows that the Aluto Langano subsurface samples from wells LA-9D and LA-10D plot mostly in the pantellerite and pantelleritic trachyte fields. In the sub-surface data of the study wells most of the rhyolite plots in pantelleritic field, except one sample; the trachyandesite and basaltic trachyandesite samples plot in the pantelleritic trachyte field and also trachyte, dacite and trachydacite samples plotted in the boundary between comenditic trachyte pantellerite trachyte fields.

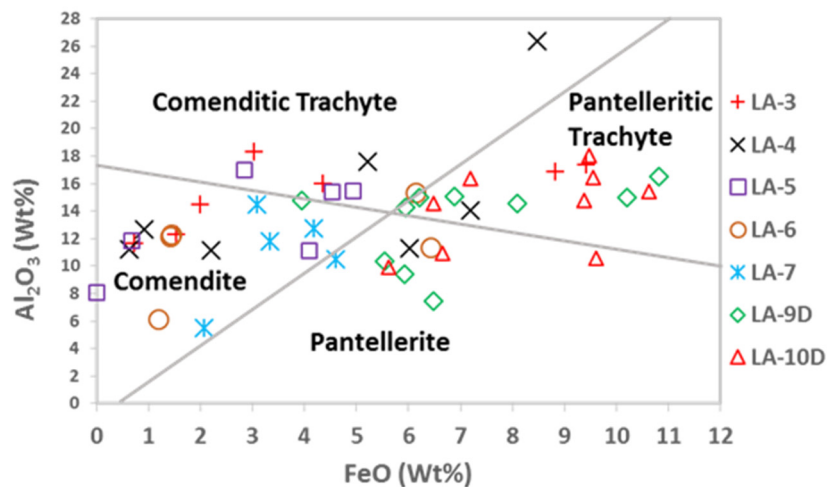


FIGURE 26: Al_2O_3 vs FeO diagram of the Aluto Langano samples from wells LA-9D and LA-10D, in addition to analyses from wells LA-3 to LA-7 (Teklemariam, 1996). Analyses of surface rocks are confined within the black broken line fields (data from Teklemariam, 1996)

4.9.2 Effects of hydrothermal alteration on the rock chemistry

Hydrothermal alteration affects the chemical composition of rocks by the interaction of hot fluid with the rock. The main factors affecting the fluid/rock interaction are permeability, porosity, temperature and pressure. In the study wells, the hydrothermal alteration minerals are found as deposition and replacement of primary minerals. To understand the effects of hydrothermal alteration the major elements (MgO, TiO_2 , Al_2O_3 , MnO, Na_2O , CaO, FeO, P_2O_5 , and K_2O) are plotted against SiO_2 . Similarly, selected trace elements (Ba, Cr, La, Rb, Sr, Y and Sc) are plotted against Zr.

In Figure 27, the major element plots of MgO, TiO_2 , Al_2O_3 , MnO, Na_2O , CaO, FeO, P_2O_5 , and K_2O vs. SiO_2 indicate that the rock composition is slightly affected by hydrothermal alteration. However, Na_2O shows significant scattering compared to the other elements, demonstrating the mobility and leaching of sodium during the hydrothermal alteration process.

Selected trace elements (Figure 28) show that Cr, La, Y and Sc plotted against Zr are not seriously affected by alteration, whilst Ba, Sr and Rb show scattering, indicating the mobility and leaching of these elements.

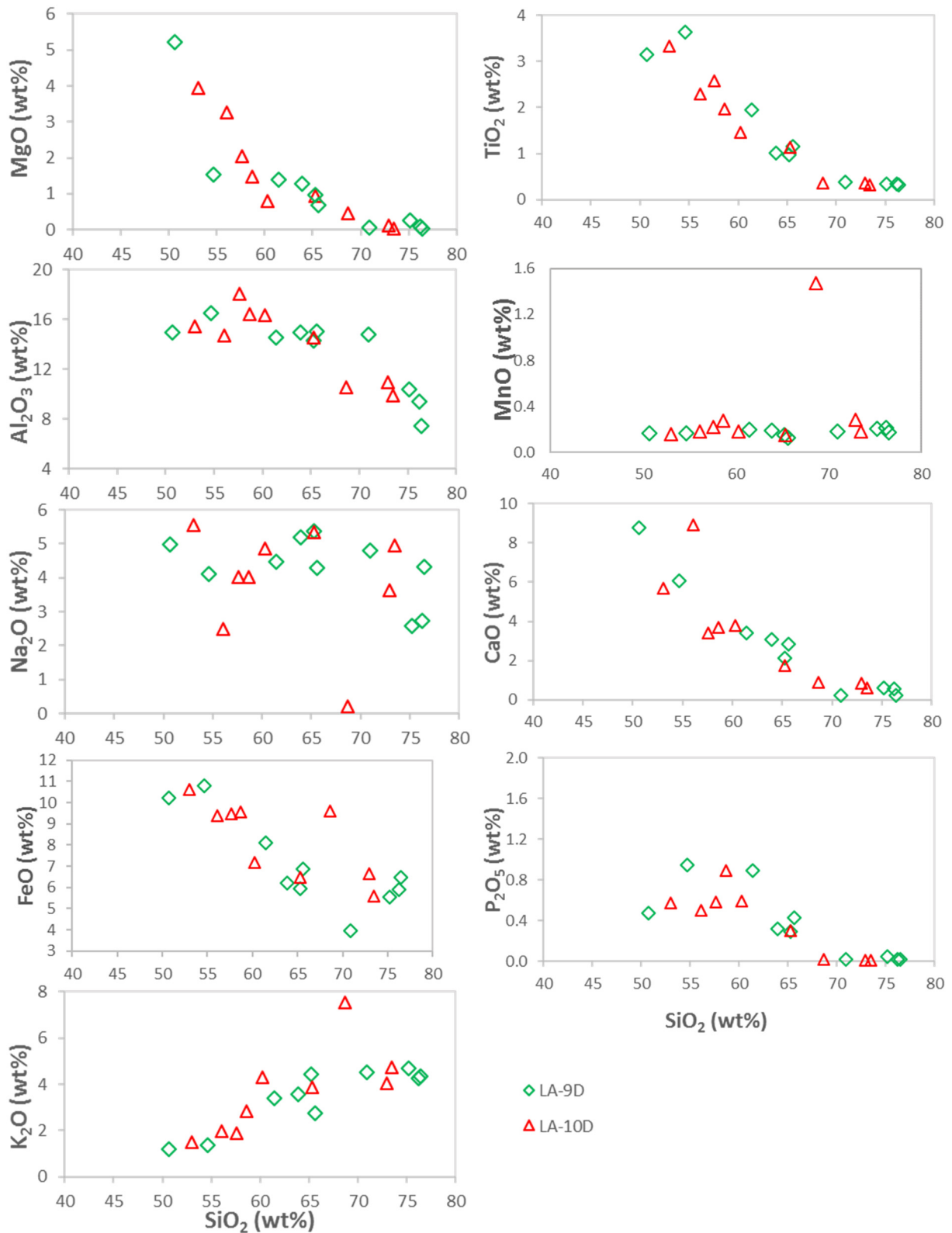


FIGURE 27: Major elements vs SiO₂ for subsurface samples of Aluto Langano geothermal field (data from wells LA-9D and 10D)

These results indicate that several major and trace elements have relatively small effect on chemical composition of the rock sample. The results are consistent with previous studies on the effects of geothermal alteration on rocks chemistry from Menengai and Olkaria in Kenya (Mbia, 2014; Musonye, 2015).

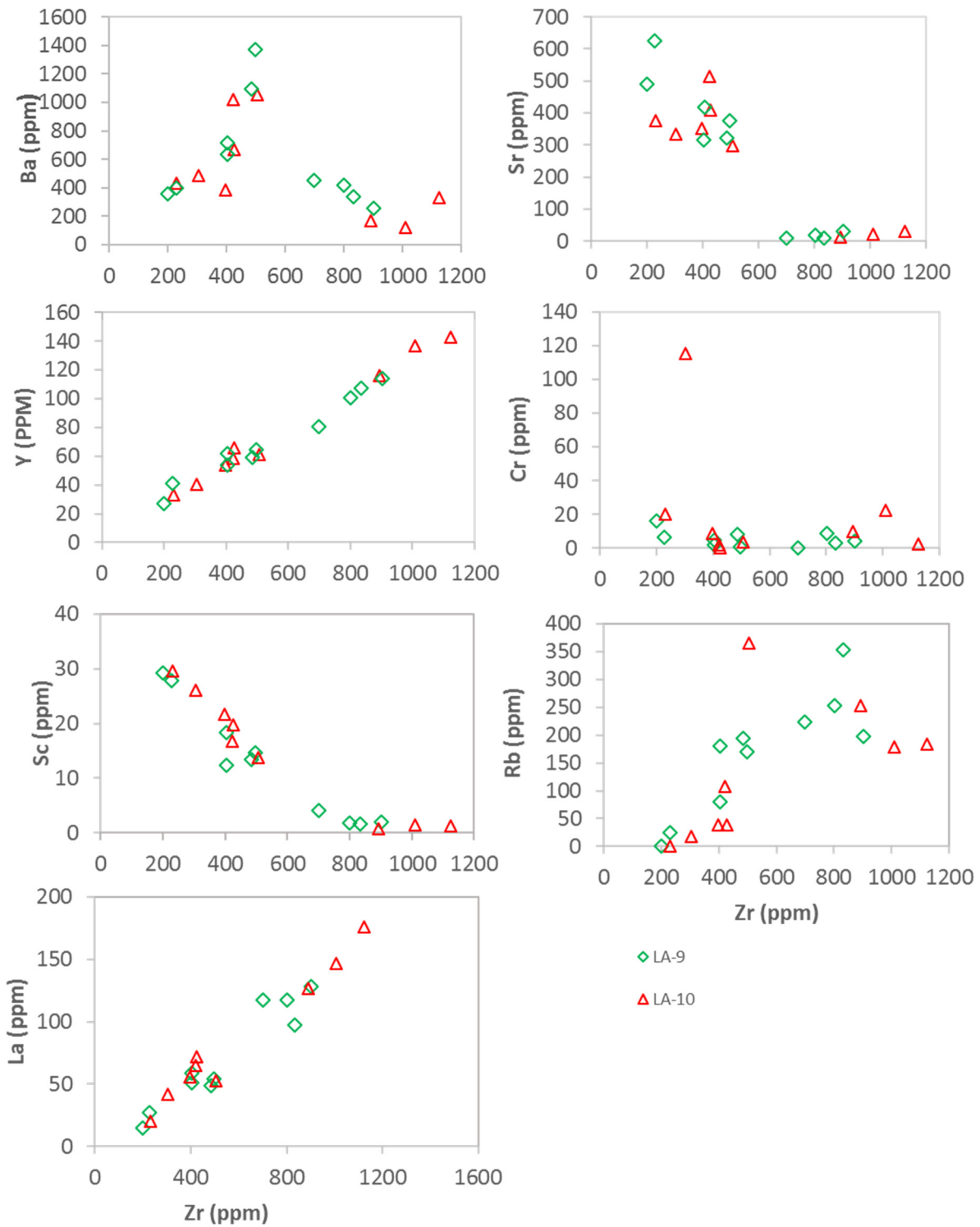


FIGURE 28: Trace elements vs Zr for subsurface samples of Aluto Langano geothermal field (data from wells LA-9D and 10D)

4.10 3D geological and geothermal model

Three dimensional models are descriptive or qualitative models, which helps to produce an integrated conceptual volume model, which may give better understanding of heat source, permeable zones, cap rock, and reservoir body that fashions the geothermal system in the subsurface. The information that is used to construct the three dimensional models are geological information which include surface mapping and subsurface data, remote sensing data, geophysical survey data, information on chemical

and isotopic content of fluid in surface manifestations and reservoir fluid samples collected from wells, temperature and pressure and drilling data from wells.

In this study, a three dimension geological and geothermal model has been produced through integration of various data such as geological and structural mapping data, data from subsurface (borehole logging), resistivity profile data and temperature data from wells. The geological and structural maps were taken from Electroconsult (2015). Also resistivity profile and cross-section were adopted from Ernst & Young and ShinNihon, LLC (2010). Stratigraphy, alteration zones, feed zones and temperature data were derived from well logging data. All these data were recreated in PETREL, 2015 software, with the aim to aid the understanding of the geological feature and structural framework within the Aluto Langanu geothermal field (Figure 29). The steps that were used to develop the 3D model include: data preparation and data import, structural modelling and 3D property modelling.

Data preparation, which is the first step and includes all relevant data used for modelling purposes. These input data were prepared and imported to the Petrel software according to their format and type of file. After the data had been imported into the software, quality control and checking was done. In the next step construction of a structural model was done and the structural model was further used to build a geological model. The structural model is developed in steps, which include creating a surface/fault model that is used to define the boundary of the stratigraphy and faults, 3D gridding, pillar gridding, making horizons and layering. Through this process a 3D grid is created, which is divided into grid cells. Each grid cell tells the property of the data, which are interpolated across the grid such as single rock type, volume of property etc. (Schlumberger, 2010). The 3D grid then consists of a number of horizons, which are intersected by faults through the process of pillar gridding. The horizons were used to separate the alteration zones in the alteration model and the main stratigraphic units (pyroclastic, rhyolite, trachyte, basalt and ignimbrite unit) in the geological model of the Aluto Langanu geothermal field. The horizons were further divided into layers, which is used to define the thickness of each stratigraphic subunit, the geological context of the subunit and to see their association with faults (Figure

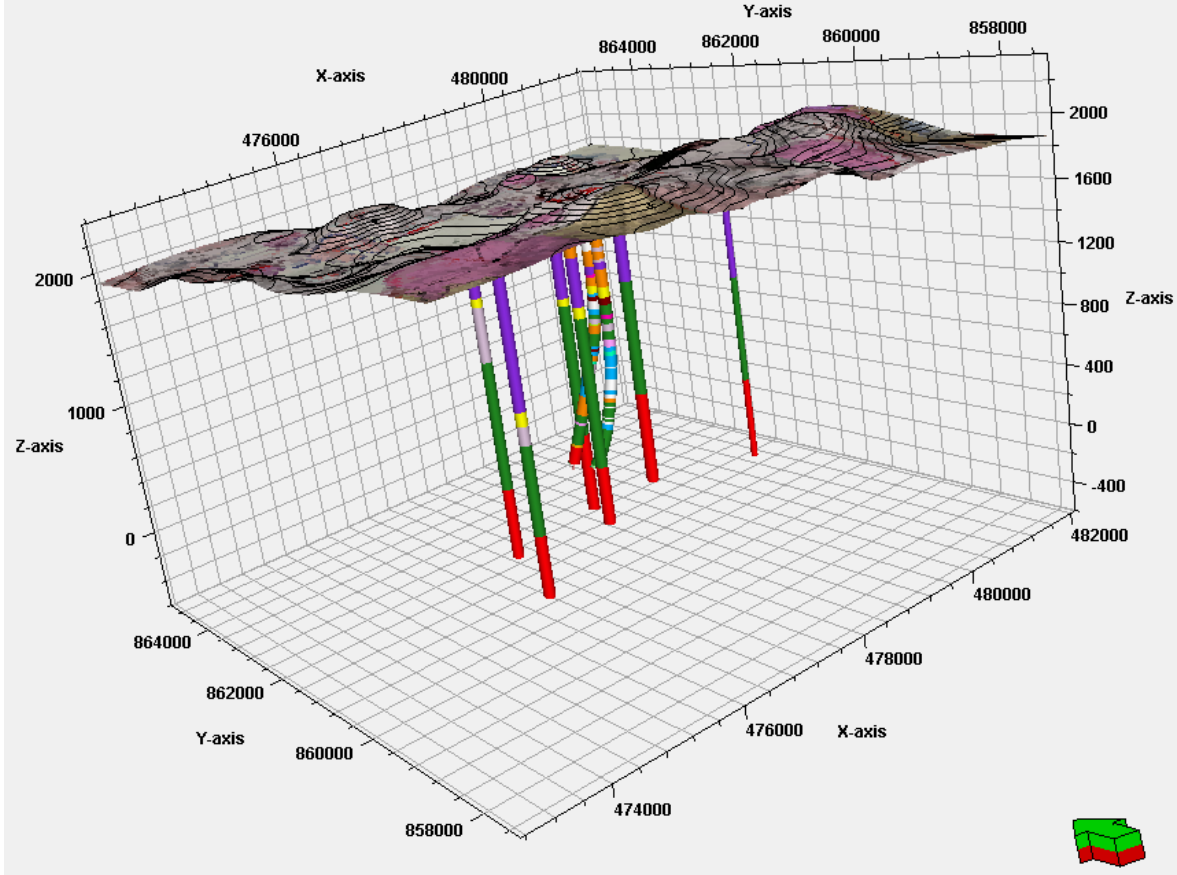


FIGURE 29: 3D view of topography map with wells (Green/red arrow is pointing north) (vertical exaggeration by factor 2x)

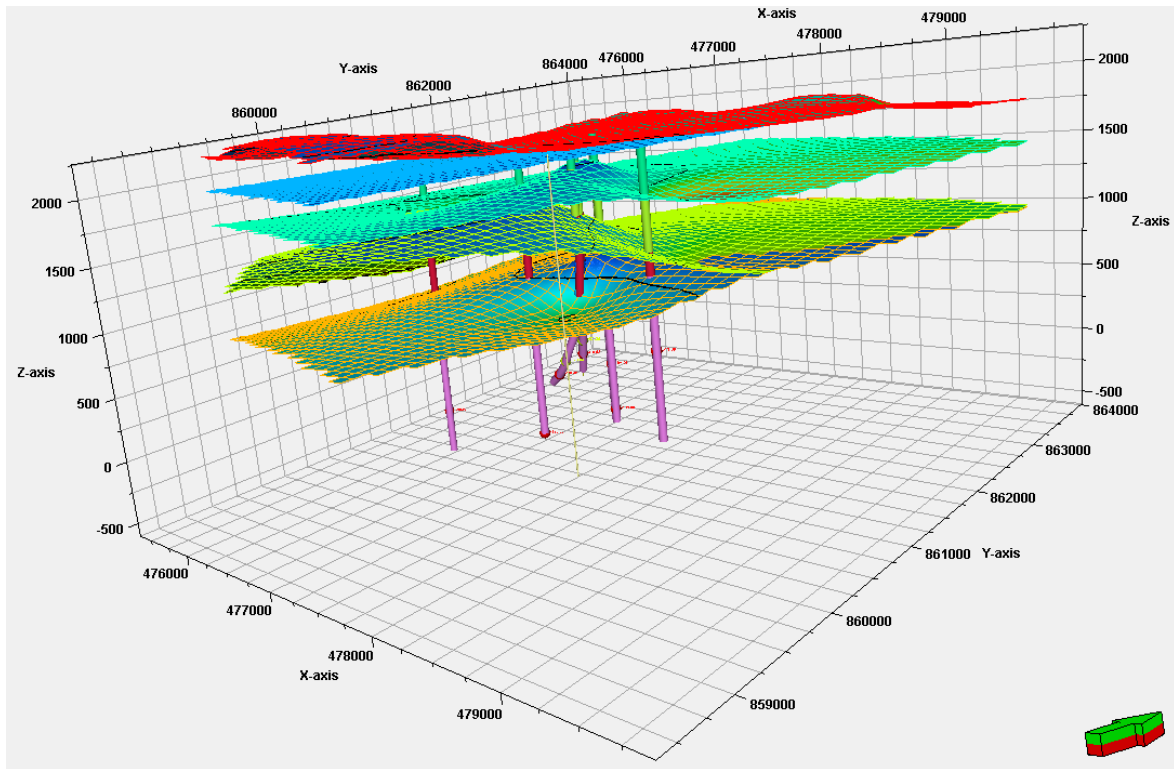


FIGURE 30: 3D view of alteration horizon with geothermal wells at Aluto Langanu geothermal field (vertical exaggeration by factor 1x) Green/red arrow is pointing to the north

30). The last step was creating a 3D property model and making a presentation of the model in both 2D and 3D visualization. The 3D property model was used to process and present the temperature and resistivity models of the geothermal area at Aluto-Langanu geothermal field (Figure 31 and 32).

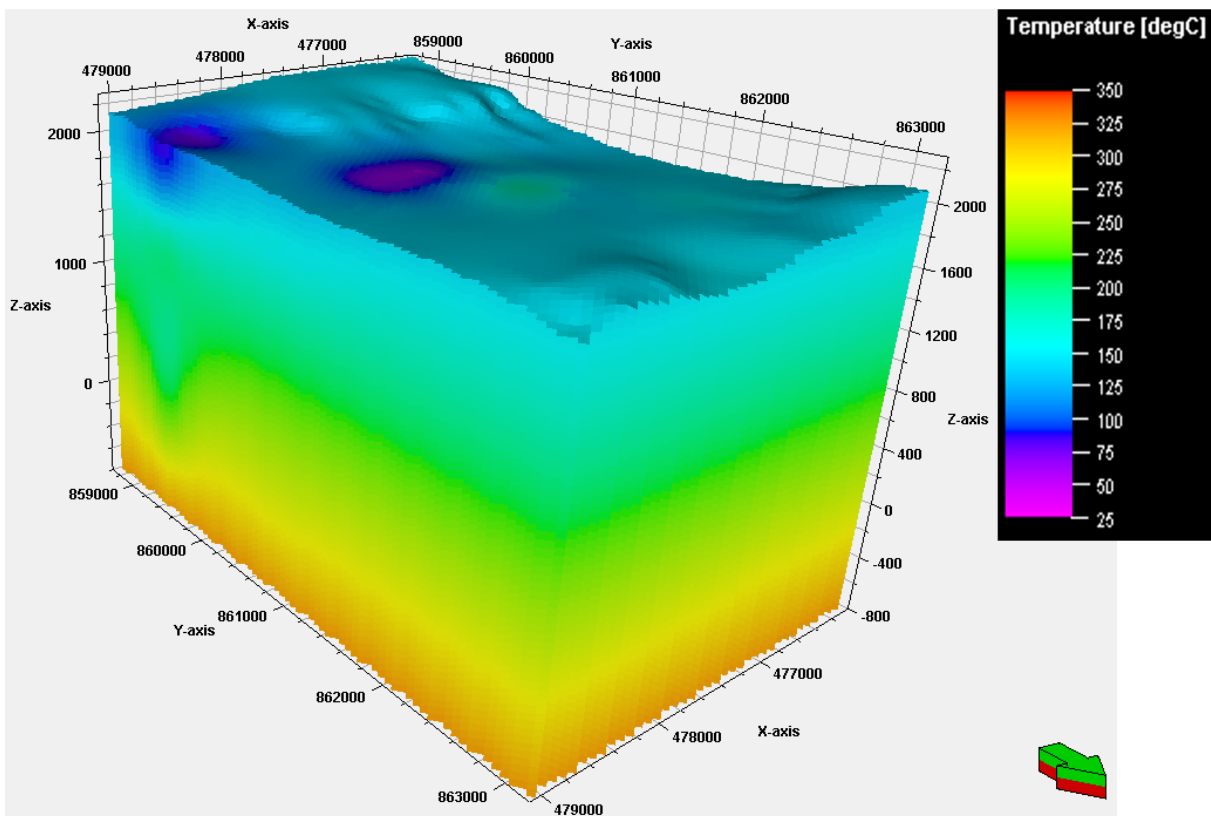


FIGURE 31: 3D property model of temperature at Aluto Langanu geothermal field

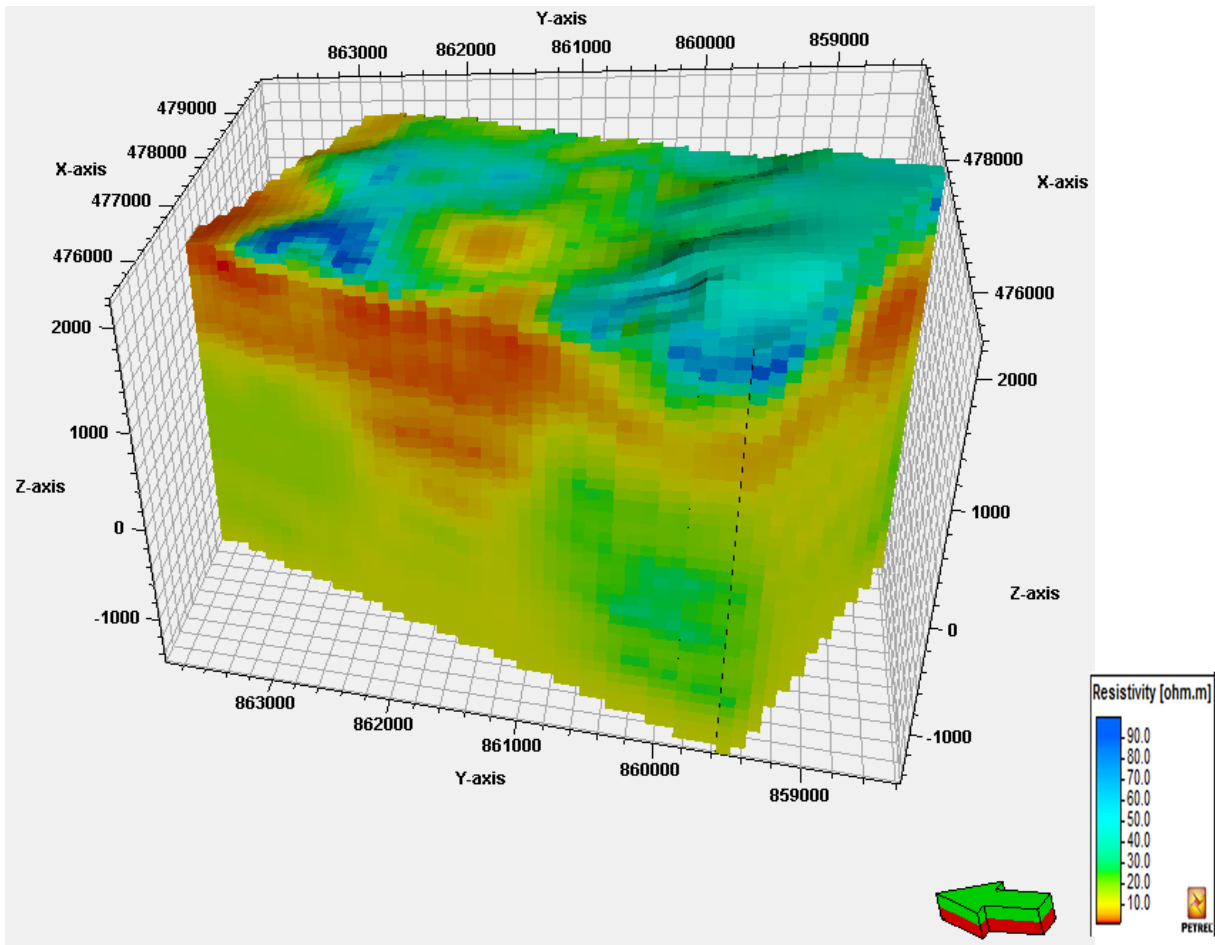


FIGURE 32: 3D property model of resistivity at Aluto Langanu geothermal field

5. DISCUSSION

5.1 Lithology

Aluto volcanic complex is a silicic peralkaline system and dominated by rhyolitic lava flows and domes, pumice cones and ignimbrite deposits (Electroconsult, 2016). In this study, the subsurface rock units were identified from directionally drilled wells such as LA-9D and LA-10D (Figure 33). The wells are located in the Aluto volcanic complex (AVC) together with six vertically drilled wells.

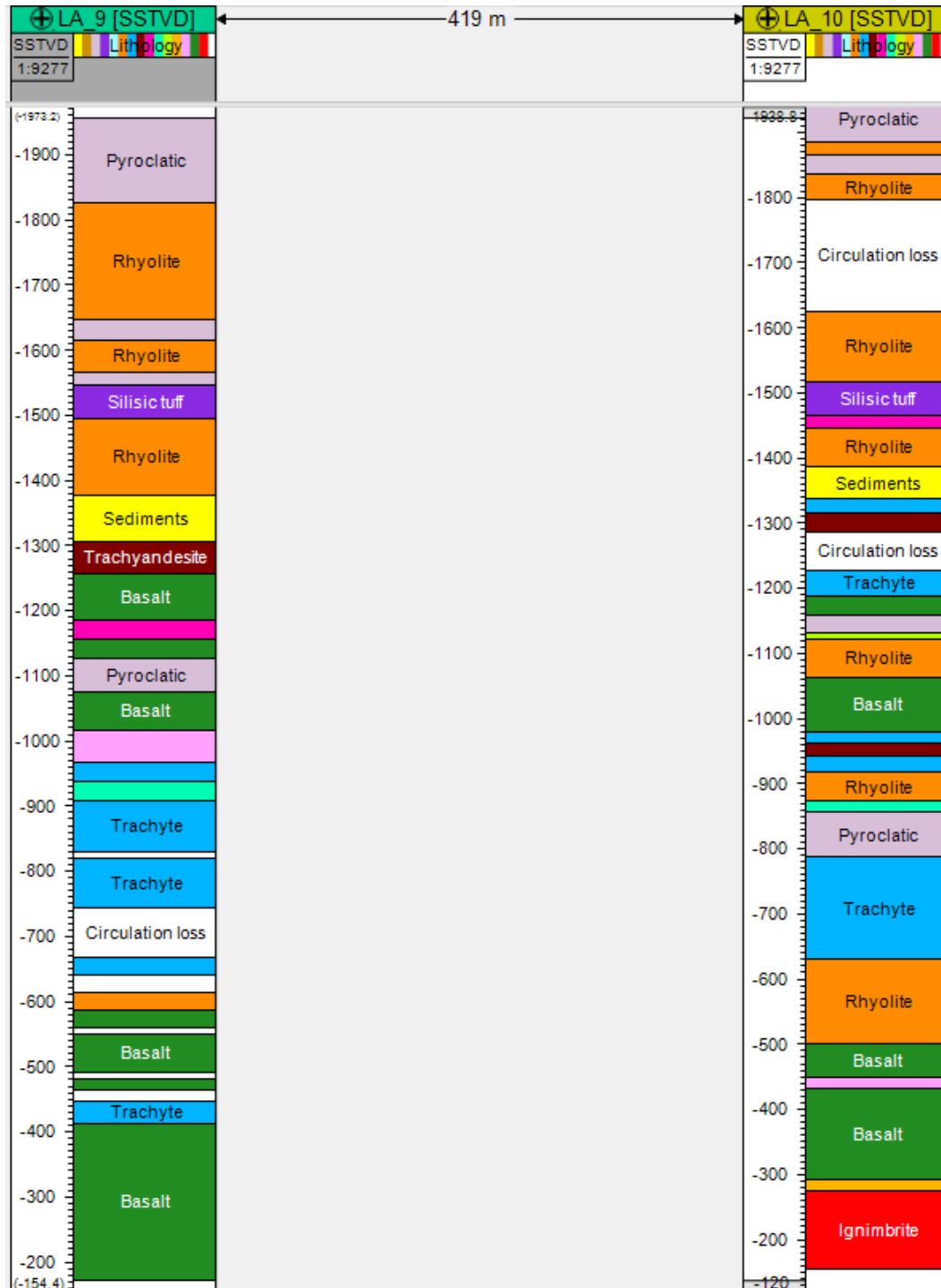


FIGURE 33: The rock units observed in well LA-9D and LA-10D, Aluto Langano geothermal field

The main lithology in the study wells are pyroclastics, silicic tuff and breccia, sediment, rhyolite, trachyte, basalt and ignimbrite. These rocks are identified and confirmed by binocular and petrography microscope.

Additionally, by ICP-OES analysis, rare transitional rock units were identified, such as trachyandesite, basaltic trachyandesite, trachydacite, basaltic andesite and andesite units. Most of the transition units show a range of medium to high alteration intensity, and are found as thin layers with intercalations of basalt and trachyte units. Ignimbrite is observed only in LA-10D wells. This might be due to the shallower depth of well LA-9D compared to the LA-10D well (Figure 34).

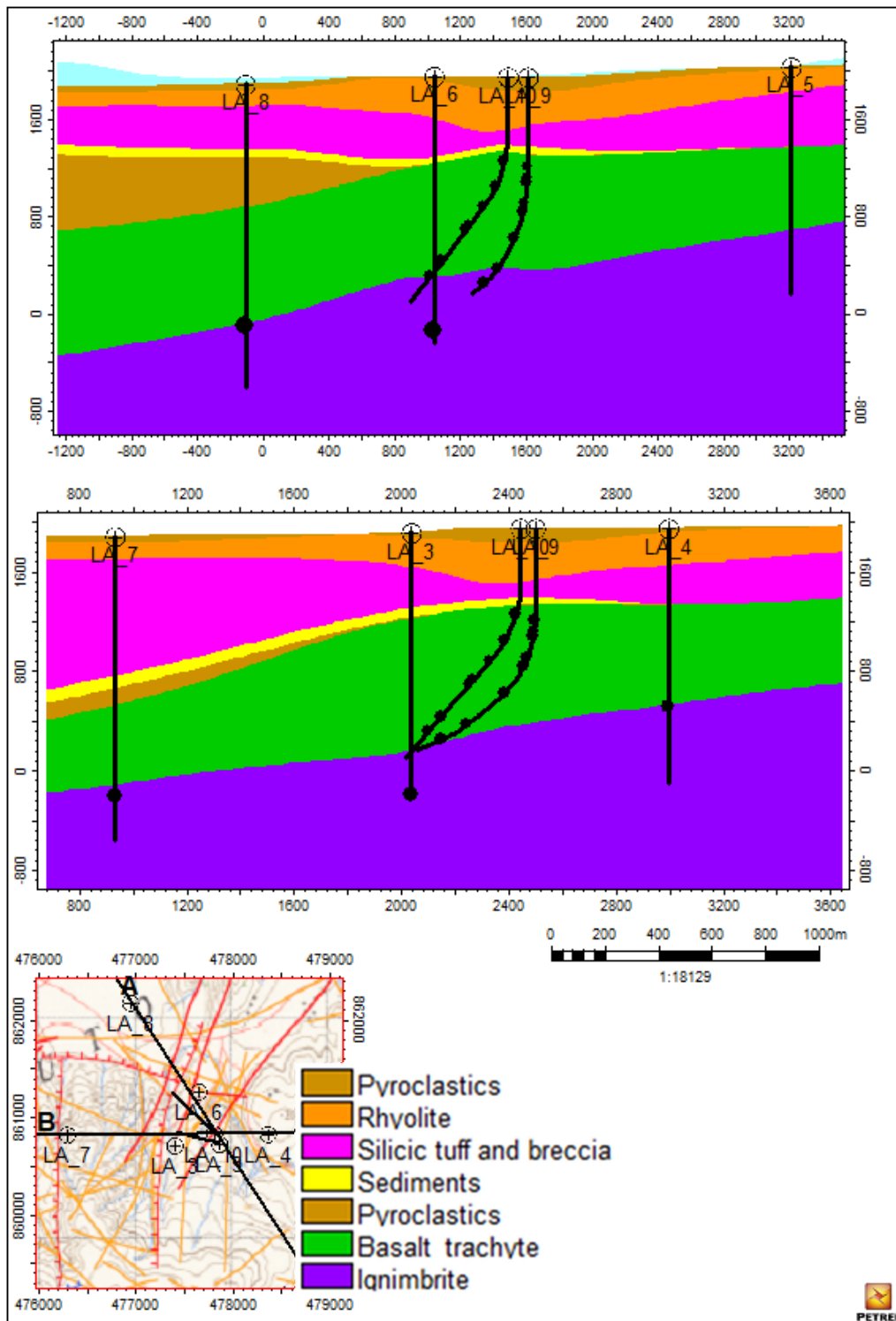


FIGURE 34: Main lithologies identified in Aluto Langanu geothermal fields (black dots represent aquifers)

From the wells in the southeastern part of the field and towards the wells in the northwestern part approximately 600 m of total displacement is observed within the Tertiary Ignimbrite formation and approximately 400 m total displacement within the Bofa basalts (Figure 35). The displacement is associated with at least three NNE-SSW trending faults, which are following the WFB trend. The displacement along the three faults indicate that a section of fault blocks is underlying the centre of up-flow in the geothermal field, but the fault blocks are dipping towards the west towards the centre of the MER.

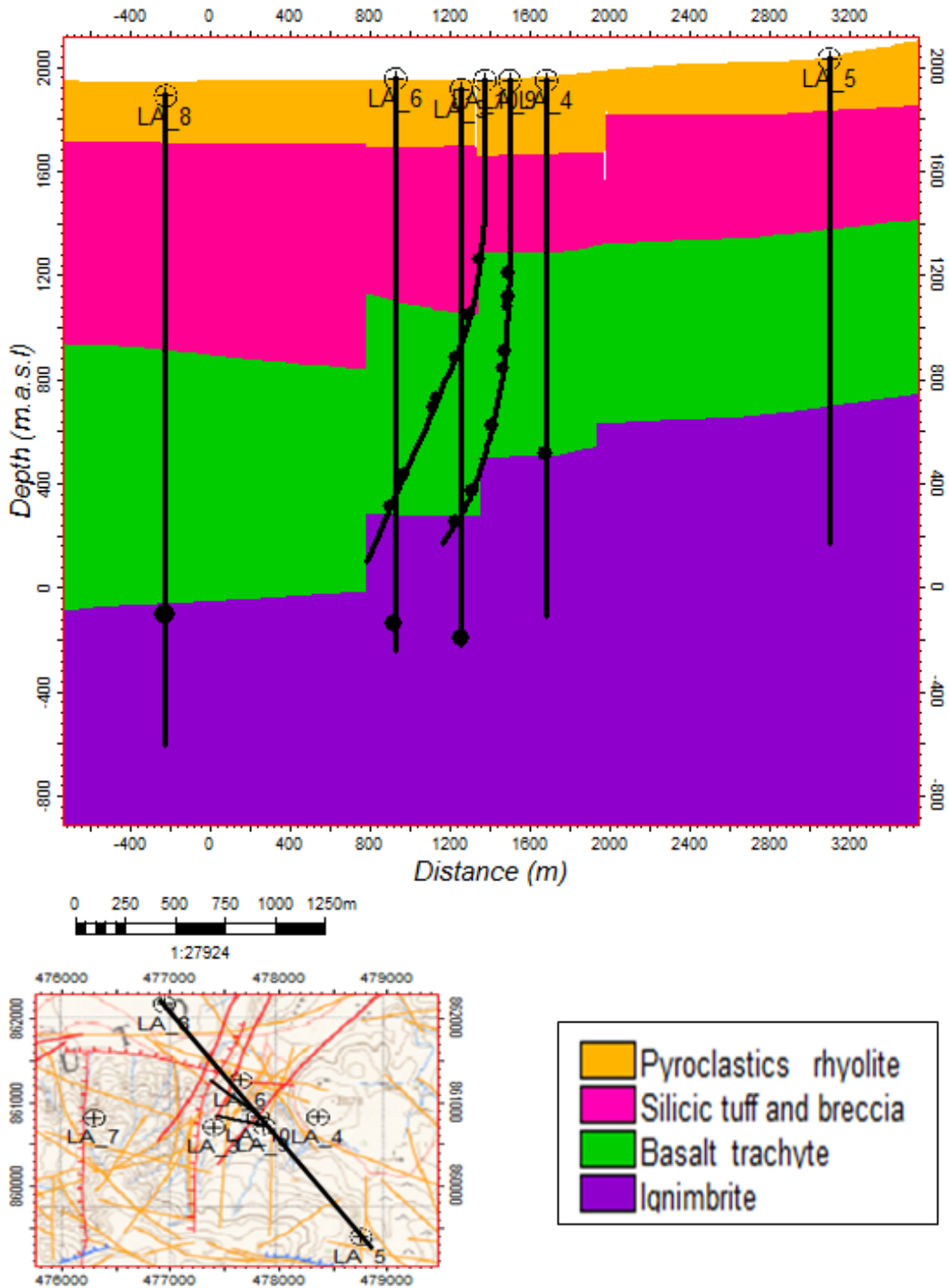


FIGURE 35: NW-SE cross-section through well field showing simplified stratigraphy and structural controls in Aluto Langanano geothermal fields (black dots represent aquifers and white broken lines indicate fault)

In Aluto Langano geothermal field a shallow permeable zone was usually encountered at a depth of 100-300 m which is a target for the shallow reinjection of residual water. The permeability in productive zone of the wells are associated lithological contacts within the Bofa basalt formation, the contact between the Bofa basalt and the Tertiary crystalline ignimbrite formation. Secondary permeability is related to the zone with the large NNW displaced fault blocks, which are located beneath the centre of the geothermal field, but it is likely to represent the zone of highest permeability.

Major and trace element analysis in the study wells indicates that the rocks are distributed continuously from basalt to trachyte/rhyolite composition. They have been plotted in a TAS diagram (Figure 25). Major elements versus SiO₂ and trace elements versus Zr indicate the effect of hydrothermal alteration on the rock chemistry. Except for K₂O, most of the major elements such as MgO, Al₂O₃, FeO, TiO₂, CaO and P₂O₅, show a negative correlation with SiO₂. On the other hand, Na₂O shows significant scattering and to a lesser extent FeO, K₂O and P₂O₅. This indicates that the hydrothermal processes have relatively small effects on the chemical composition of the subsurface rock sample from the study wells. The trace elements (Ba, Cr, La, Rb, Sr, Y and Sc) have been plotted versus Zr (Figure 27). Ba, Sr, Sc have a negative correlation with Zr, while Rb, Y and La showing a positive correlation with Zr. Rb showing significant scattering but Ba and Sr showing a geochemical trend which may indicated different groups.

5.2 Hydrothermal alteration

Various hydrothermal alteration minerals are observed in both LA-9D and LA-10D wells. The sequence of the alteration mineral deposition within the wells ranges from low-temperature to high-temperature minerals. The alteration minerals were found as replacement of primary minerals and as fillings of micro fractures, veins and vesicles in the rock units. The common primary minerals that are found in the study wells are volcanic glass (mostly found in pyroclastics, silicic tuff and breccia, to a lesser extent in rhyolite); scarce olivine is noted in the wells; pyroxene (mostly seen in basaltic rock units); sanidine (in trachytic units); plagioclase is the dominant primary mineral in most of the basaltic rock units, found as phenocrysts and in groundmass; and oxide minerals found together with alkali feldspar in groundmass.

Secondary hydrothermal alteration minerals were identified in the study wells. The minerals in the wells range from low-temperature minerals, such as chalcedony, siderite, haematite and smectite, to moderately high-temperature alteration minerals, such as mixed layer clay (MLC), illite, quartz, chlorite, epidote and actinolite. An abundance of calcite and pyrite is observed throughout the wells. It indicates that calcite and pyrite form at widely varying temperature and pressure. The abundance of calcite as vein and vesicle fillings indicates high partial pressure of CO₂ in geothermal fluid (Teklemariam,1986). The large quantity of calcite, pyrite and quartz found in the bottom parts of the wells indicates the presence of permeable zones in this part of the system. Epidote is a key index mineral related to temperature and fluid composition in geothermal systems. It is found together with quartz, illite and chlorite. Low-temperature minerals are in the upper 500 m of the wells, while the high-temperature minerals were observed below 500 m depth in both the study wells.

According to the abundance of secondary alteration minerals, the wells are divided in to four alteration zones. Unaltered zone is situated in well LA-9D and LA-10D at a depth of 0-120 m and 0-130 m, respectively. Smectite zone is at 120-500 m in LA-9D and 130-500 m in LA-10D. Illite/chlorite zone is located 500-1020 m in LA-9D and 500-860 m in LA-10D. The last alteration zone is the illite/chlorite/epidote zone, which is observed at 1080-1920 m in LA-9D and 860-1940 m in LA-10D. This division into alteration zones is defined by the first appearance of hydrothermal alteration minerals. The sequence of mineral deposition within wells shows that the hydrothermal system evolved from low to high temperature.

Based on temperature recovery data, alteration intensity, abundance of alteration minerals, lithology contacts and circulation loss data, feed zones were discovered in wells LA-9D and LA-10D. Eight feed zones were revealed in LA-9D, with one major feed zone at a depth of 1350 m and seven minor/small feed zones located at 760, 830, 940, 1000, 1140, 1640 and 1800 m depth. Most of the feed zones in this

well is located in basaltic unit. Well LA-10 has seven feed zones. The major one is found at a depth of 700 m and the six minor feed zones were discovered at 920, 1160, 1280, 1320, 1620 and 1760 m depth. Most of the feed zones are associated with high alteration intensity and medium to high abundance of calcite and pyrite minerals. In LA-10D, the feed zones are found in circulation zone, basalt and trachyte formations.

5.3 2D interpretation of hydrothermal alteration mineral zonation vs resistivity

The chemical property of minerals changes by water rock interaction, and thus changes occur in the mineralogy of the host rock. Primary minerals change or alter to secondary minerals due to temperature and chemical composition of the geothermal fluid. Alteration can be accelerated by the pH and composition of the hydrothermal fluid and result in alteration into clays and form other alteration minerals (Noor et al., 2012). At shallower depths, hydrothermal mineral assemblage can have an acidic nature (pH) with the presence of alteration minerals such as kaolin, smectite, quartz and pyrite. On the other hand, in the deeper parts of the geothermal system the hydrothermal fluid is typically neutral pH and the alteration minerals found in formations in the reservoir are epidote, calcite, chlorite and interlayer clays (Pri Utami, 2000). Four alteration zones are identified in Aluto Langanog geothermal field, which have been presented in a Chapter 4.6. The four alteration zones are also presented in a 2D model together with the resistivity model (Figure 36).

In Aluto Langanog geothermal field, MT resistivity surveys are used to identify and delineate the high-temperature geothermal system, and from the MT survey, the field is estimated to be 14 km² in size (Figure 12). The MT survey, is used to delineate the cap rock zone, which is indicated by low resistivity at shallow depth of the reservoir, but the resistivity of water saturated rocks is dependent on temperature, salinity of saturated fluid, porosity, conductivity of the rock matrix and thermal alteration (Árnason et al., 2000).

In some cases, the MT- survey may also outline structures, such as faults and fractures, due to its ability of ground penetration. The resistivity data from Aluto Langanog geothermal field was adopted Ernst & Young and ShinNihon, LLC (2010) and incorporated into the Petrel, 2015 software, where it was compared with alteration zone data from the wells (Figure 35). Two cross-sections with the hydrothermal alteration zones resistivity are presented in Figure 35. As described earlier four alteration zones were identified in the wells, except in well LA-3, where only three zones were detected.

A comparison of alteration mineral zonation and resistivity shows that from the surface down to approximately 2000-1520 m a.s.l., the formation is within the unaltered zone and is characterised by a high resistivity values, >40 ohmm. The approximate depth value of unaltered zone from wells LA-3 to LA-8 were taken from previous studies. Low resistivity <5 ohmm represents the formation of low-temperature clay minerals (smectite), but the smectite zone is at 1680-1040 m a.s.l. in well LA-8, 1680-1440 m a.s.l. in well LA-6, 1680-1520 m a.s.l. in well LA-9D, LA-10D and at 1720-1200 m a.s.l. in well LA-4 (Figure 36).

The smectite zone is at a similar depth as the low-resistivity cap outlined in the MT survey, but the low-resistivity zone outlines the cap rock of the geothermal reservoir, as well as the outer margin of the reservoir. Resistivity increases from moderate to high values of about 10-30 ohmm within the illite/chlorite zone. The illite/chlorite zone is located at various depth intervals, for example at LA-8 1120-960 m a.s.l., LA-6 1360-960 m a.s.l., LA-3 1600-880 m a.s.l., LA-7 1120-760 m a.s.l., LA-4 1200-1040 m a.s.l., LA-9D and LA-10D, 1520-1040 m a.s.l. The high-resistivity zone is located below 800 m a.s.l. with a resistivity value of >40 ohmm, but the high-resistivity zone corresponds to high-temperature alteration minerals like illite, chlorite and epidote. Within the high-resistivity zone high temperatures are observed, but the high-resistivity zone is assumed to outline the depth and extent of the high-temperature geothermal reservoir (Figures 36 and 39).

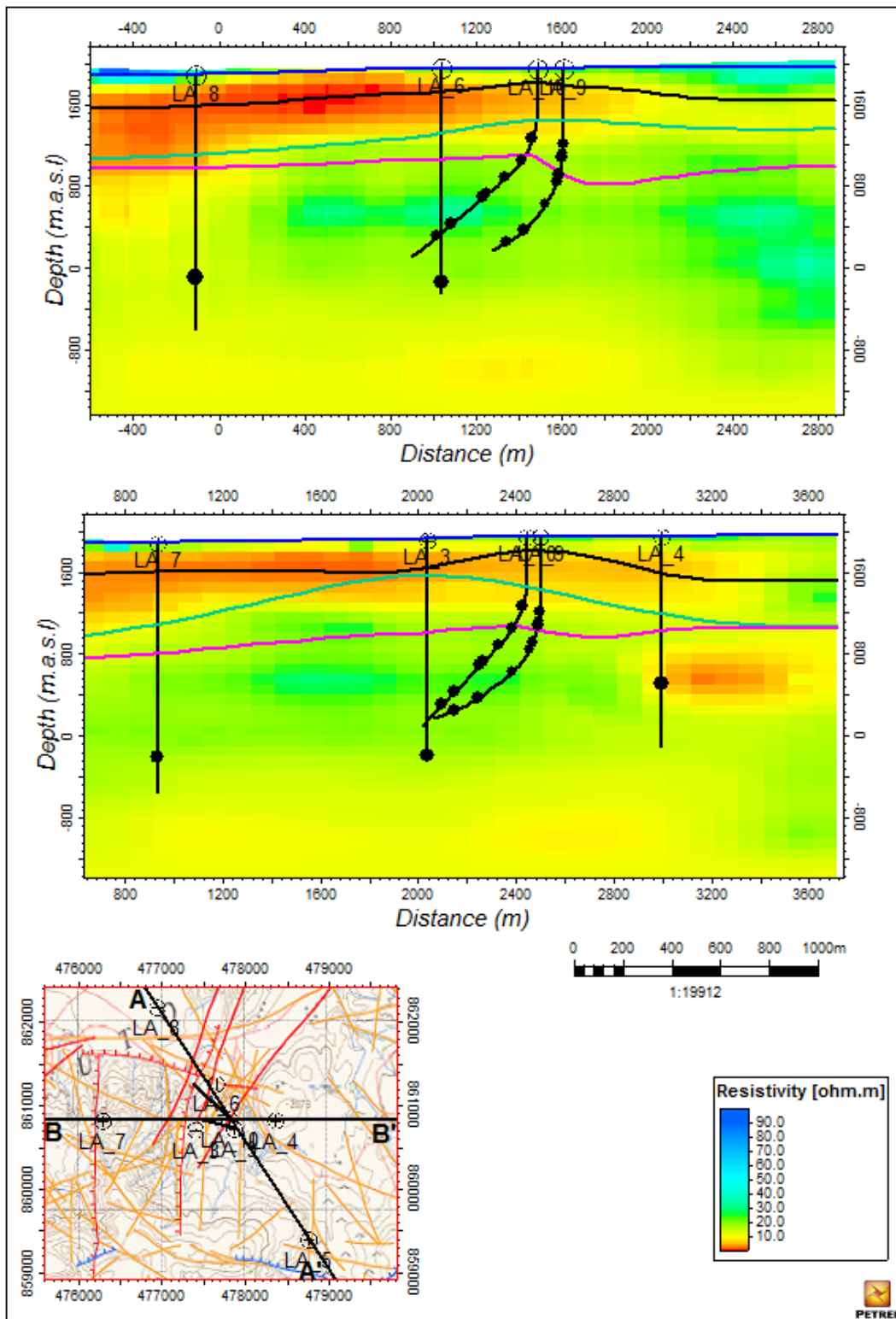


FIGURE 36: Cross-section of resistivity vs hydrothermal alteration zone. Uppermost figure shows cross-section A-A', while lower figure shows cross-section B-B'

Figure 37 shows a map of resistivity at 800 m a.s.l. in the geothermal field. The resistivity around the centre of the well field at well LA-3, LA-6, LA-9D and LA-10D is characterised by medium to high resistivity of ~30 ohmm, but this corresponds to the part of the field, where the highest temperatures have been recorded. Low resistivity, 5-15 ohmm, is observed towards the NW where well LA-7 and LA-8 are located and to the ENE where well LA-4 is located. Lower temperatures approximately 180-240°C have been observed below the production casing in all these three wells. Thus the lower resistivity

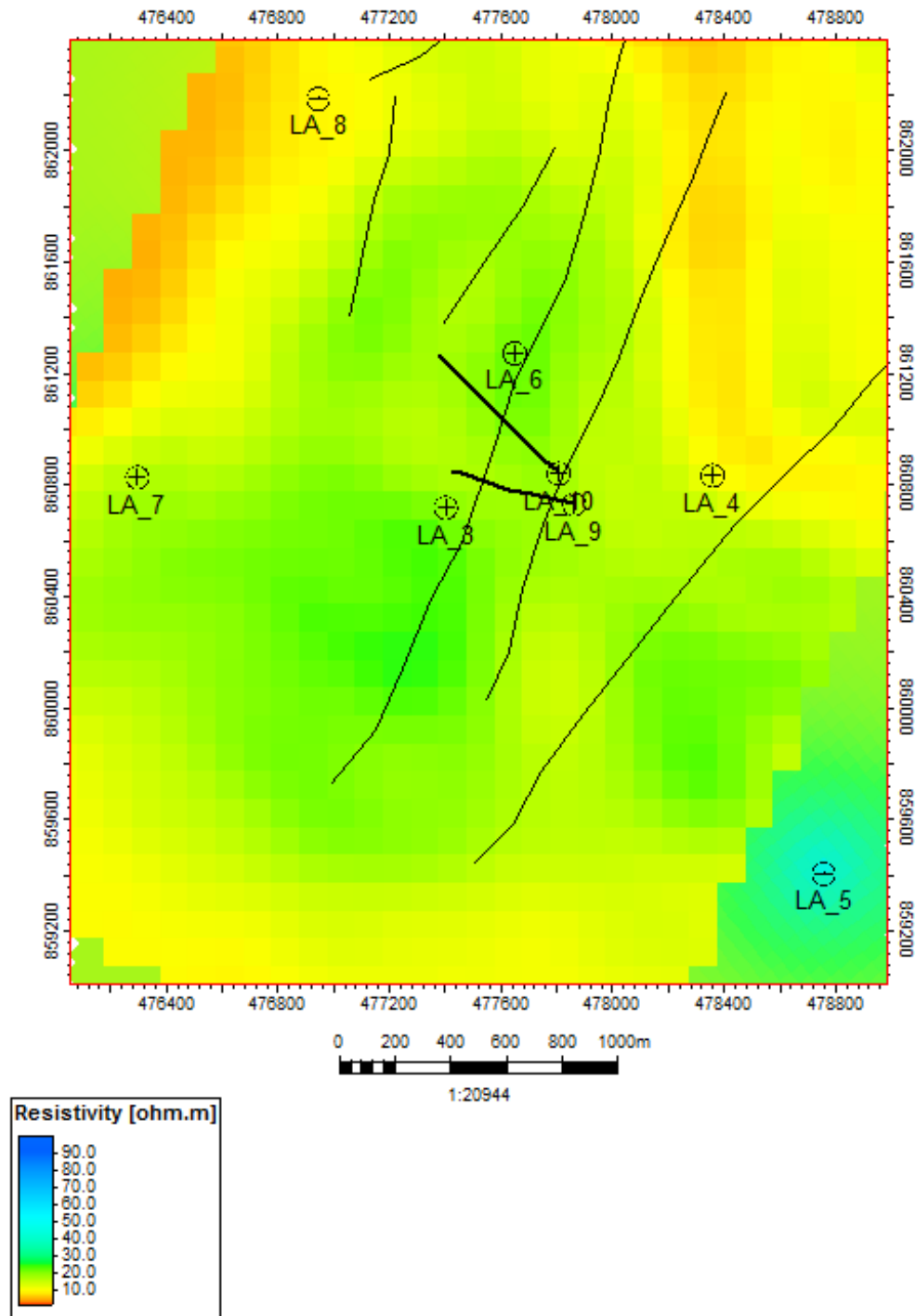


FIGURE 37: Resistivity data at 800 m a.s.l., Aluto Langanu geothermal field (black line indicating faults)

towards the NW and ENE seems to correspond to areas outside the main up-flow zone the geothermal field. The low resistivity in the NE part of the area near well LA-4 could be due to a fault structure, which is trending NNE-SSW as well as faults, associated with the caldera, while the lower resistivity in vicinity of well LA-7 and LA-8 may be associated with N-S trending faults observed at surface.

In wells LA-4 and LA-8 relatively low resistivity is recorded in the illite/chlorite/epidote zone (Figure 36). Thus the hydrothermal alteration in these wells indicate that temperatures have been higher in the past in this part of the field. The resistivity normally reflects the subsurface clay alteration, thus the difference between the alteration zones in well LA-4, LA-7 and LA-8 and the resistivity from MT-

surveys could possibly indicate that the resistivity from the MT-surveys are affected by other factors such as fractured zone with inflow of colder fluids.

According to the MT-resistivity survey a high resistivity core is centred along the NNE trending WFB faults, where the wells with highest temperature and permeability are located (LA-3, LA-6, LA-9D, LA-10D). The high resistivity anomaly extends from the centre of the well field towards the NNE and SSW along the trend of the WFB (Figure 37). This could have indicated that the up-flow zones extend along this zone of faulted blocks (Figure 35) to the NNW and SSE of the current well field and thus may represent promising areas for future drilling.

5.4 2D interpretation of formation temperature vs hydrothermal alteration mineral zonation

In geothermal fields, temperature is one of the major components defining the system. Typically, the temperature increases with depth in the up-flow zone of the geothermal system. However, in the periphery and in out-flow zones of geothermal reservoirs, temperature inversion can be observed, but cold recharge can cause temperature inversion.

The formation temperature of Aluto Langanu geothermal field has been measured during well logging, and the data imported to the Petrel software to produce a 3D model (Figures 23, 24 and 31). The distribution of formation temperature indicates that there is a narrow up-flow zone with high temperatures within the Aluto Langanu geothermal reservoir. According to the data interpretation and previous studies, the up-flow zone of the Aluto Langanu geothermal system is located beneath the LA-3, LA-6, LA-9D and LA-10D wells (Figure 38), but these wells are all located within the Wonji Fault Belt (WFB).

The temperature recorded in the upper part of the wells from surface to 2000-1840 m a.s.l. is $<50^{\circ}\text{C}$ and correlates with the unaltered zone. Temperature is slowly increasing below the unaltered zone, but the temperature change varies from well to well (Figure 38). The highest temperature at this depth is observed in wells LA-3 and LA-6, which are located above the up-flow zone. At 1840 -1260 m a.s.l., temperature is $75\text{-}150^{\circ}\text{C}$ and the formation is characterized by slight to moderate alteration of minerals. The smectite alteration zone is dominant at 120-500 m depth, which is consistent with the observed temperature. According to the information from formation temperature and resistivity data, this zone represents the cap rock of the geothermal system. Below the smectite zone, temperature increases from $180\text{-}250^{\circ}\text{C}$ at a depth interval of approximately 1200-960 m a.s.l. in the wells. In this temperature and depth interval, illite and chlorite are the dominant hydrothermal alteration minerals. The top of the illite/chlorite zone is marked with a green line zone (Figures 38 and 39). High temperature of $>250^{\circ}\text{C}$ are recorded in wells LA-3, LA-6, LA-8, LA-9D and LA-10D within the illite/chlorite/epidote zone.

The illite/chlorite/epidote zone is found at similar depth in wells LA-3 to LA-10, but it appears below 960 m a.s.l. to the bottom of these wells. The illite/chlorite/epidote zone is marked by the first appearance of epidote. Temperature in wells LA-4, LA-5 and LA-7 is $<250^{\circ}\text{C}$. In these wells, the high-temperature alteration minerals (illite/chlorite/epidote) were observed, which implies that higher temperature has existed in the past in this area of the geothermal reservoir.

The Aluto Langanu geothermal field is a water dominated, gas rich system with high reservoir temperatures ranging from 260 to $>335^{\circ}\text{C}$. In the Aluto Langanu geothermal field, the heat source is associated with magmatism associated with Aluto volcanic complex, but an obsidian flow and pumice breccia are recorded as the youngest eruption products at the age of 2000 years (Electroconsult, 1986). Meteoric water is the reservoir fluid that have penetrated through the ground from the Eastern escarpment of the rift. The water is heated by conductive process from the magmatic heat source.

Basalt and ignimbrite formations form the reservoir rocks in the system. The cap rocks that overlie the reservoir are sediments and rhyolites, intercalated with pyroclastics. The movement and up-flow of a deep hot fluids, its controlled by NNE-SSW trending faults of the WFB (Figure 39), but the up-flow zone is within a zone of NNW dipping faulted blocks with a total displacement of up to 400-600 m within the ignimbrite and basalt formations.

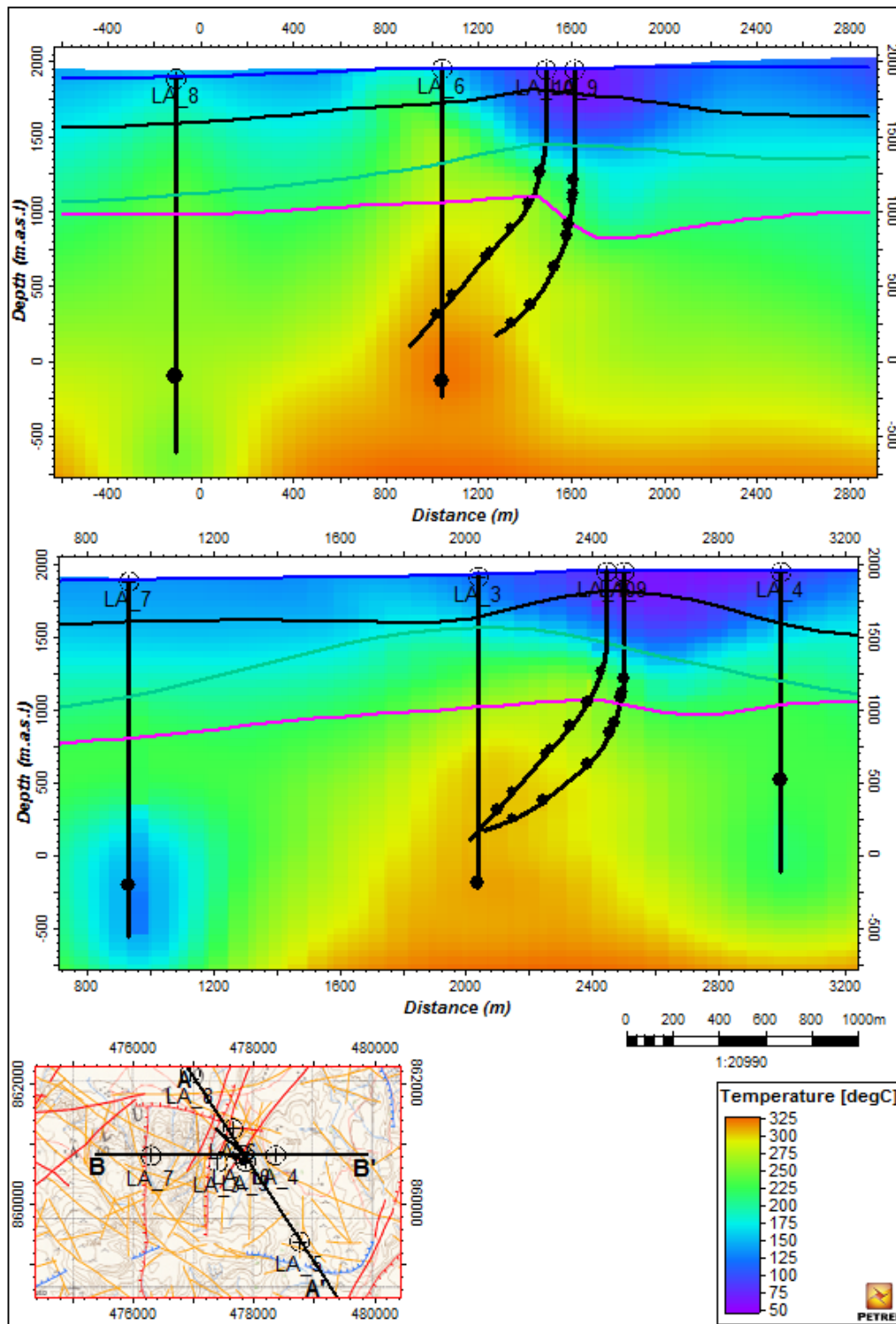


FIGURE 38: Cross-section of formation temperature vs. hydrothermal alteration zone; uppermost figure shows cross-section A-A', lower figure shows cross-section B-B'

To the ENE and NW of the main up-flow temperature reversal is observed, which could be related N-S trending faults in the NW part of the field, while the temperature reversal in the ENE part of the field may be associated with caldera faults. The main up-flow zone in Aluto-Langano geothermal field is narrow and appears to be controlled by a NNE-SSW trending fault zone characterised by NNW dipping faulted blocks. In the geothermal reservoir a high temperature gradient is observed perpendicular to the trend of the WFB. As the up-flow zone appears to be strongly controlled by NNE trending faults of the WFB, future expansion of the well field should consider gradual expansion towards the NNE and SSW along the trend of the WFB.

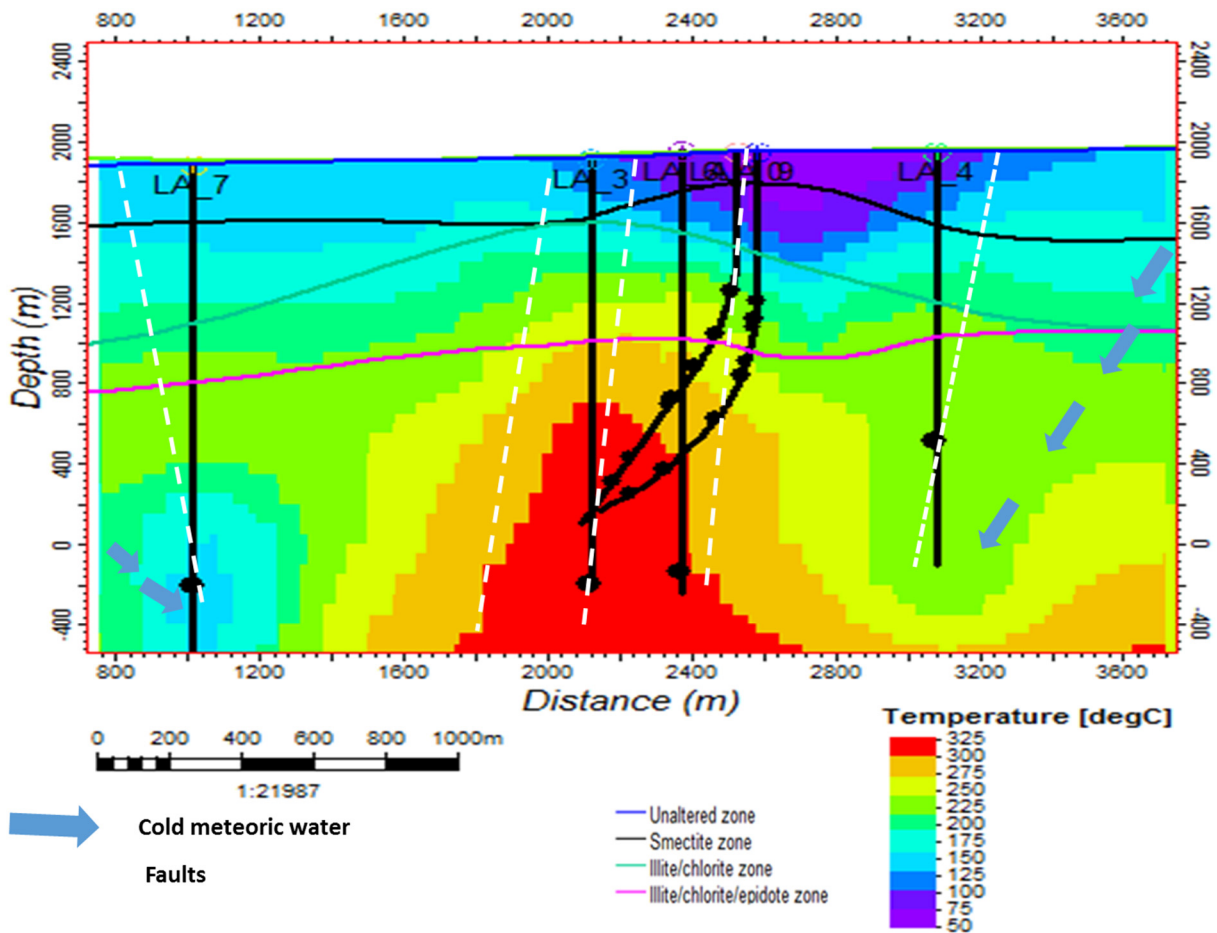


FIGURE 39: Conceptual model of Aluto Langano field in relation to alteration mineral zones and formation temperatures

6. CONCLUSION AND RECOMMENDATIONS

6.1 Conclusions

- The major rock units identified in the study wells LA-9D and LA-10D are pyroclastics, silicic tuff and breccia, sediment, rhyolite, trachyte, basalt and ignimbrite.
- The petrochemistry analysis shows that the rock composition in LA-9D and LA-10D ranges from basalt through intermediate rocks to trachyte or rhyolite compositions. Scarcity of transitional rock units are noted. Intermediate compositions should be noted with caution as they may possibly be caused by mixing of drill cuttings in the wells.
- Low to high temperature hydrothermal alteration minerals are observed in the study wells. The common alteration minerals are siderite, haematite, chalcedony, smectite, quartz, mixed layer clays, illite, chlorite and epidote.
- Four alteration zones are identified by the abundance and first appearance of alteration minerals, namely an unaltered zone, smectite zone, illite/chlorite zone and illite/chlorite/epidote zone.
- Alteration minerals, depositional sequences and formation temperature indicated that the wells (LA-9D and LA-10D) are heating up.
- The abundance of calcite and pyrite is observed throughout the wells, indicates the presence of permeable zones in the well.
- Eight feed zones were identified in well LA-9D and seven in LA-10D, which are related to lithological boundaries within the Bofa basalt formation and between the Bofa basalt and Tertiary Ignimbrite formation, as well as faults related to the NNE trending WFB.
- Major and trace elements data show that the effects of hydrothermal alteration have relatively small significant effect on the rock chemistry of the study wells.
- Basalt and Ignimbrite formations form the reservoir rocks of the Aluto-Langano geothermal system. The cap rocks that overlie the reservoir are sediments and rhyolites, intercalated with pyroclastics.
- The upflow zone in Aluto-Langano geothermal field is narrow and structurally controlled by a NNE-SSW trending fault zone of the WFB, which is characterised by NNW dipping faulted blocks.
- To the ENE and NW of the main up-flow temperature reversal is observed, which could be related N-S trending faults in the NW part of the field, while the temperature reversal in the NE part of the field may be associated with caldera faults.
- Lower temperatures to the ENE and NW of the main up-flow zone also suggests that the NNE-SSW trending fault zone of the WFB acts as a hydrological barrier.

6.2 Recommendations

By using 3D modelling, siting of further wells can be achieved in conjunction with more detailed geological and structural mapping in the proposed drilling area.

The conceptual model of the Aluto-Langano Geothermal field presented here is based only on geological mapping, well data and MT resistivity surveys. A more complete conceptual model can be achieved through further incorporation of geochemical data and data from other geophysical surveys e.g. seismic monitoring, gravity surveys and surveys of magnetic susceptibility.

Detailed fluid inclusion studies need to be carried out, specifically in wells LA-9D and LA-10D to supplement information about alteration and measured formation temperatures, to understand the evolution of the geothermal system.

Detailed surface and borehole petrochemical studies in Aluto Langano geothermal field are highly recommended to understand the geochemical evolution of the rocks.

Radiogenic isotope analysis of Sr, Nd and Hf on end-members (basalt and rhyolite) are needed to distinguish between magma sources and different magma evolution processes of the rock series.

REFERENCES

- Abebe, T., F. Mazzarini, F. Innocenti, and P. Manetti, 1998: The Yerer-Tullu Wellel volcanotectonic lineament: A transnational structure in central Ethiopia and the associated magmatic activity, *J. Afr. Earth Sci.*, 26, 135-150.
- Acoccela, A., Korme, T., and Salvini, F., 2002: Formation of normal faults along the axial zone of the Ethiopia Rift. *J. Structural Geology*, 25, 503-513.
- Agostini, A., Bonini, M., Corti, G., Sani, F., and Mazzarini, F., 2011: Fault architecture in the Main Ethiopian Rift and comparison with experimental models: Implications for rift evolution and Nubia-Somalia kinematics. *Earth and Planetary Science Letters*, 301, 479–492.
- Alemu, T., 2012: *Geology of Ethiopia*. Ethiopian Geological Survey, Addis Ababa, Ethiopia.
- Árnason, K., Karlsdóttir, R., Eysteinnsson, H., Flóvenz, Ó.G., and Gudlaugsson, S.Th., 2000: The resistivity structure of high-temperature geothermal systems in Iceland. *Proceedings of the World Geothermal Congress 2000, Kyushu-Tohoku, Japan*, 923-928.
- Bendick, R., Bilham, R., Asfaw, L., and Klemperer, S., 2006: Distributed Nubia-Somalia relative motion and dyke intrusion in the main Ethiopian rift. *Geophysical J. International*, 165, 303–310.
- Bonini, M., Corti, G., Innocenti, F., Manetti, P., Mazzarini, F., Abebe, T., and Pecsckay, Z., 2005: Evolution of the Main Ethiopian Rift in the frame of Afar and Kenya rifts propagation. *Tectonics*, 24-1.
- Corti, G., 2009: Continental rift evolution: From rift initiation to incipient break-up in the Main Ethiopian Rift, East Africa. *Earth-Science Reviews*, 96, 1–53.
- Corti, G., Philippon, M., Sani, F., Keir, D., and Kidane, T., 2013a: Re-orientation of the extension direction and pure extensional faulting at oblique rift margins: Comparison between the Main Ethiopian Rift and laboratory experiments. *Terra Nova*, 25, 396–404.
- Ebinger, C., 2005: Continental break-up: The East African perspective. *Astronomy and Geophysics*, 46, 16–21.
- Ebinger, C., Yemane T., WoldeGabriel G., Aronson J., and Walter R., 1993: Eocene-Recent volcanism and faulting in the southern Main Ethiopian rift. *J. Geol. Soc. London*, 150, 99-108.
- Electroconsult, 1986: *Exploitation of Aluto-Langano geothermal resources, feasibility report, Geothermal Exploration Project, Ethiopian Lake District Rif*. ELC, Milan, Italy, 289 pp.
- Electroconsult, 2015: *Geothermal surface exploration in Aluto Langano, Ethiopia*. ELC, Milano, Italy, report.
- Electroconsult, 2016: *Gravimetric report in Aluto Langano area, Ethiopia*. ELC, Milano, Italy.
- Endeshaw, A., 1988: Current status of geothermal exploration in Ethiopia. *Geothermics*, 17, 477–488.
- Ernst & Young and ShinNihon, LLC, 2010: Study on geothermal power development project in the Aluto Langano Field, Ethiopia. Japan External Trade Organization (JETRO).
- Franzson, H., 1998: Reservoir geology of the Nesjavellir high-temperature field in SW-Iceland. *Proceedings of the 19th Annual PNOC-EDC Geothermal Conference, Manila*, 13-20.
- Hou, X., and Jones, T.B., 2000: *Inductively coupled plasma/optical emission spectrometry*. Wake Forest University, Winston-Salem, NC, USA.

Hutchison, J.W., Mather, T.A., Pyle, D.M., Biggs, J., and Yirgu, G., 2015: Structural controls on fluid pathways in an active rift system: A case study of the Aluto volcanic complex. *Geosphere*, 11-3, 542-562.

Kazmin, V., 1980: Transform faults in the East African Rift system. *Atti Convegna Lincei*, 47, 65-73.

Kazmin, V., Berhe, S.M., Nicoletti, M., and Pertucciani, C., 1980: Evolution of the northern part of the Ethiopian rift. *Atti Convegna Lincei*, 47, 275-292.

Kebede, S., 2012: Geothermal exploration and development in Ethiopia: Status and future plan. *Presented at Short Course VII on Exploration for Geothermal Resources, organized by UNU-GTP, GDC and KenGen, at Lake Bogoria and Lake Naivasha, Kenya*, 16 pp.

Kebede, Y., Kebede, S., Teklemariam, M., and Amdeberhan, Y., 2002: *Compiled summary report on Aluto-Langano*. Geothermal Survey of Ethiopia, Addis Ababa, report.

Kebede, S., Mamo, T., and Abebe, T., 1984: *Geothermal exploration project Lakes district*. Geological Survey of Ethiopia, Addis Ababa, report.

Kebede, S., Travi, Y., Asrat, A., Alemayehu, T., Ayenew, T., Tessema, Z., 2008: Groundwater origin and flow along selected transects in Ethiopian rift volcanic aquifers. *Hydrogeology Journal*, 16, 1431–2174.

Keir, D., Ebinger, C.J., Stuart, G.W., Daly, E., and Ayele, A., 2006: *Strain accommodation by magmatism and faulting as rifting proceeds to breakup: Seismicity of the northern Ethiopian rift*. *J. Geophysical Research*, 111, 1-17.

Koestono, H., 2010: *Lahendong geothermal field, Indonesia: Geothermal model based on wells LHD-23 and LHD-28*. University of Iceland, Reykjavik, MSc thesis, UNU-GTP, Iceland, report 3, 90 pp.

Kristmannsdóttir, H., 1979: Alteration of basaltic rocks by hydrothermal activity at 100-300°C. In: Mortland, M.M., and Farmer, V.C. (editors), *International Clay Conference 1978*. Elsevier Scientific Publishing Co., Amsterdam, 359-367.

Lagat, J., 2009: Hydrothermal alteration mineralogy in geothermal fields with case examples from Olkaria domes. *Paper presented at Short Course IV on Exploration for Geothermal Resources, organized by UNU-GTP, KenGen and GDC, Naivasha, Kenya*, 24 pp.

Laury, R.L., and Albritton, C. Jr., 1975: Geology of middlestone age archeological sites in the Main Ethiopian Rift Valley. *Geol. Soc. of Am. Bull.*, 86, 999-1011.

Le Bas, M.J., Le Maitre, R.W., Streckeisen, A., and Zanettin, B., 1986: A chemical classification of volcanic rocks based on the total alkali-silica diagram. *J. Petrology*, 27-3, 745-750.

Lloyd, E.F., 1977: *Geological factors influencing geothermal exploration in the Langano region, Ethiopia*. NZ Geological Survey, Rotorua, NZ, unpubl. report, 73 pp.

Macdonald, R., 1974: Nomenclature and petrochemistry of the peralkaline oversaturated extrusive rocks. *Bulletin Volc.*, 38, 498-516.

Mbia, P., 2014: *Sub-surface geology, petrology and hydrothermal alteration of Menengai geothermal field, Kenya*. University of Iceland, MSc thesis, UNU-GTP. Iceland, report 1, 99 pp.

Mohr, P., 1962: The Ethiopian Rift System. *Bull. Geophys. Obs., Addis Ababa*, 5, 33–62.

- Mohr, P., 1983: Volcanotectonic aspects of the Ethiopian Rift evolution. *Bulletin Centre Recherches Elf Aquitaine Exploration Production*, 7, 175–189.
- Molin, P., and Corti, G., 2015: Topography, river network and recent fault activity at the margins of the. *Tectonophysics*, 664, 67-82.
- Munsonye, X.S., 2015: *Sub-surface petrochemistry, stratigraphy and hydrothermal alteration of the domes area. Olkaria geothermal field, Kenya*, University of Iceland, MSc thesis, UNU-GTP, report 3, 100 pp.
- Noor, Y., Suwaili, J., and Kangogo, D., 2012: Correlating resistivity with temperature and alteration mineralogy in Menengai geothermal field, case study of Menengai well MW-01. *Proceedings of the ARGeo-C4 Conference, Nairobi, Kenya*, 6 pp.
- Paola, G.M., 1986: *Development of geothermal resources*. United Nations, NY.
- Pri Utami, 2000: Characteristics of the Kamojang geothermal reservoir (West Java) as revealed by its hydrothermal alteration mineralogy. *Proceedings of the World Geothermal Congress 2000, Kyushu-Tohoku, Japan, 1921-1926*.
- Peccerillo, A., Donati, C., Santo, A., Orlando, A., Yirgu, G., and Ayalew, D., 2007: Petrogenesis of silicic peralkaline rocks in the Ethiopian. *ScienceDirect*, 13.
- Reimann, C., Bjorvatn, K., Frengstad, B., Melaku, Z., Tekle-Haimanot, R., and Siewers, U., 2003: Drinking water quality in the Ethiopian section of the East African Rift Valley – data and health aspects. *Science of the Total Environment*, 311, 65-80.
- Reyes, A.G., 1990: Petrology of Philippine geothermal systems and the application of alteration mineralogy to their assessment. *J. Volcanic & Geoth. Res.*, 43, 279-309.
- Reyes, A.G., 2000: *Petrology and mineral alteration in hydrothermal systems: from diagenesis to volcanic catastrophes*. UNU-GTP, Iceland, report 18-1998, 77 pp.
- Ring, U., 2014: The East Africa Rift System. *Austrian J. Earth Science*, 132-146.
- Schlumberger, 2010: *Petrel introduction course*. Schlumberger, 493 pp.
- Stamps, D.S., Calais, E., Saria, E., Hartnady, C., Nocquet, J.-M., Ebinger, C.J., and Fernandes, R.M., 2008: A kinematic model for the East African Rift. *Geophysical Research Letters*, 35-5.
- Tadesse, S., Milesi, J.P., and Deschamps, Y., 2003: Geology and mineral potential of Ethiopia: a note on geology and mineral map of Ethiopia. *Journal of African Earth Sciences*, 36, 273-313.
- Tassew, M., 2015: Expansion work and experience gained in operation of Aluto Langano geothermal power plant. *Proceedings of the World Geothermal Congress 2015, Melbourne, Australia*, 6 pp.
- Teclu, A., 2004: *Geochemical study of the Aluto-Langano geothermal field, and the surrounding areas*. Geothermal Survey of Ethiopia, Addis Ababa, report.
- Teklemariam, M., 1985: *Hydrothermal alteration in LA-3, LA-4 and LA-6 Langano-Aluto, Ethiopia*. UNU-GTP, Iceland, report 9, 53 pp.
- Teklemariam, M., 1986: Petrography of the cores and cutting samples from wells LA-3, 4, 5 and 6. Aluto-Langano, Ethiopia. Geological Survey of Ethiopia, Addis Ababa, report.

Teklemariam, M., 1996: *Water-rock interaction process in the Aluto- Langano geothermal field*. University of Pisa, Italy, PhD thesis, 295 pp.

Teklemariam, M., Battaglia, S., Gianelli, G., and Ruggieri, G., 1996: *Hydrothermal alteration in the Aluto Langano geothermal field, Ethiopia*. Pisa, Italy. *Geothermics*, 25-6, 679-702.

Teklemariam, M., and Beyene, K., 2000: *Geochemical monitoring of the Aluto-Langano geothermal field, Ethiopia*. Geological Survey of Ethiopia, Addis Ababa, report.

UNDP, 1986: *Development of geothermal resources Ethiopia*. UNDP, report.

WoldeGabriel, G., Aronson, J.L., Walter, R.C., 1990: Geology, geochronology, and rift basin development in the central sector of the Main Ethiopia Rift. *Geol. Soc. Am. Bull.*, 102, 439–458.

Zanettin, B., Justin-Visentin, E. Nicoletti, M., and Petrucciani, C., 1978: Evolution of the Chench escarpment and the Ganjiuli graben (Lake Abaya) in the southern Ethiopian rift. *Nues. Jahrb. Geol. Paleontol. Monatsh.* 8, 473 – 490.

APPENDIX I: Description of stratigraphy for well LA-9D as observed under binocular and petrography microscope analysis

10-130 m Pyroclastics. Light grey to yellowish, fine to medium grained rock sample. Slightly altered rock sample and hint of oxidation is noted. It contains crystalline rhyolite showing flow bands with spherulitic texture, slightly vesicular pumice breccia and dark grey to black obsidian. The amount of pumice and siliceous material increases from depth of 40-100 m. Alteration minerals: haematite, siderite, feldspars, kaolinite chalcedony, primary quartz and fresh glass.

140-310 m Rhyolite. Light grey to brownish and light greenish colour, aphanitic to porphyritic texture, slightly to moderately altered rock sample. Some vesicles are filled with silica and chalcedony at the depth of 260 and 280m; and vesicles are observed at 250, 260, 270 and 280 m depth. The rock shows hint of oxidation. Fragments of fresh and silicified obsidian, pumice breccia and siliceous material also noted in the sample. Alteration minerals: pyrite, chalcedony, siderite, quartz, chlorite, smectite, and magnetite.

320-340 m Pyroclastic. Light grey to greenish colour, with fragments of pale greenish rhyolite with spherulitic texture, pumice, slightly silicified obsidian and tuff. Slightly altered rock unit with hint of oxidation. It is vesicular and the vesicles are filled with siliceous material. Magnetite and aegirine (pyroxene) are observed as the ground mass, glasses are slightly altered to clay but most of them are fresh. Alteration minerals: pyrite, quartz, siderite (white), chalcedony, smectite and glass/opaque minerals. Mineral sequence is noted at the depth of 320 m, such as fine grained chalcedony < coarse grained clay < clay.

350-390 m Rhyolite. Light grey to light pinkish colour and medium grained rock unit with phenocryst of plagioclase. A few fragments of obsidian and cement are found. It is vesicular and fractured, the vesicles filled by greenish clay. Slight alteration and oxidation noted. Alteration minerals: pyrite, smectite, illite, amphibole, and feldspar.

400-410 m pyroclastic. Light grey to brownish, fine grained, scarcely pores rock sample A few fresh and fractured obsidian grains, vitric tuff and reddish siliceous material noted. Little oxidation and slight to moderate alteration observed. Aegirine and feldspars are found as the ground mass. Alteration minerals: pyrite, MLC, smectite, quartz, plagioclase and magnetite.

420-460m Silicic tuff and breccia. Reddish to brownish, fine to medium grained units. Fragments of fractured and silicified obsidian and rhyolite with plagioclase phenocrysts are observed. The alteration intensity is medium to high with very slight oxidation. Circulation loss was encountered at 450m. Alteration minerals: pyrite, smectite and clays.

470-580 m Rhyolite. Light greyish and greenish, fine grained scarcely pores, found together with fragments of pumiceous Pyroclastics, tuff and fewer obsidian. It is slightly altered rock unit. Fragment of rocks observed below this unit are partly silicified obsidian, pumice and silicic materials. Fractures and vesicles are filled by secondary minerals and siliceous material and a few quartz vein also found at depth of 480m and 490m. No cuttings found at depth of 450 m. Plagioclase and sanidine are found as a phenocryst and hint of oxidation noted. There is no sample at depth of 510 m. Alteration minerals: disseminated pyrite, quartz, smectite, MLC, chalcedony, plagioclase, fresh glass and magnetite.

590-650 m Sediments. Black to light grey, fine to medium grained with black fine grained silt like material. Fragments of tuff, altered basalt silicified obsidian, rhyolite and siliceous material. From 610-615 m and 630-635 m circulation loss occurred. Feldspars are found as ground mass in basalt and rhyolite. Some calcite and quartz veins are observed. Moderately to highly altered with hint of oxidation. Alteration minerals: pyrite, calcite, MLC, chlorite, quartz, illite and magnetite.

660-700 m. Trachyandesite. Light grey to brownish, fine to medium grained with trachytic texture rock unit. Partly oxidized and moderately altered. There are fragments of fractured tuff and some altered

basalts. Alteration minerals: calcite, siderite, pyrite, chlorite, MLC, and plagioclase. Mineral sequence indicates MLC < quartz < calcite.

710-770 m. Basalt. Dark grey to black, porphyritic texture, with plagioclase phenocrysts and fine grained feldspar ground mass. Vesicle and veins are filled by calcite. Slightly altered and oxidized. Alteration minerals: calcite, pyrite, chlorite, chalcedony and magnetite.

780-800 m. Dacite. Light grey to brownish, porphyritic texture and moderately altered rock type. It is identified by its chemical composition by using ICP-OES method. Dacite seen together with fragment of altered basalt. Alteration minerals: calcite, pyrite, chlorite, secondary quartz and magnetite.

810-830 m. Basalt. Dark grey to brownish, fine to coarse grained, containing phenocrysts of plagioclase. It is found together with few brownish tuffs. Slightly oxidized and moderately altered rock unit. Alteration minerals: epidote (found at 710 m), pyrite, calcite (vein filling), MLC, smectite, chlorite, chalcedony, quartz and opaque minerals. Mineral sequence is also noted: chlorite < MLC < Smectite.

840-880 m. Pyroclastics. Light greenish to whitish crystalline welded tuff with a few dark grey porphyritic basalt grains. Fine to medium grained with well-developed secondary quartz. Hint of oxidation noted and alteration is recorded from moderate to high. Alteration minerals: disseminated pyrite, quartz, calcite chlorite (with vesicle filling), smectite and opaque minerals.

890-940 m. Basalt. Black to reddish, porphyritic with fragments of fine grained greyish rhyolite and greenish tuff units. It is containing phenocrysts of plagioclase and sanidine with magnetite groundmass. Hint of oxidation noted and alteration is recorded from slight to moderate. Alteration minerals: disseminated pyrite, biotite, quartz, calcite, chlorite, MLC, illite, smectite and magnetite. Mineral sequence showing chlorite < calcite and chlorite < MLC < Smectite.

950-990 m. Basaltic trachyandesite. Light grey to greenish, fine to medium grained, with plagioclase phenocryst. Vesicles are filled with calcite and quartz. Alteration minerals: pyrite, calcite, quartz, chlorite, magnetite, clays and opaque minerals.

1000-1020 m Trachyte. Dark grey to brownish, fine grained rock unit, with plagioclase phenocrysts and feldspars ground mass but the feldspar getting altered. It is vesicular and fractured, moderate oxidation and alteration noted. Few fragments of fine grained rhyolite and black basalt are found. Alteration minerals: pyrite, calcite, albite, chlorite quartz, magnetite and illite.

1030-1050 m. Trachydacite. Dark grey to brownish, fine grained with plagioclase phenocryst. Few fragments of tuff and basalt grains are observed. Few vesicles are noted and it is filled with calcite. Alteration minerals: pyrite, calcite, magnetite and clays.

1060-1120 m. Trachyte. Light greyish to brownish crystalline, fine to medium rock unit with ground mass of feldspar and sanidine, and plagioclase as phenocrysts. Fragments of dark grey/black, porphyritic basalt and a dark greyish rhyolites are found. Moderately to highly altered and slightly oxidized. Alteration minerals: calcite, pyrite, clays, chlorite, epidote, quartz and opaque minerals.

1130-1140 m. Circulation loss.

1150-1220 m. Rhyolite. Light grey to brownish, aphyric rock unit with altered aphanitic basalt fragments and siliceous material. Hint of oxidation and alteration noted. Alteration minerals: pyrite, calcite, quartz, haematite, chlorite and clays.

1230-1300 m. Circulation loss

1310-1325 m Trachyte. This rock unit occurred at a depth of 1270, 1285, 1310 and 1325 m. It is light grey colour with plagioclase phenocrysts. Few fragments of basalt are seen. Moderate oxidation and

high alteration noted at this depth. Alteration minerals: calcite, pyrite, clay, quartz, epidote, chlorite, MLC and magnetite.

1330-1360 m. Circulation loss.

1370-1390 m. Trachyte. Light greyish to whitish in colour with fragments of aphanitic basalt. Slightly oxidized and moderately altered. Alteration minerals: calcite, pyrite, magnetite, illite, epidote and chlorite.

1400-1410 m. Basalt. Dark grey porphyritic texture, feldspars found as ground mass and plagioclase as phenocrysts. Quartz are found in vein filling. Slight oxidation and alteration seen. No cuttings observed at 1400m. Alteration minerals: calcite, pyrite, quartz, epidote and chlorite. Mineral sequence indicated that chlorite < calcite.

1420-1430 m. Circulation loss.

1440-1490 m. Basalt. Black shiny to dark grey porphyritic basalt with plagioclase phenocrysts. Few vesicles and fractures filled with calcite and siliceous materials. Fragments of fine to medium grained rhyolite. Slightly oxidized and altered. Alteration minerals: calcite, pyrite, quartz, magnetite and epidote. Mineral sequence indicated that quartz < chlorite.

1500-1510 m. Circulation loss.

1520-1530 m. Basalt. Black shiny to dark grey porphyritic texture with fragments of light greenish rhyolite. Slight oxidation and alteration seen. Alteration minerals: calcite, pyrite, quartz, epidote and plagioclase.

1540-1550 m. Circulation loss.

1560-1590 m. Trachyte. Light green crystalline unit with fragments of light pinkish rhyolite and dark grey basalt. Moderately altered and hint of oxidation noted. Alteration minerals: calcite, pyrite, quartz, chlorite, epidote and opaque minerals.

1600-1920 m. Basalt. Black to dark grey, shiny rock, fine-medium grained with fragments of light greenish rhyolite and ignimbrite. Phenocrysts of plagioclase seen. Veins and vesicles are filled by quartz and calcite. Moderate to highly altered and hint of oxidation noted. Circulation loss occurred at a depth of 1610, 1670, 1720, 1740, 1790, 1840, 1850 and 1870 m. Alteration minerals: calcite, disseminated pyrite, quartz, chlorite, haematite, magnetite and epidote.

APPENDIX II: Description of stratigraphy for well LA-10D as observed under binocular and petrography microscope analysis

10-70 m. Pyroclastics. Light grey, fine to medium grained. Fragments of light grey to pinkish, slightly silicified rhyolite, few layered obsidian grains, pumice and siliceous materials are noted. Hint of oxidation and a few primary amphibole crystals, hornblende, plagioclase and quartz are seen in this rock unit.

80-90 m. Rhyolite. Light grey to brownish, with micro phenocrysts of amphibole. It is observed together with pumice, obsidian and cement fragments. Very slight alteration observed. Few vesicles are noted filled with siliceous material.

100-120 m. Pyroclastics. Light to dark grey rock unit with fresh and silicified obsidian, pumiceous tuff, few vesiculated pumice, fine grained rhyolite and cement fragments. Fine to medium grained, showing banded texture and vesicular. Vesicles and fractures filled by clays and calcite. Plagioclase found as phenocrysts and amphibole, glass, aegirine, as ground mass. Slight alteration has occurred. Alteration minerals: calcite, primary quartz, smectite and chalcedony.

130-150 m. Rhyolite. Light greyish to light pinkish, moderately vesicular, amphibole rich and ashy rock unit. It is found together with welded tuff and glassy obsidian grains. Amphiboles and primary quartz grains are noted. Very slight alteration observed.

160-330 m. Circulation loss.

340-440 m. Rhyolite. Light greyish, fine- medium grained, fresh rhyolite with fragments of obsidian and lithic tuff. Plagioclase found as phenocrysts; and feldspar, aegirine, riebeckite and opaque minerals found as a ground mass. Few vesicles and veins are filled with quartz and clay. Slight to moderate alteration and oxidation seen. Alteration minerals: pyrite, calcite, smectite, primary quartz, clay and magnetite.

450-490 m. Silicic tuff and breccia. Light grey, fine grained, vesicular rock type. Some veins and vesicles are filled with siliceous material. Fragments of rhyolite with plagioclase phenocrysts and fragment of obsidian units are noted. High alteration and slight oxidation observed. Alteration minerals: few pyrite, chalcedony, quartz and clays.

500-510 m. Dacite. Light grey to brownish colour, fine grained, shows strong alteration and very slight oxidation. Rare micro veins noted. The rock unit observed together with highly altered flow banded silicified rhyolite and minor amount of tuff. Vesicles are observed at 480 m and filled by siliceous material. Alteration minerals: chalcedony, fine grain quartz, pyrite, biotite, greenish clays and siderite.

520-570 m. Rhyolite. Light grey to pinkish, fine grained rock unit. Feldspar is found as micro phenocrysts. Micro veins and vesicles are filled with quartz and clay minerals. The rock is found together with tuff fragments. Hint of little oxidation and moderate alteration noted. Alteration minerals: calcite, pyrite, smectite, quartz and illite.

580-620 m. Sediments. Dark grey to brownish, fine grained rock unit, no crystals were not seen. Black fine grained like silt fragments are dominated. Also fragments of fractured basalt, altered pumice, rhyolite and tuff are found. The ground mass is rich in quartz and feldspars. It is vesicular and fractured, the vesicles and veins are filled with quartz, calcite and clays. High alteration noted in this rock unit. Alteration minerals: pyrite, calcite, quartz (the amount increased compare to the previous depth), altered glass, chlorite, magnetite and MLC.

630-640 m. Trachyte. Dark to light greyish, highly altered with trachytic texture rock unit. Fragments of few brownish altered tuff and altered rhyolite are observed. There is intergrowth of calcite with quartz also seen through petrography microscope at depth of 640 m. Mineral sequence shows calcite < chlorite < quartz. Alteration minerals: calcite, pyrite, clays and quartz.

650-670 m. *Trachyandesite*. Light grey to brownish, fine to medium grained. Plagioclase found as phenocrysts and feldspar as ground mass together with microphenocrysts of pyroxene. A few vesicles and veins are noted and filled by calcite, clays and quartz. Hint of oxidation and moderate alteration observed. Alteration minerals: calcite, pyrite, magnetite, quartz and MLC.

680-730 m. *Circulation loss*.

740-770 m. *Trachyte*. Light grey, fine to medium grained rock unit with trachytic texture and phenocrysts of altered plagioclase. Fragments of rhyolite, pumiceous tuff, few basalt and siliceous material are found. Few fractures and veins filled by calcite. Hint of oxidation and high alteration noted. Alteration minerals: calcite, pyrite, quartz, MLC, illite and clays.

780-800 m. *Basalt*. Black shiny, fine grained rock unit with light grey to whitish tuff and obsidian fragments. Slightly altered and hint of oxidation seen. Mineral sequence observed quartz > chlorite. Alteration minerals: calcite, pyrite, quartz, chlorite and oxide minerals. no cutting observed at a depth of 780m.

810-820 m. *Pyroclastics*. A mixture of glassy basalt, vesiculated tuff, rhyolite and black consolidated clay fragments are observed. It is slightly altered and oxidized. Alteration minerals: calcite, pyrite, chalcedony and clays.

830-840 m. *Andesite*. Brownish with fragments of black shiny aphyric basalt and white tuff. Moderate to high alteration and oxidation noted in the rock unit. Alteration minerals: chalcedony, calcite (vesicle filling), pyrite, chlorite and quartz.

850-900 m. *Rhyolite*. Light grey to dark grey, fine to medium grained, plagioclase and quartz as phenocrysts with feldspar ground mass. Fragments of brownish vesicular basalt and welded tuff are seen. Vesicles dominate at 880m depth and some are filled by calcite and quartz. Slight alteration and very slight oxidation noted. Alteration minerals: calcite, disseminated pyrite, quartz, epidote, chlorite, MLC, illite, magnetite and haematite.

910-930 m. *Basalt*. Brownish to light grey, fine grained rock unit. Fragment light grey lithic tuff and fine grained rhyolite. High to moderate alteration and, oxidation noted. Alteration minerals: quartz, chlorite, pyrite, calcite, epidote and magnetite. There is also intergrowth of quartz and epidote.

940-950 m. *Basalt*. Light grey to black, fine grained rock unit with tuff and light pinkish rhyolite. The rhyolite is more dominant unit than tuff. The colour of rhyolite changes from greenish to light greenish when the depth increases. Slight to moderate alteration and slight oxidation noted. Alteration minerals: pyrite, quartz, chlorite, calcite, epidote and opaque minerals.

960-990 m. *Basalt*. Light grey to greenish, fine grained rock unit with light pinkish rhyolite. It is vesicular and some vesicles are filled with quartz. Highly altered and slightly oxidized. Alteration minerals: epidote, calcite, quartz, pyrite and chlorite. Mineral sequence seen as epidote < quartz and plagioclase; epidote < calcite and chlorite < quartz.

1000-1010 m. *Trachyte*. Light greenish, fine to medium grained with moderately altered plagioclase phenocrysts and feldspar ground mass. It is vesicular, the vesicles and the veins are filled with quartz, chlorite and calcite. Fragments of porphyritic black basalt, tuff and fine grained rhyolite are observed. Alteration minerals: epidote, calcite, chlorite, pyrite, quartz, MLC and magnetite. The mineral sequence indicated that quartz < MLC and quartz < chlorite.

1020-1030 m. *Trachydacite*. Whitish to light greenish with fragments of black basalt, tuff and rhyolite. Phenocryst of plagioclase noted. Slightly altered and slightly oxidized. Alteration minerals: calcite, pyrite and chlorite.

1040-1060 m. *Trachyte*. Light grey to greenish, trachytic texture, fine to medium grained rock unit with plagioclase and few quartz phenocrysts and ground mass of sanidine and feldspars. Fragments of

greenish grey welded tuff, partially altered basalt and fine grained rhyolite noted. Slightly altered and oxidized. Alteration minerals: calcite, pyrite, quartz, epidote, MLC, illite, magnetite and chlorite. There is intergrowth of quartz and calcite minerals.

1070-1100 m. Rhyolite. Light grey to brownish, fragment of aphanitic basalt and tuff. Trachytic texture with magnetite and feldspar ground mass and plagioclase phenocrysts. It is moderately altered and oxidized. Alteration minerals: quartz, calcite, epidote, pyrite, MLC and chlorite.

1110-1130 m. Trachydacite. Light grey to brownish, observed together with fine to coarse grained basalt. Slight to moderate alteration and oxidation seen. Alteration minerals: pyrite, calcite and chlorite.

1140-1210 m. Pyroclastic. Light grey, fine to medium grained, brecciated, plagioclase phenocrysts and pyroxene micro-phenocrysts with feldspar and magnetite ground mass. Fragments of pinkish and yellowish fine grained rhyolite with light grey basalt noted. Moderately altered and slightly oxidized. Circulation loss occurred at a depth of 1190m. Alteration minerals: pyrite, calcite, epidote, chlorite, MLC and quartz.

1220-1390 m. Trachyte. Light grey to brownish, trachytic texture, fine to medium grained rock unit with fragments of basalt, rhyolite and welded tuff. Feldspars are surrounded the magnetite as ground mass and plagioclase phenocrysts. Veins and vesicles are filled with calcite and quartz. Moderately altered and slightly oxidized. Circulation loss occurred at 1290m depth. From 1360m to 1400m the amount of basalt fragment increased with vesicles and strong alteration and oxidation are also recorded. Alteration minerals: epidote, calcite, pyrite, chlorite, magnetite, illite, MLC and quartz. Mineral sequence indicates quartz < chlorite < fine grained clay and calcite < epidote.

1400-1540 m. Rhyolite. Light grey to brownish, fine grained rock unit with basalt and tuff fragments. It is vesicular and vesicles filled with quartz. At 1440m the amount of black shiny basalt increased together with white coloured tuff. This rock unit is moderately to highly altered and hint of oxidation noted. Alteration minerals: pyrite, chalcopyrite, platy calcite, quartz, chlorite and epidote. Mineral sequence indicates that clay < quartz.

1550-1600 m. Basalt. Black, shiny, aphyric rock unit together with light greenish rhyolite, whitish tuff and ignimbrite grains. Plagioclase occurs as phenocrysts. Circulation loss happened at 1580m depth. Slightly to moderately altered. Alteration mineral: pyrite, calcite, quartz, chalcopyrite and epidote.

1610-1620 m. Basaltic trachyandesite. Light greenish aphyric rock unit with fragments of black shiny basalt and tuff. Moderately to highly altered and hint of oxidation noted. Alteration minerals: calcite, pyrite, chalcopyrite, chlorite, illite and epidote.

1630-1780 m. Basalt. Fine-medium grained, black shiny rock unit with tuff and ignimbrite fragments. Moderately altered plagioclase and sanidine are found as phenocrysts and pyroxene as micro-phenocrysts. The amount of epidote increases at a depth of 1670 m. Moderate alteration and hint of oxidation noted. Alteration minerals: calcite, pyrite, chalcopyrite, quartz, chlorite, MLC, magnetite and epidote (replacing feldspars). Intergrowth of quartz and epidote are seen. Mineral sequence indicating that calcite < chlorite < quartz and chlorite < quartz.

1790-1800 m. Basaltic andesite. Pale greenish, fine grained rock unit, with fragments of rhyolite and ignimbrite is noted. It is vesicular and fractured unit. Slight oxidation and alteration observed. Alteration minerals: chalcopyrite, pyrite, quartz, epidote and calcite.

1810-1940 m. Ignimbrite. Light greenish to greyish, fine to medium grained rock unit with feldspars and magnetite, which are found as groundmass. Also plagioclase and quartz as phenocrysts. A few fragments of black basalt, rhyolite, tuff and siliceous material. A few fractures are seen and filled by quartz and calcite. Moderate to high alteration and hint of oxidation seen. Alteration minerals: calcite pyrite, quartz, chalcopyrite, chlorite, illite, magnetite, MLC, epidote and actinolite (formed by replacing pyroxene).

APPENDIX III: Procedure for ICP-OES analysis

First prepare a homogeneous sample from the drill cuttings by removing other fragments.

The homogenous rock cuttings were grinded in agate mortar to get about 100 mesh powder

After getting the cuttings sample powder, weight 100 mg±1mg in an epicure graphite crucible and mix with 200mg±1mg of lithium metaborate (LiBO₂).

Prepare six working standard samples (K-1919, BIR-1, BGM-1, A-THO, B-THO and B-ALK).

250mg±1 mg of A-THO, B-ALK and B-THO standard samples were mixed with 500mg±1mg of lithium metaborate flux (LiBO₂).

The samples melted at 1000°C in an electric furnace for 30 minutes and formed as a pellets. This took about 15-20 minutes to cool down.

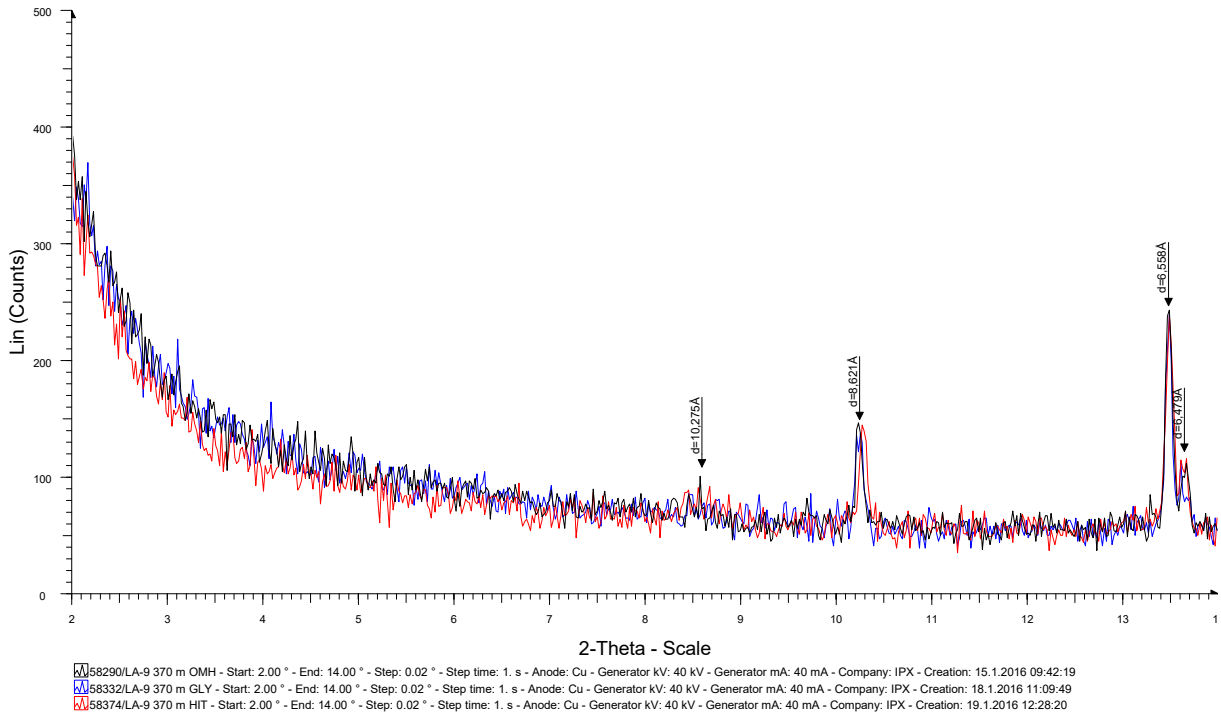
After the melt has cooled down or changed to pellet, put in to the bottle which has 30ml of Rockan complexing acid, which is a mixture of 5%HNO₃, 1.33%HCL and 1.33% semi saturated oxalic acid.

The three calibrated standards, i.e. A-THO, B-THO and B-ALK, were mixed with 75ml of the Rockan complexing acid. To monitor the drift during analysis, Reference (REF) was prepared by mixing 33% A-THO, B-THO and B-ALK. After mixing put in to a shaker machine for more than 2hr until the mixture was completely dissolved, which helps to avoid silica precipitation problem.

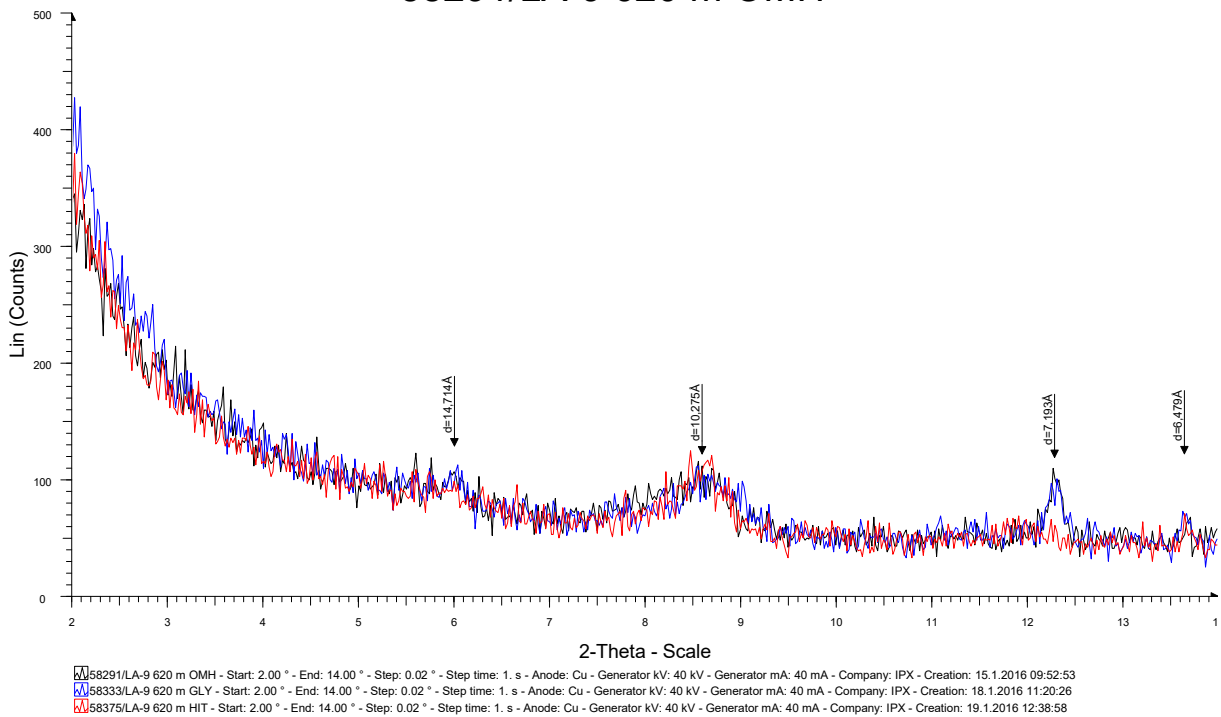
After this process, the samples become ready for ICP-OES analysis. To calibrate the instrument, the three standards K-1919, BIR-1 and RGM-1 were run first. The REF was done at every 10 sample interval.

**APPENDIX IV: X-ray diffractograms from wells LA-9D and LA-10D,
Aluto Langanu geothermal field**

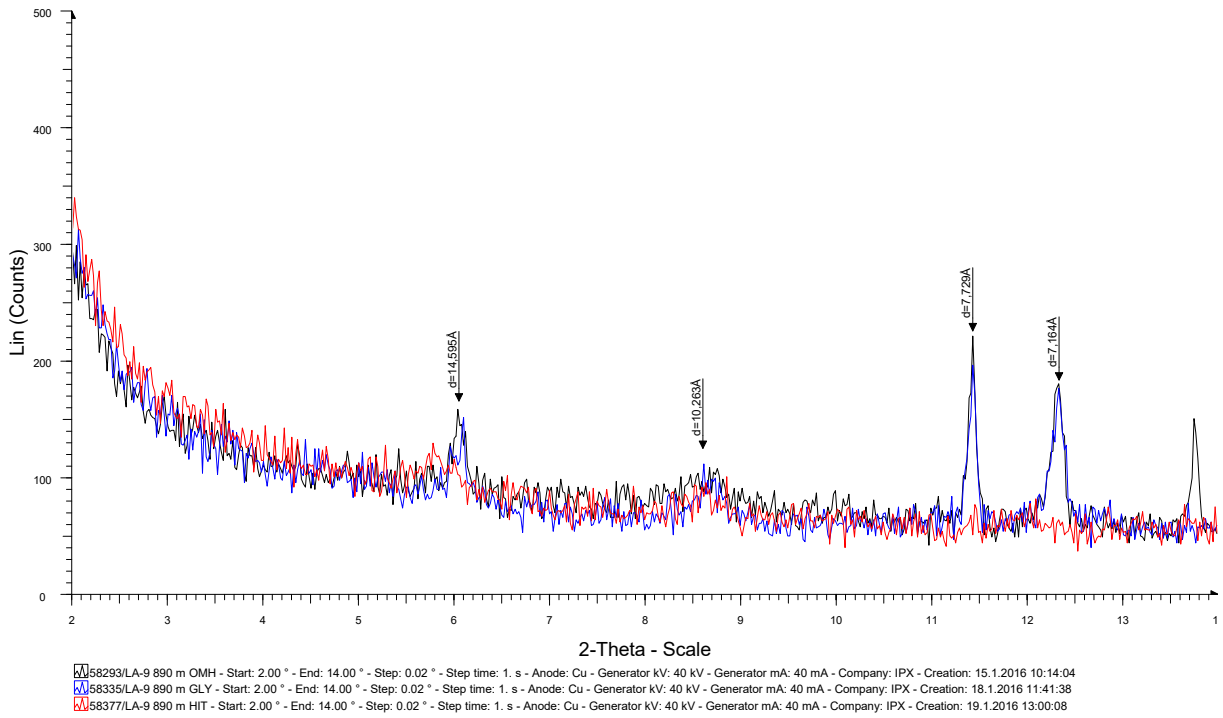
58290/LA-9 370 m OMH



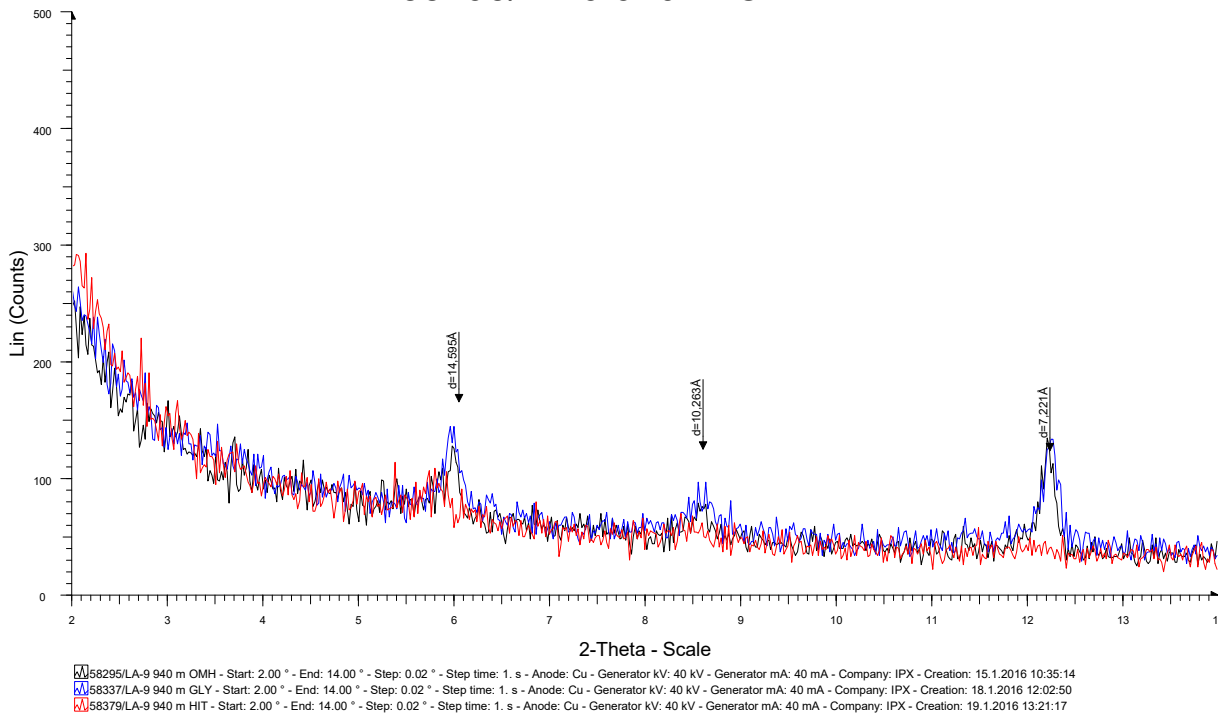
58291/LA-9 620 m OMH



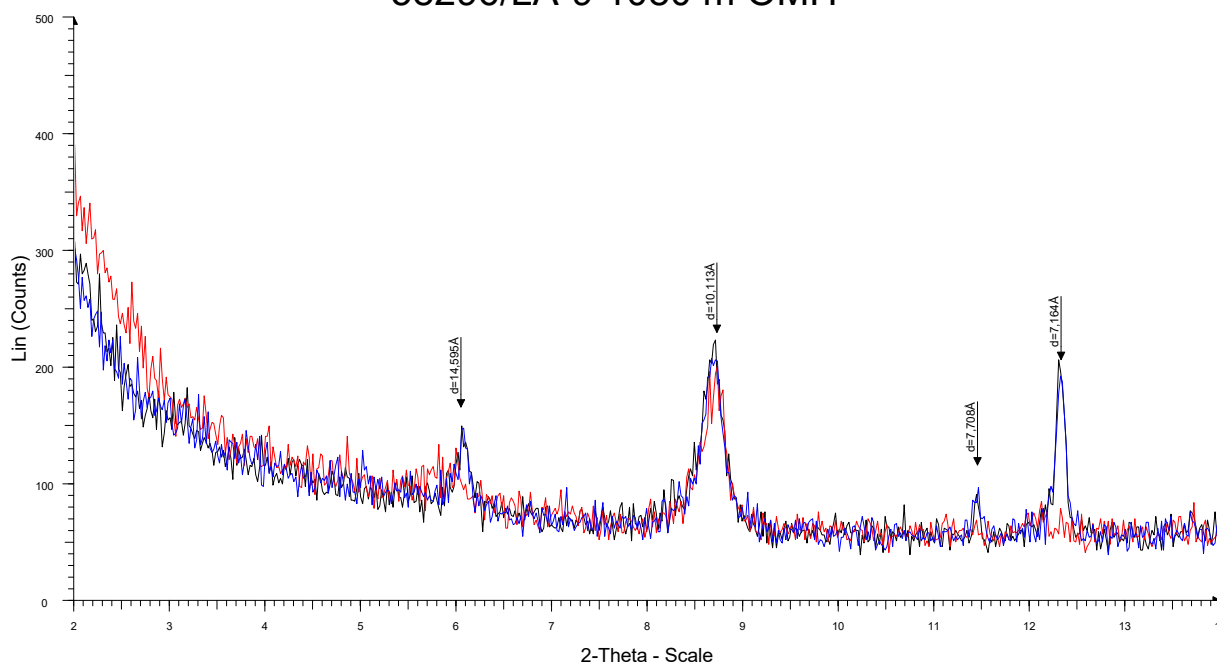
58293/LA-9 890 m OMH



58295/LA-9 940 m OMH

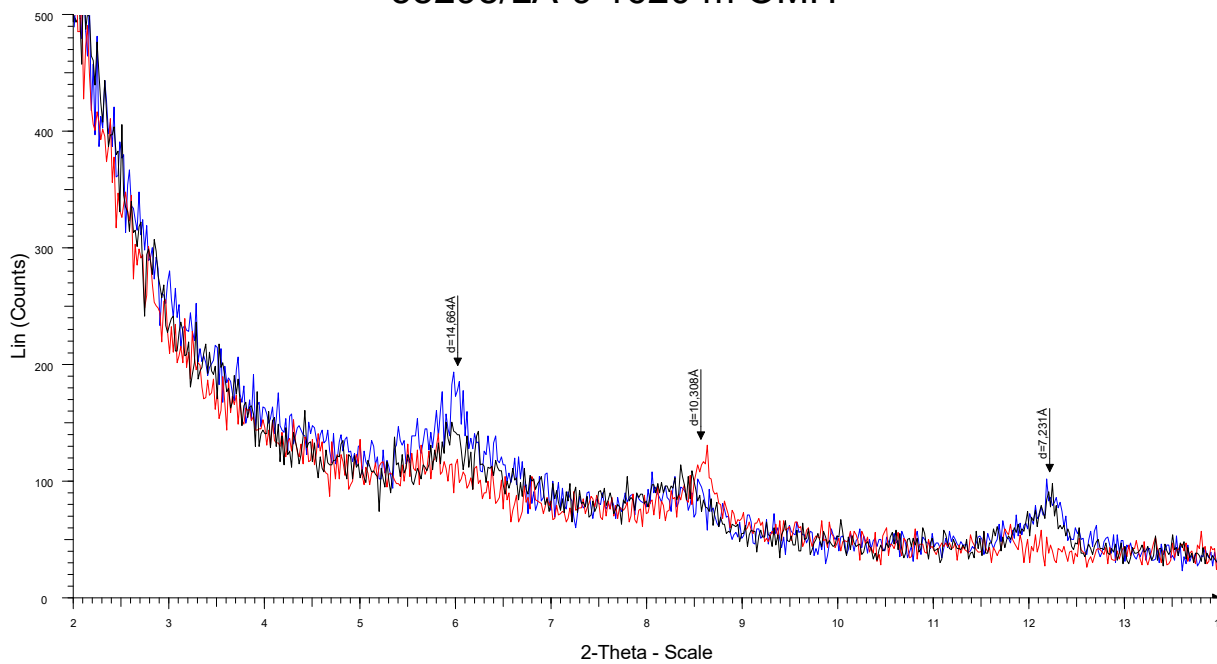


58296/LA-9 1080 m OMH



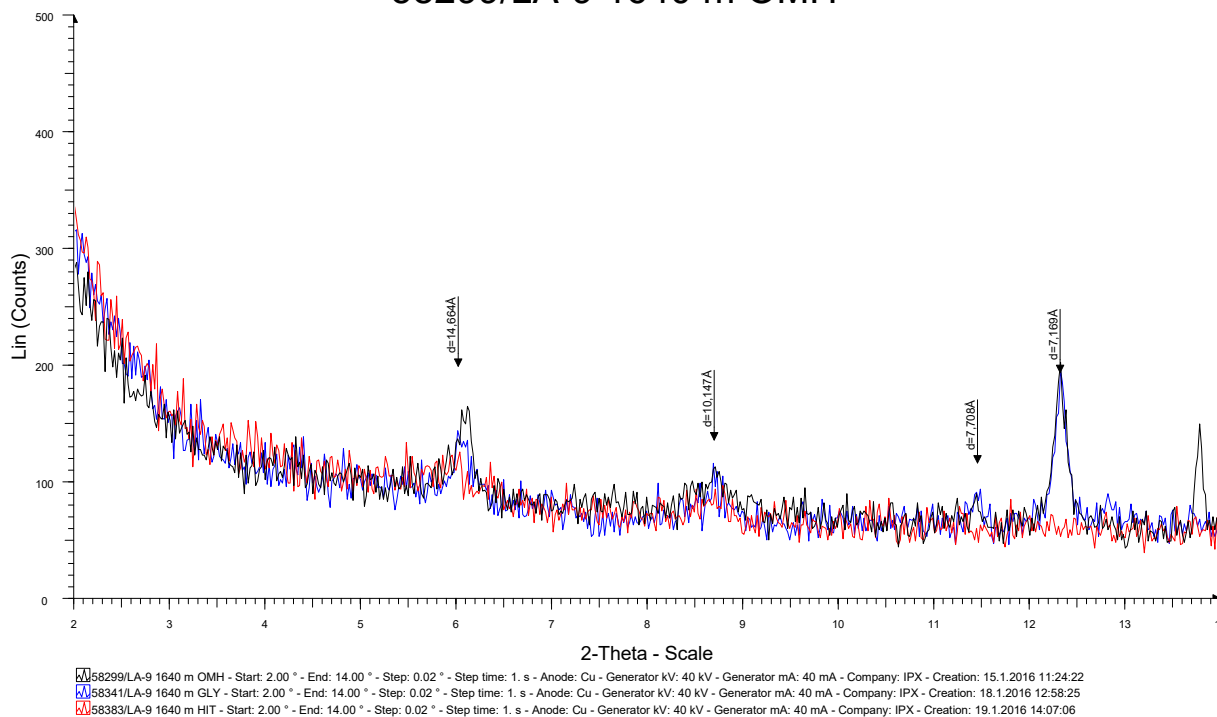
58296/LA-9 1080 m OMH - Start: 2.00 ° - End: 14.00 ° - Step: 0.02 ° - Step time: 1. s - Anode: Cu - Generator kV: 40 kV - Generator mA: 40 mA - Company: IPX - Creation: 15.1.2016 10:45:48
58338/LA-9 1080 m GLY - Start: 2.00 ° - End: 14.00 ° - Step: 0.02 ° - Step time: 1. s - Anode: Cu - Generator kV: 40 kV - Generator mA: 40 mA - Company: IPX - Creation: 18.1.2016 12:13:25
58380/LA-9 1080 m HIT - Start: 2.00 ° - End: 14.00 ° - Step: 0.02 ° - Step time: 1. s - Anode: Cu - Generator kV: 40 kV - Generator mA: 40 mA - Company: IPX - Creation: 19.1.2016 13:31:52

58298/LA-9 1620 m OMH

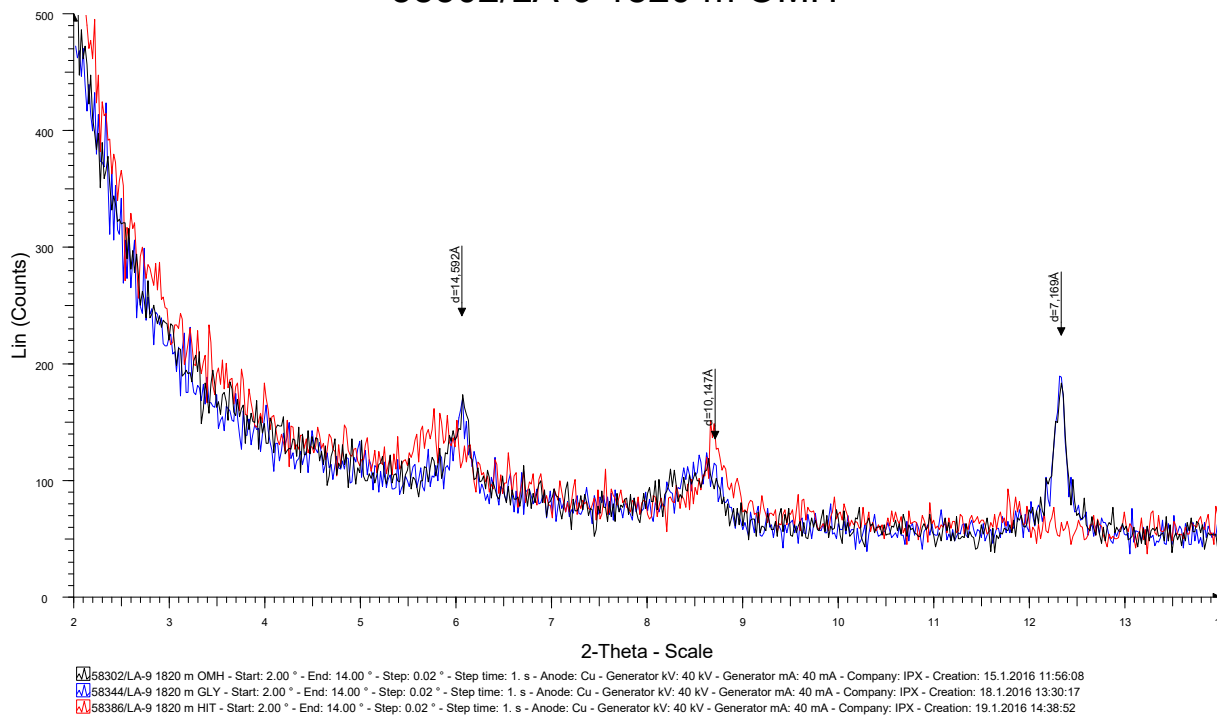


58298/LA-9 1620 m OMH - Start: 2.00 ° - End: 14.00 ° - Step: 0.02 ° - Step time: 1. s - Anode: Cu - Generator kV: 40 kV - Generator mA: 40 mA - Company: IPX - Creation: 15.1.2016 11:13:45
58340/LA-9 1620 m GLY - Start: 2.00 ° - End: 14.00 ° - Step: 0.02 ° - Step time: 1. s - Anode: Cu - Generator kV: 40 kV - Generator mA: 40 mA - Company: IPX - Creation: 18.1.2016 12:47:51
58382/LA-9 1620 m HIT - Start: 2.00 ° - End: 14.00 ° - Step: 0.02 ° - Step time: 1. s - Anode: Cu - Generator kV: 40 kV - Generator mA: 40 mA - Company: IPX - Creation: 19.1.2016 13:56:29

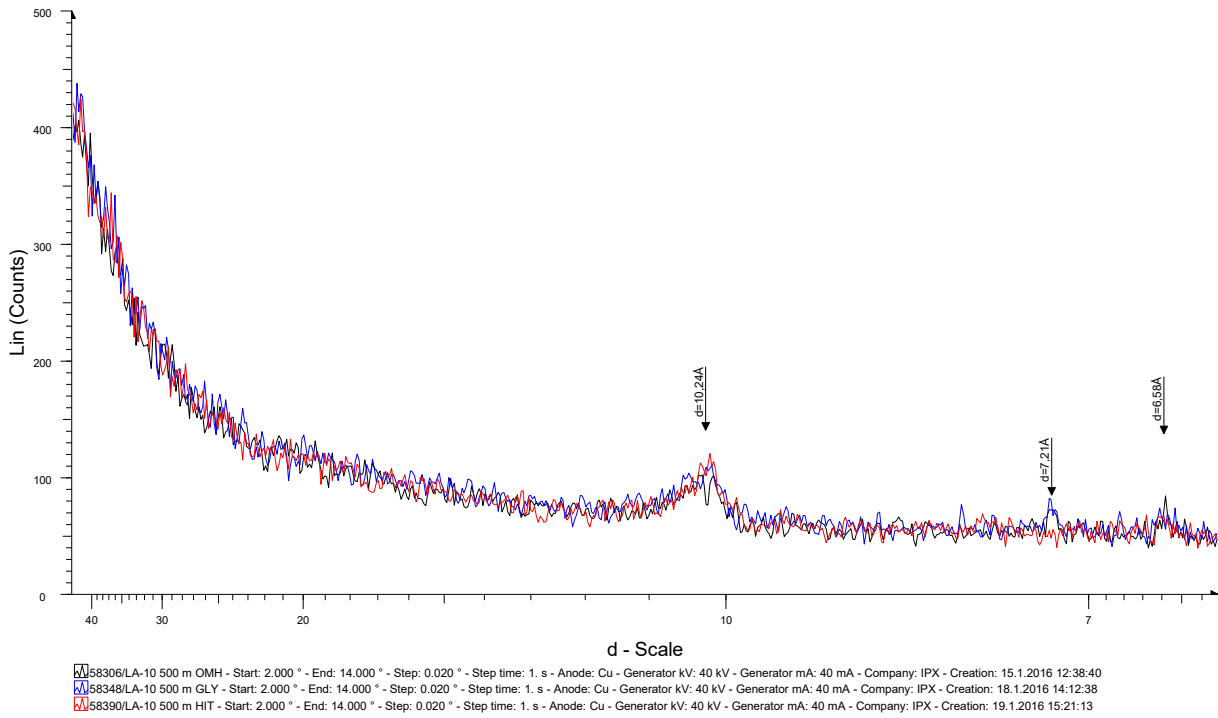
58299/LA-9 1640 m OMH



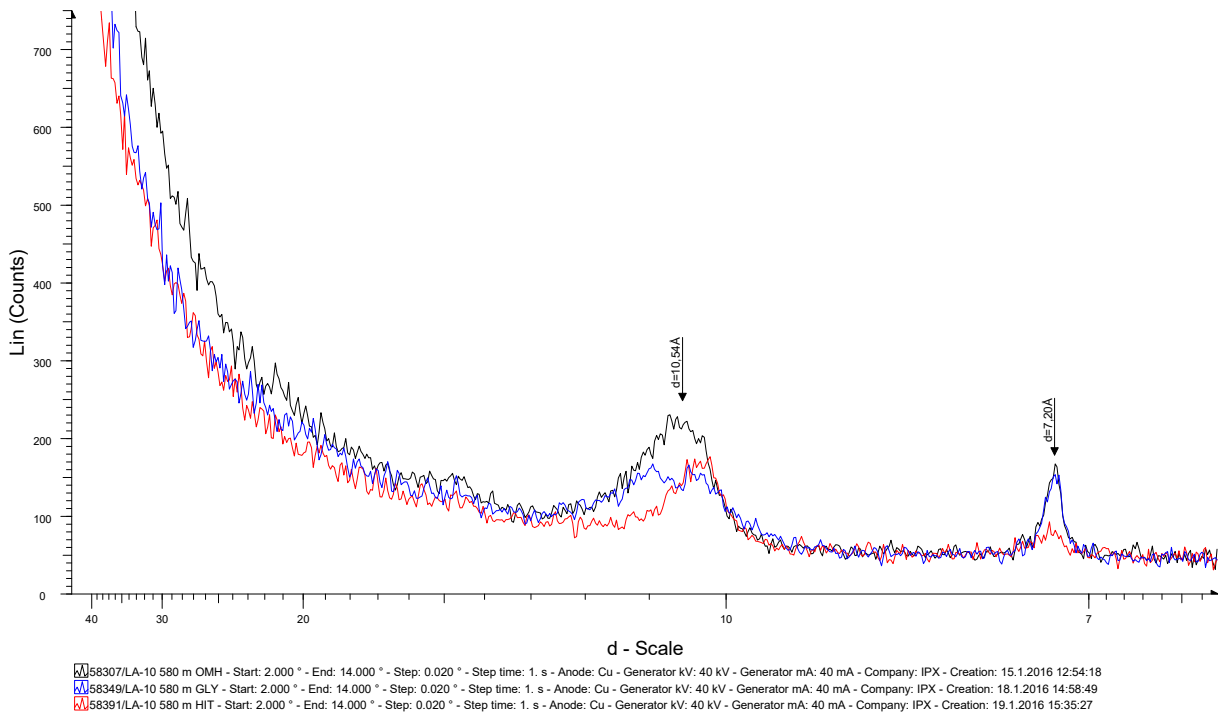
58302/LA-9 1820 m OMH



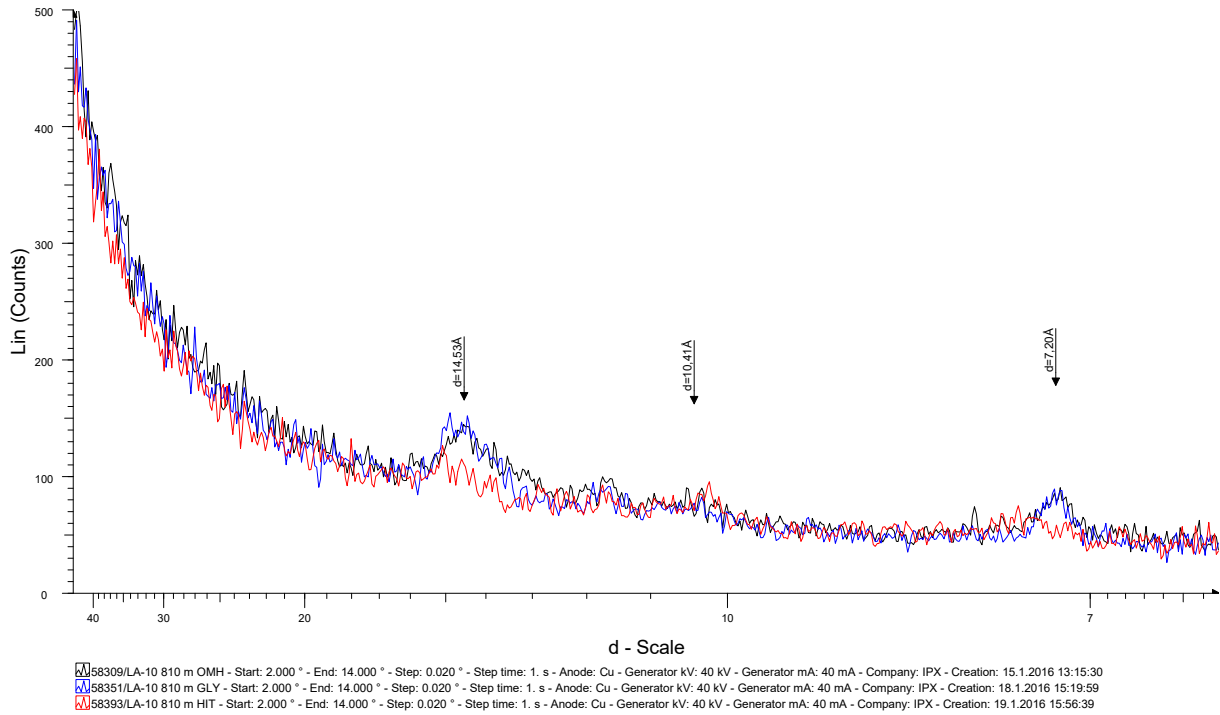
58306/LA-10 500 m OMH



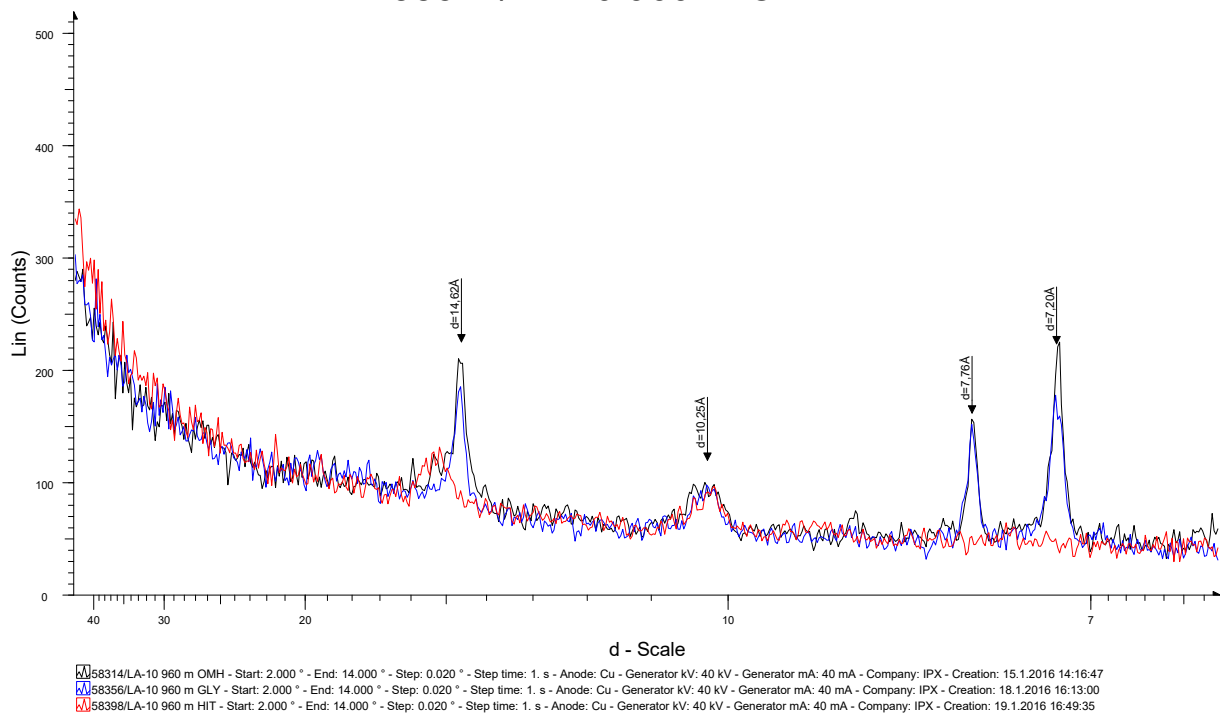
58307/LA-10 580 m OMH



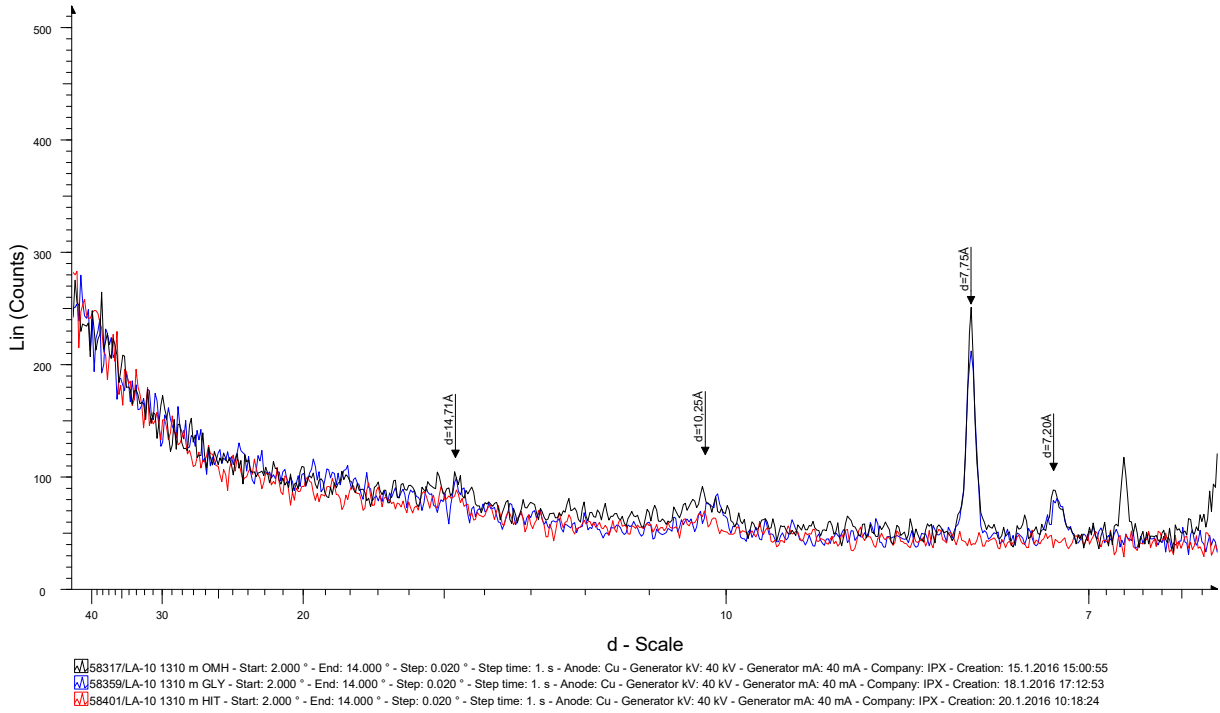
58309/LA-10 810 m OMH



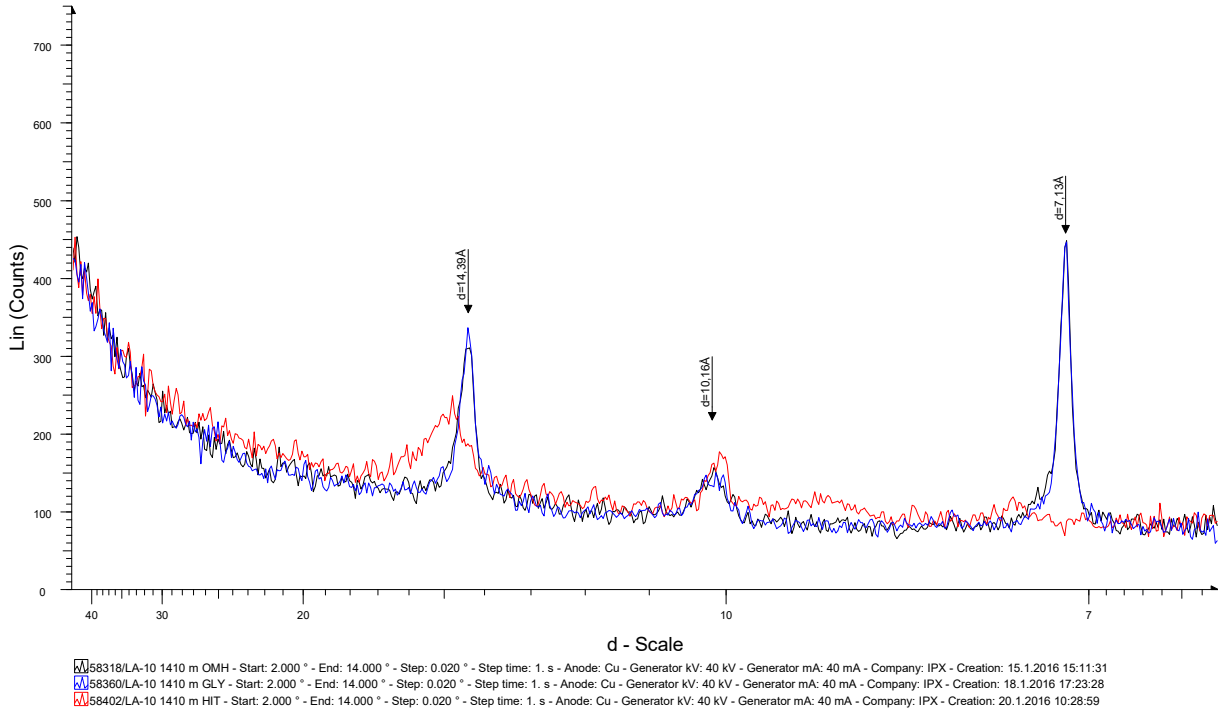
58314/LA-10 960 m OMH



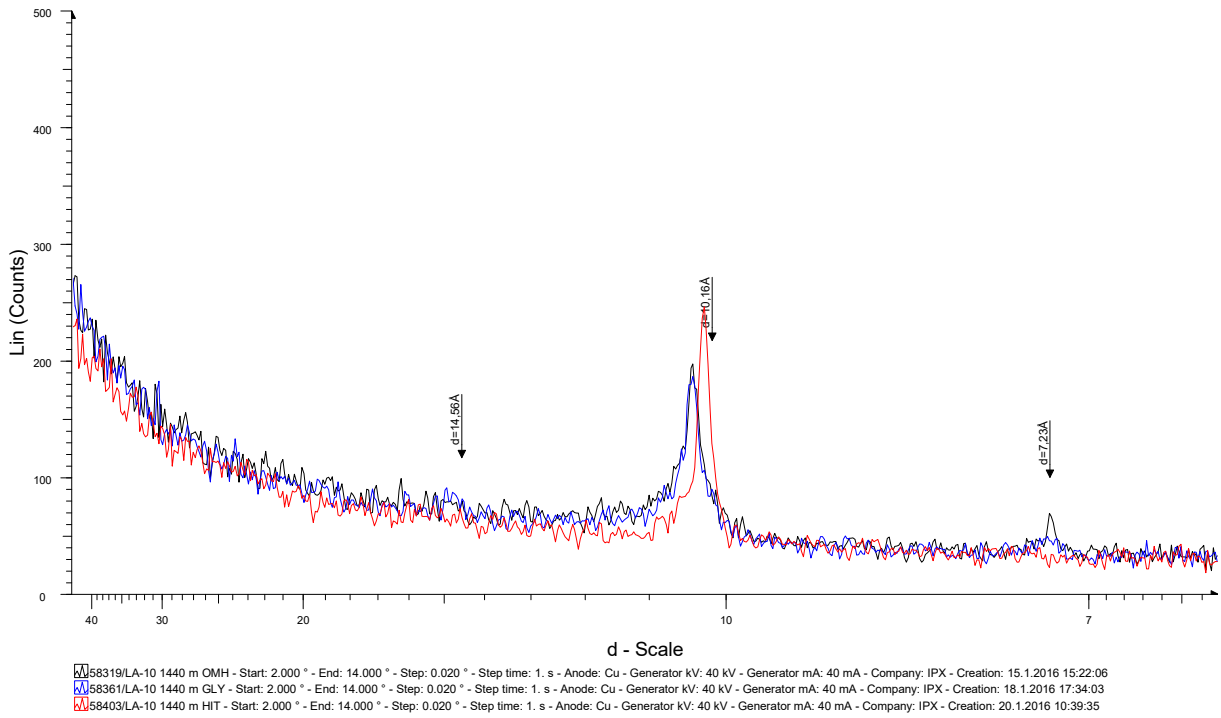
58317/LA-10 1310 m OMH



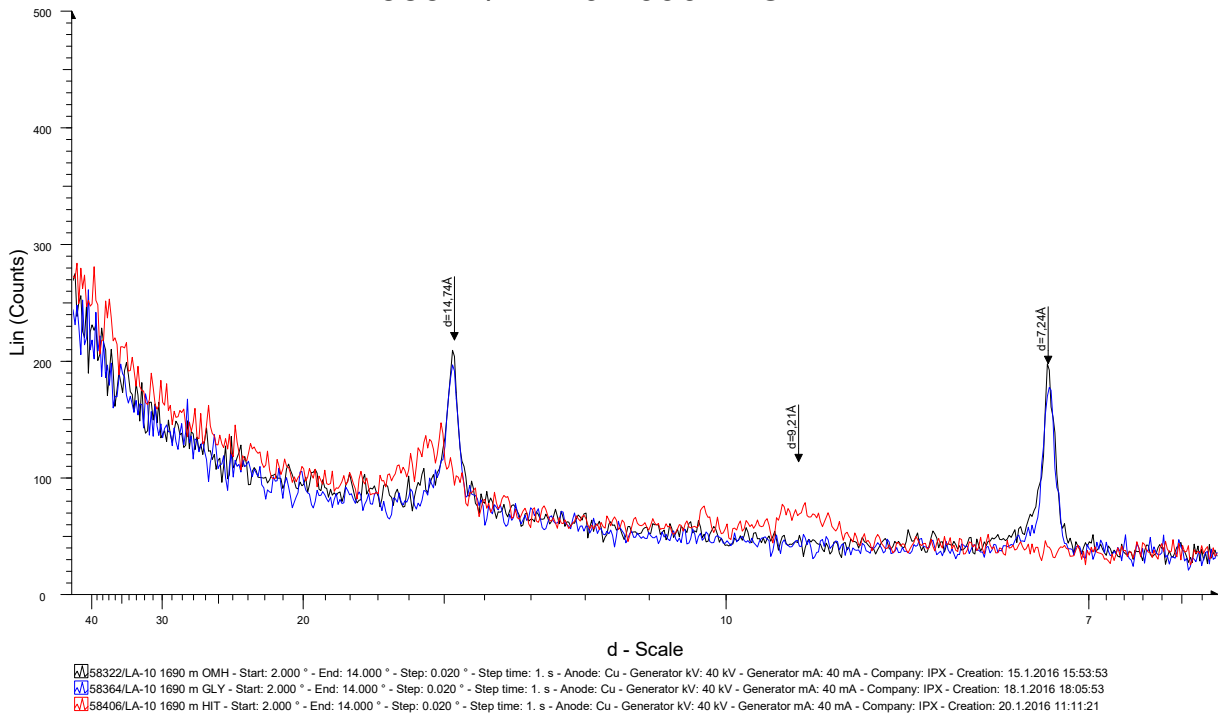
58318/LA-10 1410 m OMH



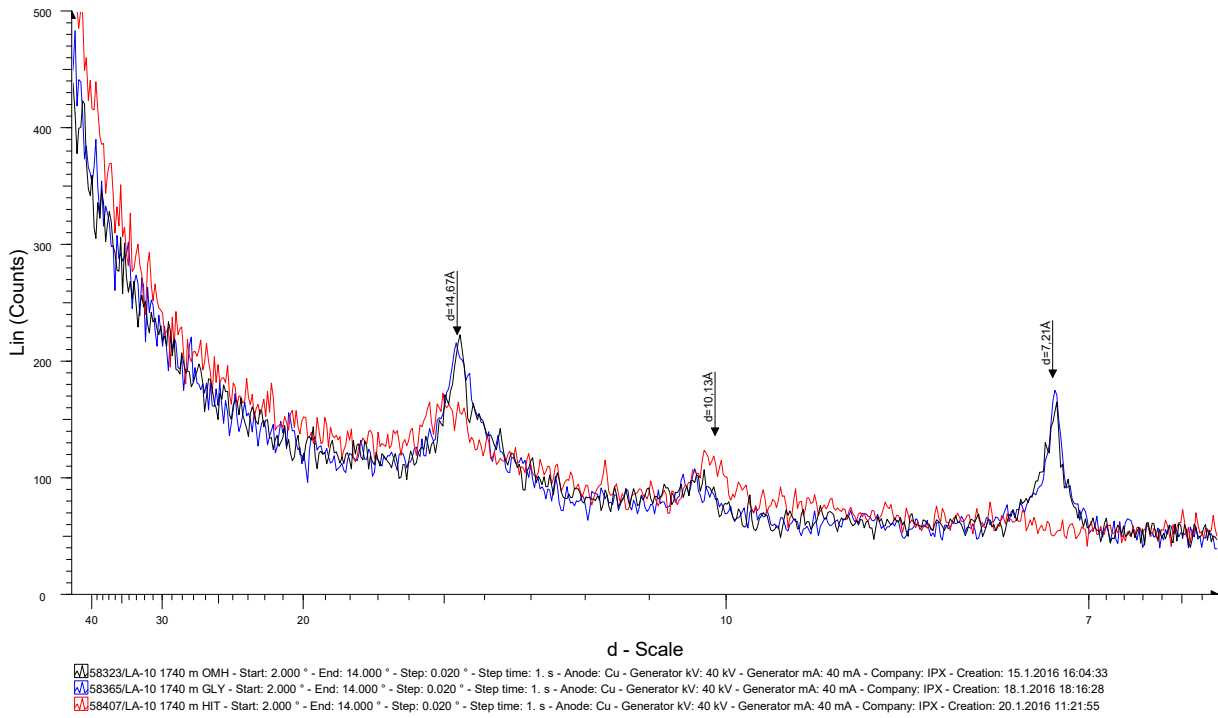
58319/LA-10 1440 m OMH



58322/LA-10 1690 m OMH



58323/LA-10 1740 m OMH



58324/LA-10 1910 m OMH

